ISSN 2294-4931

# IAS

NwLtr 271-272

January 2018

www.sedimentologists.org

# International Association of Sedimentologists

# IAS Council



Link to **IAS National Correspondents:**
https://www.sedimentologists.org/society/correspondents

# CONTENTS

# EDITORIAL

Newsletter 271 collects reports of the founded undergraduated students on 2nd sessions 2015 and 2016.

The Newsletter continues with announcements of the forthcoming meetings sponsored or just supported by IAS.

Student Grant applications guidelines close the Newsletter.

On behalf of the work carried by Early Career Scientists Committee IAS is on Facebook.

IAS has restyled the webpage (www.sedimentologists.org): please have a look at it, log in and fill the spaces under your profile, and renew your membership for 2018.

You can renew your membership quickly and safely on the IAS website (after log in).

Basic membership fees for 2018 remain at 25 Euro for full members (or 20 Euro if you renew for 5 years at once) and 10 Euro for student members. Please check our Membership Benefits page to find out what your membership buys you.

Remember that being an IAS member gives you the following benefits:

- access to the online versions of Sedimentology and Basin Research, including all issues ever published;
- access to the printed versions of Sedimentology and Basin Research at very favourable rates;
- access to the IAS Member Directory;
- the Friendship Scheme which gives free membership to people in less-developed countries;
- the electronic Newsletter;
- a network of National Correspondents, which report on the activities in their countries;
- International Sedimentological Congress every four years at reduced fees;
- annual Regional Meeting and meetings sponsored by the IAS at reduced fees;
- pecial lecturer tours allowing sedimentology groups to invite a well-known teacher to give talks and short courses in their

country;
- travel grants for PhD student members to attend IAS sponsored meetings;
- research grants for PhD student members (maximum 1.000 Euros);
- institutional grants for capacity building in 'Least Developed Countries' (LDC), (maximum 10.000 Euros)
- biannual Summer Schools focused on cutting edge topics for PhD student members.

The 20th International Sedimentological Congress will take place in Quebec City (Canada) on 13-17 August 2018. Following previous gatherings on four different continents (Africa, Asia, South America and Europe), the congress will now return to North America... 36 years after Hamilton in 1982. For the first time, the congress will also be co-sponsored by IAS's privileged partner organization SEPM (Society for Sedimentary Geology).

The Call for Abstracts has now been launched. Abstracts are invited for 49 Sessions distributed over 7 General Scientific Themes. Deadline for submission of abstracts is 19 March 2018.

The Call for (early-bird) Registration will be launched in the coming weeks.

- Info@ http://isc2018.org

IAS Student Members can apply for a travel grant from IAS, provided they have an accepted presentation (oral or poster). Deadline for applying for these travel grants via the IAS website is 1 May 2018.

All information and updates about the 20th ISC can be found on the Conference Website and on Twitter.

## ANNOUNCING: 7th IAS International Summer School of Sedimentology

The 7th IAS International Summer School of Sedimentology 2018 for PhD students will be held in Zapala, Argentina, near Neuquén, Argentina from 21 to 28 October 2018. The title of the school is: Processes, stratal architecture and controlling factors of continental to deep-marine systems at the foot of the Andes. It will include field excursions to the worldwide renown outcrops of the Neuquén Basin. Three days of lecturers alternating with three days of field activities are planned. Lecturers will address the latest advances in depositional processes and controls on deep-marine, shallow-marine and continental settings. Jurassic and Lower Cretaceous siliciclastic and carbonate strata of the Neuquén Basin will be used as case studies. The Neuquén Basin, the most extensively studied petroleum basin in Argentina, has been used for fieldtrips and geoscientists training courses for decades. It provides an excellent opportunity to observe geology in the field and to experience superb outcrops along the Andean Fold and Thrust Belt. Zapala, situated in the centre of the basin, is located approximately 180 km west from the Neuquén Airport and represents a northern gateway to the scenic regions of western Patagonia. The meeting point for participants will be at the Neuquén Airport, which can be reached by direct airplane connections from the capitol Buenos Aires and also from Santiago, Chile, as well as by flights arriving from Cordoba, Mendoza and Comodoro Rivadavia. Topics to be addressed: Recent advances in process sedimentology have demonstrated the need to better record and understand depositional facies in a wide range of depositional environments, as well as the need to improve our understanding of how depositional

signals are propagated at basin scale over geologically short periods of time. The core goal of this Summer School will be to provide the students lectures on recent topics regarding depositional processes and environments, as well as the governing controls that can be expected in different siliciclastic and carbonate systems (from deep marine to continental in different geodynamic settings (e.g., early post-rift, late post-rift, foreland). The students will then apply these concepts in the field on outcrops to analyse the stratigraphic architecture of deep-marine, shallow-marine, and continental deposits. Selected examples will be explored at different scales, from high-frequency cycles, to system-scale architectural patterns (i.e., seismic scale), and eventually to large-scale, source-to-sink scales.

The Summer School will comprise approx. 40 % lectures and 60 % field studies, focused on the theme of "Processes, stratal architecture and controlling factors of continental to deep-marine systems at the foot of the Andes". The Neuquén Basin provides an excellent opportunity to observe the geology and superb outcrops of the most extensively studied petroleum basin of Argentina. Participation is limited to IAS Post-graduate student members only. Look for more information coming soon to the IAS website.

### *Important Dates:*

- 25 May 2018 - Application Deadline
- 29 June 2018 - Notification of Acceptance
- 27 July 2018 - Registration Fee (300 EUR) Payment Deadline
- 10 August 2018 - IAS Travel Grants Announced
- 21 October 2018 - Arrival in Zapala

Note: Students must make their own travel arrangements to Neuquén Airport and apply for visas, if required

## Travel grants for IAS Student Members

- 7th International Maar Conference (Olot, Spain; 21-25 May 2018)
  Application deadline: 15 March 2018
- 4th Meeting of the Working Group on Sediment Generation (Dublin, Ireland; 27-29 June 2018)
  Application deadline: 1 May 2018
- Cyclostratigraphy Intercomparison Project Workshop (Brussels, Belgium; 30 July - 1 August 2018)
  Application deadline: 1 June 2018
- 20th International Sedimentological Congress (Quebec, Canada; 13-17 August 2018)
  Application deadline: 1 May 2018
- VII Argentinean Meeting on Quaternary and Geomorphology (Puerto Madryn, Argentina; 8-21 September 2018)
  Application deadline: 1 July 2018

All travel grants are also listed on the website in the members-only Events Timeline. The listings include the option for downloading the deadline in your calendar.

IMPORTANT: The application rules and eligibility criteria for IAS Student Travel Grants have been updated:

- Applicants must be active IAS Student Members;

- Applicants can apply for a travel grant twice per calendar year: once for an IAS meeting (IMS or ISC) and once for any other IAS-sponsored meeting;
- Applicants must have an active and approved (oral or poster) presentation at the meeting.

### *Meetings with IAS support*

- 2018 Flügel Courses (Erlangen, Germany; 5-16 March 2018)
- 2018 Western Pacific Sedimentology Meeting (GwangJu, South Korea; 19-20 March 2018)
- EGU 2018 General Assembly (Vienna, Austria; 8-13 April 2018
- 7th International Maar Conference (Olot, Spain; 21-25 May 2018)
- International Conference Resources for Future Generations 2018 (Vancouver, Canada; 16-21 June 2018)
- 4th Meeting of the Working Group on Sediment Generation (Dublin, Ireland; 27-29 June 2018)
- Cyclostratigraphy Intercomparison Project Workshop (Brussels, Belgium; 30 July - 1 August 2018)
- 20th International Sedimentological Congress (Quebec, Canada; 13-17 August 2018)
- VII Argentinean Meeting on Quaternary and Geomorphology (Puerto Madryn, Argentina; 8-21 September 2018)

All meetings with IAS support are also listed on the website in the members-only Events Timeline. The listings include the option for downloading the event period in your calendar.

I would like to remind all IAS members that:

- the IAS Newsletter 271 is published on-line and is available at: http://www.sedimentologists.org/publications/newsletter

The Electronic Newsletter (ENIAS), started in November 2011, continues to bring monthly information to members. For information on ENIAS contact ias-office@ugent.be

Check the new Announcements and Calendar. Meetings and events shown in CAPITAL LETTERS and/or with * are fully or partially sponsored by IAS. For all of these meetings, IAS Student Member travel grants are available. Students can apply through the IAS web site. To receive the travel grant, potential candidates must present the abstract of the sedimentological research they will present at the conference. More info @ www.sedimentologists.org

*Vincenzo Pascucci*
*(IAS General Secretary)*

# IAS POST GRADUATE GRANT SCHEME REPORT

Postgraduate Student Grant –2nd Session 2015

# Fluvial Processes and Evolution of Quaternary Landscape in the Ajay River Basin of West Bengal, Sujay Bandyopadhyay

## Department of Geography The University of Burdwan Golapbag,

## Burdwan-713104 West Bengal, India

*Sujay Bandyopadhyay*
*Department of Geography The University of Burdwan Golapbag, Burdwan-713104 West Bengal, India*
*Ph.D. Student Department of Geography The University of Burdwan Golapbag, Burdwan-713104 West Bengal, India*

### 1. Introduction

Fluvial archives and depositional styles are vitally important in Quaternary palaeoclimatic and palaeoprocess research. These are appropriate to link river behaviour with long term climate and more specifically, to search for possible causal relationship between climate and landscape development. Since the fluvial record is highly discontinuous, consisting mostly of sediments deposited during short, high-energy events, the study of long-term landscape evolution has serious implications for understanding the dynamicity of fluvial processes and interplay between autocyclic (intrinsic) and allocyclic (extrinsic) variables. On this background, the current research work is aimed at providing an integrated sedimentological, stratigraphic and luminescence (OSL) chronological study on fluvial sequences of Ajay River and the adjacent region from western Bengal Basin, eastern India which has allowed a better understanding about the late Quaternary palaeo-depositional and palaeo-environmental conditions. The study area known by the name of Rarh plains, form a part of lower Ganga plain and deltaic plains (LGP) (Bagchi and Mukherjee 1979; Chaudhuri 1985; Biswas 1987; Bandyopadhyay et al. 2015) lie between the Chottanagpur plateau on the west and the Ganges-Brahmaputra delta (GBD) on the east that comprise lateritic uplands and alluvial plain along with recent deposits (Fig. 1B). It falls in the western marginal fault-scarp and shelf zone (morpho-tectonic zones of western part of Bengal basin) (Fig. 2) locating more than ~200 km upstream of the modern day tidal limit (Fig. 1A). On the basis of geophysical data, Sengupta (1966) suggested that the Pre-

Cambrian formations continue beneath the Quaternary sediments of LGP as buried ridges before finally disappearing near its eastern boundary in a series of normal faults into the deeper part of Bengal Basin. The modern climate system of the area is dominated by Indian monsoon system and the rainfall generally decreases as one proceeds from the south-east to north-west except for pockets of high or low rainfall (Fig. 1C). During the summer months of May and June, land temperature reaches 40 C, driving monsoonal circulation and drawing oceanic moisture (Sarkar et al. 2014). A major portion of the discharge of the river systems in this area is contributed by run-off from the southwest Indian Monsoon (SWIM), making the systems sensitive to any major changes in monsoonal precipitation over time.

Mostly contributed by the western tributaries of Bhagirathi-Hooghly river system (a distributary of the Ganges system), the area is long considered as the oldest part of GBD (Bagchi 1944; Basu 1973; Niyogi 1975). However, there has been a great deal of controversy among researchers regarding the western boundary of the GBD beyond the present course of the Bhagirathi-Hooghly which include paradeltas (After Strickland 1940: paradelta refers the deltaic plain that is no longer undergoing deposition and has began to be degraded) formed by the western tributaries (Rudra 2015). These rivers are represented by five major tributaries: the Kopai-Mayurakshi-Babla System, the Ajay, the Damodar, the Dwarakeswar¬Silabati-Rupanarayan System and the Kangsabati-Keleghai-Haldi System which brought down Craton¬derived alluvium and formed coalescing paradeltas on the continental shelf -the Bengal basin -that continued to prograde into the sea till the formation of the wider GBD, much later (Deshmukh et al. 1973; Agarwal and Mitra 1991; Das Gupta and Mukherjee 2006; Rudra 2014; Bandyopadhyay et al. 2014). In the present study, we attempted to document the sedimentary facies and establish the depositional environment of the sedimentary sequences of Ajay, Damodar and Kopai rivers (Fig. 3). The region has a well preserved alluvial record accessible through drilling, trench and river cliff sections. These record form important continental archives for understanding landscape dynamics against the backdrop of Quaternary environmental changes. We proposed Quaternary stratigraphy of the region based on lithologs of bore holes in Ajay valley supplied by State Water Investigation Directorate (SWID), Government of West Bengal, Kolkata (Fig. 4). The four major Quaternary depositional units in order of relative ages (oldest to youngest) are: (a) Unit Q4: The Laterite formation; (b) Unit Q3: Calcrete formation; (c) Unit Q2: Older Flood Plain formation; and (d) Unit Q1: Present-day floodplain formation. While interpreting stratigraphic development, relationships between temporal changes in river hydrology, sediment flux and depositional units are established in this report.

## 2. Methods

### *2.1 Facies and depositional units*

During the field work in the Rarh plains, data were collected with a focus to study the lithosections exposed both, along the present day channel and the away from the main channel to investigate the Quaternary stratigraphic units (aided with chronology) and obtain sediments. Five exposed and trenched stratigraphic sections (Fig. 7) were cleaned and carefully chosen at specified locations (spatially cover major portion of the study area) for the documentation of grain size, colour (using

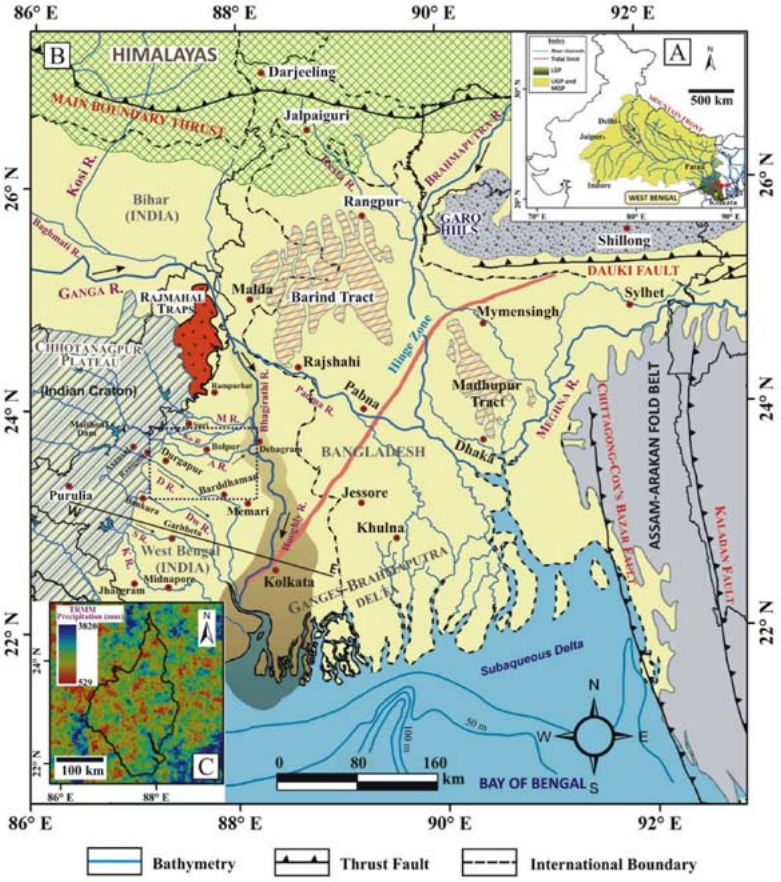


*Figure 1: (A) Location of the Ganga basin in India and division of the plains into Upper (UGP), Middle (MGP) and Lower (LGP) Ganga plains. The thick red line represents the present day tidal limit in LGP (compiled from Singh 1994; Sinha and Sarkar 2009). (B) Regional map of Bengal Basin including lower Ganga plains (Rarh plains) where Ganges, Brahmaputra, and Meghna are the major rivers in Bengal Basin, which formed one of the largest delta systems in the world. The Bhagirathi-Hooghly River acted as main conduit of sediment supply (shown by dark grey shaded region) during initial Ganges-Brahmaputra delta (GBD) growth in Holocene subsequent to which progradation proceeded from west to east (Sarkar et al. 2009). Transect line (W-E) shown on this map corresponding to regional cross-section representing the structural units as shown in Fig. 2. Position of Hinge Zone from Shamsudduha and Uddin (2007). The study area is approximated by the dotted line boxed area showing position of Fig. 3. Key for main riversof Rarh plains: M R.=Mayurakshi River; Ko R.= Kopai River; A R.=Ajay River; D R. = Damodar River; Dw R.=Dwarakeswar River; S R.= Silabati River; K R.= Kangsabati River. (C) TRMM-derived precipitation pattern for the LGP (http://www.geog.ucsb.edu/wbodo/TRMM/).*

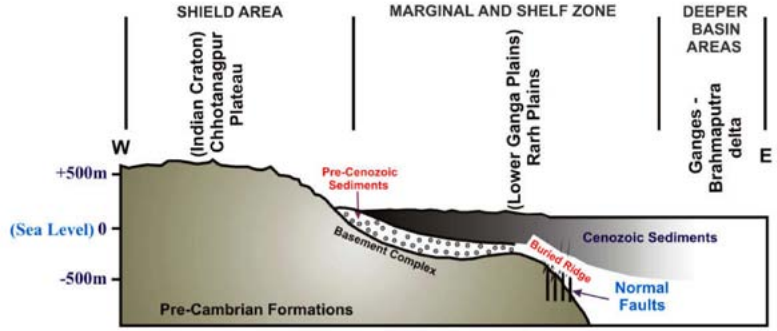


*Figure 2: Schematic cross-section of the western fringe of Bengal basin showing various structural components and subsurface conditions (modified after Sengupta 1966).*

Munsell soil color charts with genuine Munsell color chips, Year 2009, Revised 2015, Production: Munsell Color x-rite), matrix percentage, physical structures, lateral geometry and bounding contacts of the individual unit which recorded on centimeter scale. Thickness of the alluvial fill was measured using tapes and rods. The lateral extensions were also examined in the field and recorded in the form of descriptive sketches and log supported by photographs. The valley-fill deposits were studied through three drilled boreholes collected along the Ajay valley by sludging method. The detail sludging methodology is described in UNICEF (2009). The boreholes locations were selected where past fluvial features (paleochannels) were observed. Locations of boreholes were determined by a Garmin GPS (Model: OREGON®550) accurate to less than ~3 m. Some representative samples were

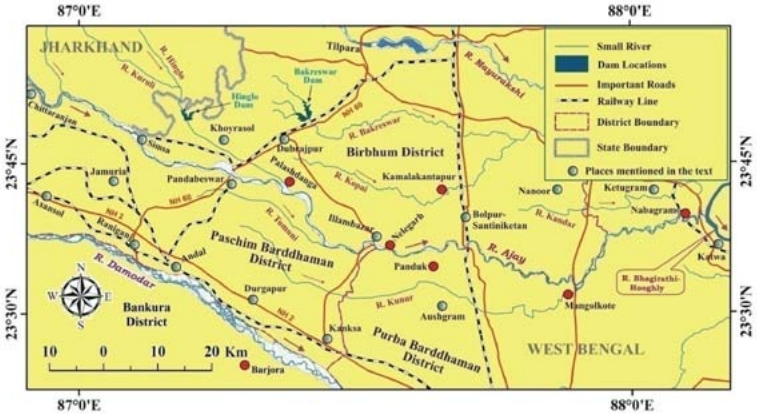


*Figure 3: Map showing the study area and the Ajay River Systems through West Bengal. Major cultural features like lines of communication and administrative boundaries are incorporated in it. Red circles are locations of cliff sections (trench and river bank sections) and bore holes where sediment samples are collected for Quaternary studies.*

selected for particle-size analysis from the borehole section (Borehole-II). The samples were then treated with dilute Hydrochloric acid (HCl) and hydrogen peroxide (H2O2), followed by washing with distilled water to remove carbonate and organic matter. After washing and cleaning, the samples were subjected to grain-size analysis by means of a Malvern Mastersizer 2000 Laser Particle Size Analyzer (LPSA) in the Sedimentology Laboratory of the Wadia Institute of Himalayan Geology (WIHG), India. Optically Stimulated Luminescence (OSL) samples were collected which are also been processed and analyzed in Luminescence laboratory of WIHG under the mentorship of Dr. Pradeep Srivastava. The sampling and mapping of lithofacies was completed in three field works during January 2016,

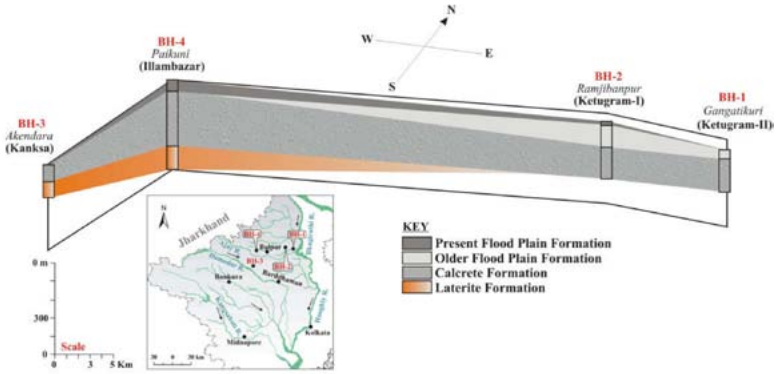


*Figure 4: Lithological column of bore-holes in Rarh plains showing broad correlation of Quaternary stratigraphy (Lithologs of bore holes supplied by State Water Investigation Directorate, Government of West Bengal, Kolkata). Borehole locations shown in inset map.*

February 2016 and October 2016.

### *2.2 Optically Stimulated Luminescence (OSL) dating*

The chronology was established based on optically stimulated luminescence (OSL) dating. The OSL dating technique is based on the assumption that during denudation the sediment exposed to sunlight and leads to zeroing the stored luminescence. The burial accelerates reaccumulation of luminescence signals because of irradiation from natural radionuclides. Total nine samples for OSL dating were taken from a freshly cleaned surface; four from Barjora (Damodar River) (Fig. 10a), three from Nelegarh (Ajay River), one from Kamalakantapur (Kopai River) and one from trench at Mongalkote (Ajay River) using opaque iron pipes (~15 cm long and 2.5 cm diameter). To avoid daylight exposure, standard precautions are taken which was accompanied by the details study of these sections. The rest three samples were retrieved during night time from the boreholes (Borehole-I) at Panduk (Ajay River). This time we paid special attention to avoid exposure to light during the drilling and subsequent procedures. The drilling was performed at night (new moon phase). The sections and boreholes locations are mentioned in Fig. 3. In the laboratory, the pipes

were opened under subdued red light conditions and the 2 centimeter sediments from both ends of the pipes scraped out to avoid potential contamination due to bleaching which would have been used for dose rate measurements later. The sediments were pre-chemically treated with 1N HCl to digest carbonates, followed by H2O2 (30%) treatment to remove organic materials and washed with water (Srivastava et al. 2006). The treated samples were sieved to obtain 90 and 180  m grain size fraction. Quartz and feldspar grains were separated by density separation method using heavy liquid of Sodium Polytungstate (2.62 gm/cc). The separated quartz grains etched using 40% hydrofluoric acid (HF) for 80 min, followed by 20 min of 35% HCl treatment to remove an alpha irradiated outer layer of approximately 10 µm and fluorides formed during the HF treatment and also to eliminate any feldspar contamination present if any. Infrared-Stimulated Luminescence (IRSL) measurement was performed on every sample to check the feldspar contamination. All samples except LD-1642 showed low IRSL counts (100-150 counts) and thus no or little feldspar contamination was found (Fig. 5). The samples LD-1642 and LD-1643 were treated with an additional etching (to remove feldspar contamination). Amonolayer of quartz grains were then mounted on stainless steel discs of 10 mm diameter using Silko-Spray silicone oil. Luminescence measurements were carried out on a Riso TL/OSL-20 system via blue LEDs as a source for stimulation to the quartz grains. The photon detection optical filters comprise Schott BG-39 and Hoya U¬340 were used in front of an EMI 9235 QA photomultiplier tube. 90Sr/90Y sealed source was used for beta irradiations (radiation dose 5.5 Gy/min). The OSL and IRSL measurements were recorded for 40s at 125°C and 100 s at 60°C respectively.

In this study, 5-point single aliquot regenerative (SAR) protocol, suggested by Murray and Wintle (2000), was used to determine the paleodose (De). An additional step of IRSL cleaning (for 100s at 60°C) was introduced before every OSL measurement to reduce luminescence signals coming from feldspar (Jain and Singhvi 2001). A preheat of 220°C/10s for removing unstable traps and a cut heat of 160°C for test doses were used. Total 30-35 aliquots were used for measurement, out of which aliquots yielding (i) recycling ratio within 10%, (ii) paleodose error was less than 10% and (iii) recuperation was below 5% were considered and the mean of around 9-24 aliquots were taken for the estimation of De and final age calculations. The radial plots were prepared to illustrate the precision on the dose estimates (Galbraith et al. 1999) (Fig. 6). The dose distribution of De's showed well constricted data around the average values (over dispersion was found less than 20% and hence minimum age model was not applied even though the three ages are young as a few hundreds of years old) and thus the mean age model (MAM) was applied for age calculations. The U, Th and K measurements to estimate dose rate were done using X-ray Fluorescence (XRF) or Inductively Coupled Plasma Mass Spectrometer (ICP-MS). The cosmic ray contribution was obtained using the relationship between sample burial depth and site altitude, latitude and longitude suggested by Prescott and Stephan (1982). A value of 10 ± 3% by weight was used as the best estimate of the water content during the period of burial for all samples due to the presence of fine-grained sediments in an alluvial monsoon-dominated setting. Details of the various parameters including radioactive concentration of U, Th and K in the sediments, dose rate, paleodoses and ages calculated are presented in Table 1. In this report, seven samples from different stratigraphic units were dated and the additional analysis of rest of the samples is under progress.

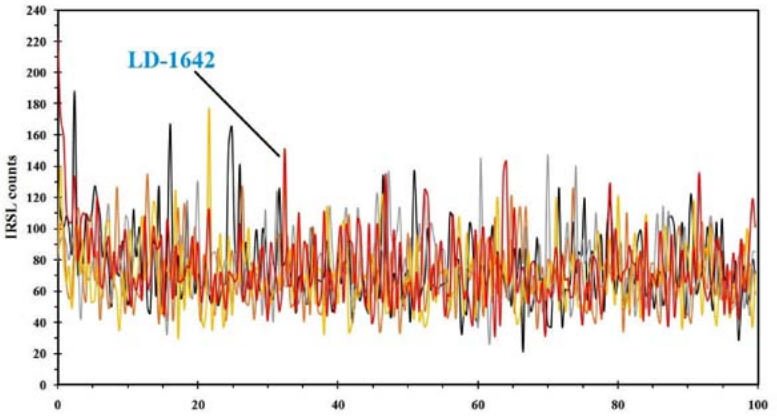


*Figure 5: The IRSL counts of samples LD-1638 to LD-1642. Note that sample (LD-1642; from Nelegarh) is showing the highest feldspar counts (222) among all samples.*

## 3. Results

The stratigraphic profiles from the study area represent a complex history of erosion, sedimentation, and landscape stability followed by soil formation. Field observations indicate the presence of four startigraphic units chronologically constrained using OSL ages. The five exposed sections are studied composing of clay, silt and sand sheets with centimeter to metre-scale thickness (Fig. 7). Two depositional facies groups were identified, namely floodplain (FF) with five component facies and channel (Ch) with seven facies. Three stratigraphic units; i.e. Unit Q4, Unit Q3 and Unit Q1 were identified on the photo and field logs (Fig. 7 and 10). Unit Q4 is the Quaternary oldest unit in this region exhibits induced ferricrete facies and trough cross-stratified pebble-gravel (Ch7) with varying stratigraphic and bedrock settings. It is resting on Precambrian boulder conglomerate of quartzite, amphibolites, schist, and granite in the western side; Gondwana formation and Tertiary (pre-Mio-Pliocene) rocks in the eastern side. This unit is characterized by reworked, remobilized and redeposited nodular ferricretes and cemented by the ferruginous sandy silt or clay. It also comprises lateritic hard-pan with reddish brown latosol cover followed downward by a lithomargic part consisting of brownish white sandy clay with few iron nodules. The gravelly sediments (Fig 10c) in this unit are crossed cut by small channel fills formed due to later surges. It is identified in the litho-section-I (base not exposed), having a thickness of 2.2 m. The abundance of trough crossbed and planar crossbed with gravel (Gt) point to a well-established high energy flow with low rate of sedimentation and this is probably due to the intensified SW monsoon. The formation has been named as Lalgarh formation (Fig. 10b) which has been described in the adjacent Kasai basin (Ghosh and Majumder 1981) and occurs in physical continuity of the same area (Fig. 10d). Unit Q3 (Calcrete formation) is composed of calcretized mud (FF5), grey (2.5Y6/1 to 5Y4/1) sticky slity clay (FF1) and clayey silt (FF4), underlain by Unit Q4. It consists mainly of scattered to concentrated calcareous concretions

(kankars) of various sizes (size 0.5 -200 mm). Sometimes micaceous and iron nodule is not uncommon. Besides, silty sand (Ch1) is also present in the 5.8 m thick litho-section-V. The maximum thickness is 11.5 m (litho-section-I), and it has a vast aerial extent. This formation represents a distal floodplain environment as inferred from muddy deposits that are moderately pedogenised. The presence of a considerable proportion of calcretes, some of which forms more concentrated layers, suggests periods of minimal deposition or discontinuities. This unit generally fines up but slightly coarser sediments at the top suggest that the area was closer to a fluvial conduit, or experienced a high-energy flood peak. A composition of silty clay, clayey silt and sandy silt, together with poorly developed palaeosols and the fill of a shallow channel, suggests deposition as a natural levee.

| Sl. No. | Lab. No. | Type | Depth (m) | U (ppm) | Th (ppm) | K (%) | Cosmic dose rate (μGy/a) | Palaeodose (Gy) | Dose rate (Gy/a) | Age (ka) |
|---|---|---|---|---|---|---|---|---|---|---|
| **Barjora (N 23°26'45"/ E 87°17'55"E)** | | | | | | | | | | |
| 1 | LD-1643 | ES | 5 | 1.03±0.1 | 7.9 ± 0.79 | 2.556±0.25 | 140.5 ± 42 | 141.3 ± 20.15 | 2.94 ± 0.25 | 48.09 ± 7.97 |
| **Panduk (N 23°35'07.2"/ E 87°38'35.3")** | | | | | | | | | | |
| 2 | LD-1588 | BH | 11.6 | 1.15± 0.1 | 2.1± 0.21 | 2.199± 0.22 | 121.1 ± 36 | 2.92 ± 0.22 | 2.33 ± 0.21 | 1.26 ± 0.14 |
| 3 | LD-1638 | BH | 13.0 | 1.0 ± 0.1 | 6.2 ± 0.62 | 2.008 ± 0.2 | 118.3 ± 35 | 4.68 ± 0.78 | 2.38 ± 0.19 | 1.97 ± 0.36 |
| 4 | LD-1639 | BH | 16.0 | 1.0 ± 0.1 | 5.7 ± 0.57 | 2.083 ± 0.2 | 113.8 ± 34 | 5.72 ± 0.91 | 2.40 ± 0.20 | 2.38 ± 0.43 |
| **Nelegarh (N 23°36'35"/E 87°32'58")** | | | | | | | | | | |
| 5 | LD-1640 | ES | 4.9 | 1.5±0.15 | 11.7±1.17 | 2.432±0.24 | 146.0 ± 44 | 2.47 ± 0.52 | 3.26 ± 0.25 | 0.76 ± 0.17 |
| 6 | LD-1641 | ES | 1.1 | 1.0 ± 0.1 | 6.0 ± 0.6 | 2.29 ± 1.17 | 182.0 ± 54 | 0.57 ± 0.08 | 2.71 ± 0.22 | 0.21 ± 0.03 |
| 7 | LD-1642 | ES | 2.8 | 1.0 ± 0.1 | 7.4 ± 0.74 | 2.241±0.22 | 163.2 ± 49 | 0.78 ± 0.13 | 2.75 ± 0.22 | 0.28 ± 0.05 |

*Table 1. OSL chronology of the sediments collected from the cliff section and drill boreholes of the Ajay valley and the adjacent region.*

Notes: 1. ES: Exposed Section
2. BH: Borehole

Quartz fractions of 90-180 μm from this unit yielded OSL dates of 48±7 ka (litho-section-I) indicates high-energy channel activity (medium to coarse sands) and the relative depth suggests that incision occurred prior to alluviation. After that, floodplain development during this period was interrupted by multiple pedogenic events (calcrete formation), possibly indicating slow sedimentation or short-term discontinuities, and more intense pedogenesis is apparent in the topmost beds. Levee deposits of Unit Q3 before 48 ka imply the formation from small channel body. The sedimentary sequence of Unit Q1 is represented in this area by the present day flood plain deposits of the rivers (Fig. 10f). The vertical litho-sections in the Ajay River exhibits trough cross-laminated medium to coarse sand (Ch6a), overlain and underlain by a sequence of planar cross-laminated (Ch6b) and parallel laminated sands with intervening thin mud bands with mottled pigmentation of iron oxides. The sediments of Ch6b overlie the sediments of Ch6a separated by a sharp and erosional contact (Fig. 2). It seems that after deposition of coarse sand, the surface was eroded to by a large surge produce an undulatory surface. The

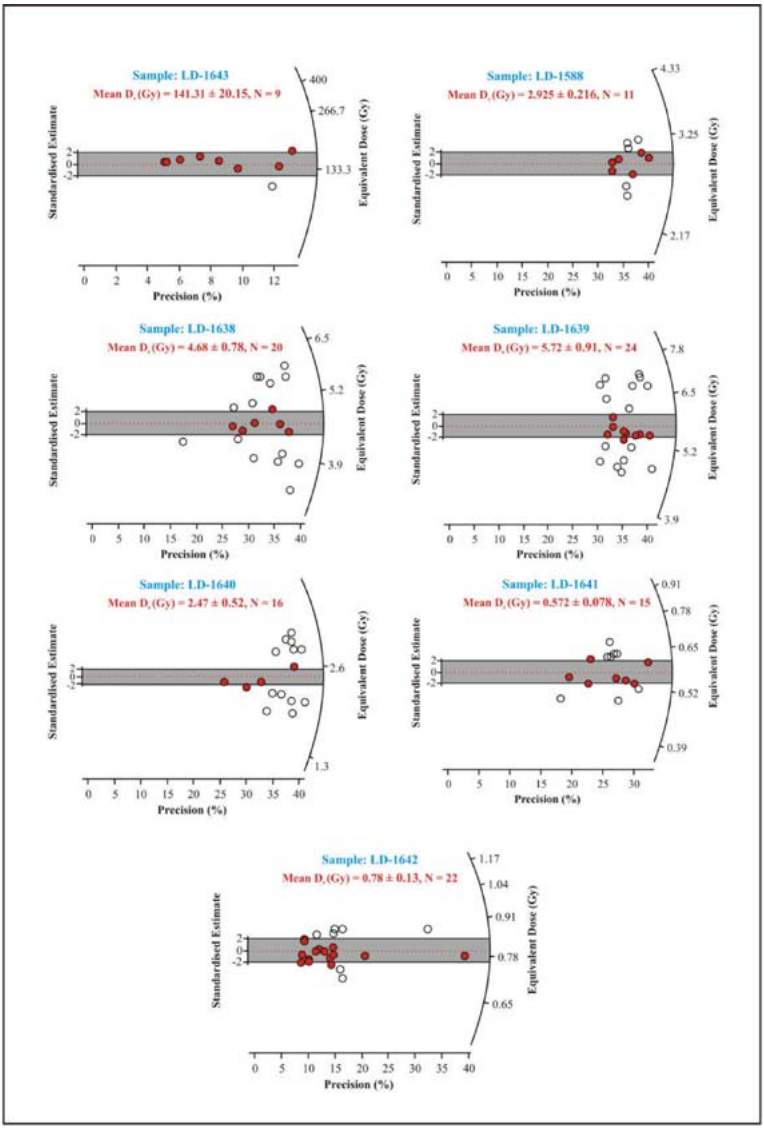


*Figure 6: Radial plots for age calculations showing the dose distribution.*

sediments are yellowish brown in colour and poorly sorted. In the channel bar deposits of litho-section-II, deformation structures (convolution) are found, where sands are quarrying. The OSL ages of sediments from this units at Nelegarh (litho-

section-III) dated to 700±200 years to 200±30 years indicating that the last 1000 years experienced by recurrent flooding events. The deposition began shortly after CE 1250 (700 years BP) and continued until about CE 1750 (200 years BP). This finding is consistent with qualitative historical data showing intense ploughing in the area from the end of the Middle Age to the 18th century. In between 700 years BP and 300 years BP, the high sedimentation rate was triggered by the reduced fluvial activity. The Older Flood Plain unit (Unit Q2) identified in the boreholes (Fig. 8) consists of Channel facies (Ch) and Floodplain facies (FF). This unit comprises mainly of loose, brownish grey silty clay without any calcareous concretions. The topmost part of the succession is made up of 5 to 7 m thick muddy sediments revealed occurrences of craton derived sediments. The channel facies are present, namely silty sand (Ch1), fine sand (Ch3), medium sand (Ch4) and coarse sand (Ch5), are composed of discrete fine to coarse grained sand bodies up to 4 m thick, and are interpreted to represent former channel deposits. The fine-grained facies have been termed as floodplain facies (FF) and subdivided into grey silty clay (FF1), pale yellow silty clay (FF2), brown silty clay (FF3) and clayey silt (FF4) here based on grain size and colour. Grain-size variations within the vertical litho-architectural arrangement of the floodplain deposits formed the basis for lithofacies description and interpretation of depositional conditions. The grain-size distributions of 20 representative samples from borehole-II were used to calculate textural parameters such as mean size, standard deviation, skewness and kurtosis (Fig. 9). Mean size values range from 8.2 -9 (phi) in the top 4 m section and the sorting being 1.0 -1.8 (phi). So, the samples are mostly poorly sorted and some very poorly sorted. Skewness ranges from 0.35 to (-) 0.05 and the little temporal variation suggest that the same conditions prevailed during repeated monsoonal floods and that these may in fact have been cyclical. Among the channel facies, the finer grained facies Ch3 generally occurs as relatively thin bodies in the borehole-II that are inferred to represent small tributary or floodplain channels. In contrast, up to 4 m thick fine sand found in borehole-III. The medium to coarser channel sands (Ch4 and Ch5) have found in borehole-I, separated by <2 m of silty clay that are interpreted as the deposits of major trunk rivers. The silty sand facies (Ch1) generally occurs within muddy successions and contains mottles, defined by a change from clayey silt to clay with high moisture content. Floodplain facies are found abundantly in borehole-II; consist mainly of silty clay with pedogenic features that include dark brown, yellow brown and grey mottles where the thickness varies upto 9 m, attributed to floodplain marsh deposits. In borehole-I, bottom medium sand layer yielded an OSL date of 2.4 ± 0.4 ka. Another two samples from the same borehole gave dates of 1.9 ± 0.4 ka and 1.2 ± 0.1 ka for this unit. One major migration phases has been detected between 2.4 ka to 1.9 ka. Based on three OSL dates; initially the sediment filling was high, i.e. 7.1 m/103 yr during 2.6 to 2.1 ka while the sedimentation rate after 2 ka is 1.8 m/103 yr., reflected the pronounced decline in monsoon intensity and transport capacity.

## 4. Discussion

The Rarh region exposures and subsurface deposits are illustrated schematically in Fig. 7 and 8, along with OSL chronology. In interpreting our records, we have drawn strongly on the range of dates provided by the seven finite OSL dates to establish the late Quaternary paleoenvironment and the evolution of the

depositional units. Although more dates are necessary to provide a comprehensive understanding, the dates were obtained from precisely documented strata, commonly to test the age of key boundaries, and they suggest several distinct periods of fluvial activity. The OSL chronology indicates that the pedogenesis under ponding condition began prior to 48 ka. At the study section, the lack of exposure of the basal portions of the gravel bed means that the age of the onset of the Unit Q4 is unknown. The Ch7 facies is overlain by large volume of sandy alluvium is suggestive of a high competency stream and aggradational fluvial activities probably during the high-stand of MIS-5. The formation of lateritised pebble to gritty sand layer at the base of the laterite profile at the lithosection-I and Illambazar section area indicates the age before MIS-5. Renewed fluvial activity is recorded in the litho-section-I of Damodar River in MIS 3 period (48 ka). The Damodar River deeply incised, effectively terminating this long phase of overbank sedimentation. Incision and the overbank sedimentation were followed by a phase of channel aggradation involving the deposition of sand fills, before a second phase of overbank succession. The monsoon intensification produced a braided channel pattern, represented by relatively coarser grain size during 48 ka. The stream power continues increased due to high rainfall as inferred from the occurrence of poor imbricated gravel. No such major channel deposits are recorded after 48 ka, suggesting that this interval, which includes the global Last Glacial Maximum (LGM), experienced reduced fluvial activity. Relatively strong pedogenesis is observed below much younger deposits in the topmost muddy parts of Unit 3 in Section-I, and an interval of soil formation may accord with reduced activity, although these strata are constrained by dates. The similar kind of succession also observed in the litho-section-IV (Kopai River) (Fig. 10e) and litho-section-V (Mongolkote, Ajay River) above the channel fill deposits. It has been postulated that these result in a relatively stable landscape and pedogenesis, and that in turn has prompted the formation of a pedocal soil and caliche nodules in the strata (<29 ka) of terraced alluvial geomorphic unit (Unit Q3) in LGP. Simultaneous occurrence of channel fill deposits and overbank mud deposits in the Unit Q2, observed in the boreholes indicates the lateral migration of rivers in this alluvial setting. It also connotes the environmental change likely from overbank sedimentation distal to the channel. Late Holocene channel bodies aggraded across much of the present valley area, and sediments accumulated within a short period of 2.7 to 1 ka. Based on three OSL dates; initially the sediment filling was high during 2.6 to 2.1 ka, but later stage accreted at a fairly steady rate. The lowermost floodplain deposits (Unit Q1) of the study area are bracketed between 700 and 200 years BP and sediments accumulated within a short period of time, based on three OSL dates. This unit (Fig. 10f) was observed in the Ajay valley (litho-section-II and III) is characterised by deposition of sand and silt (slack water deposit) with upward fining sequences and convolution structure indicating the flooding phenomena during the last 1000 years BP. The occurrence of pedogenic Fe-Mn nodules is implying

incursion of low flow regime and dominance of overbank deposition under warm and humid climate. During the period of 700 yr BP to 300 yr BP, this episode of low fluvial activity may be occurred due to Little Ice Age (LIA).

## 5. Conclusion

The exposed cliff section and valley cores from the Ajay valley and the adjacent

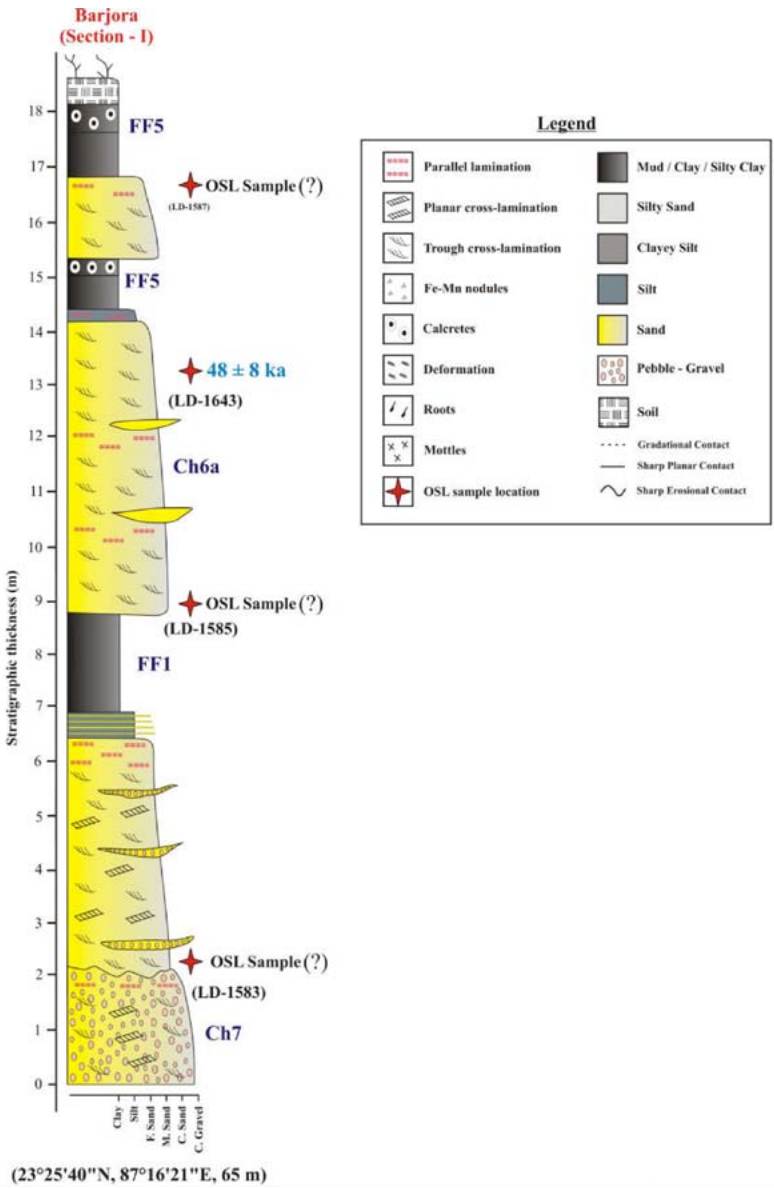


*Figure 7: Cliff section logs showing stratigraphic units. The available OSL data are shown (see Table 1 for details). Based on the facies associations, the cliff section have been subdivided into three major depositional units. For discussion see the text.*

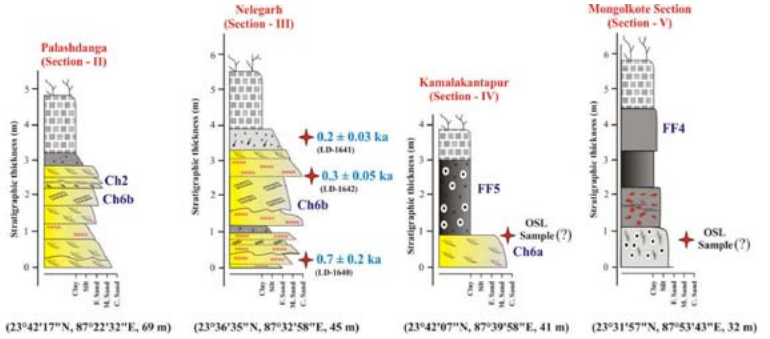


*Fig. 7 (continued).*

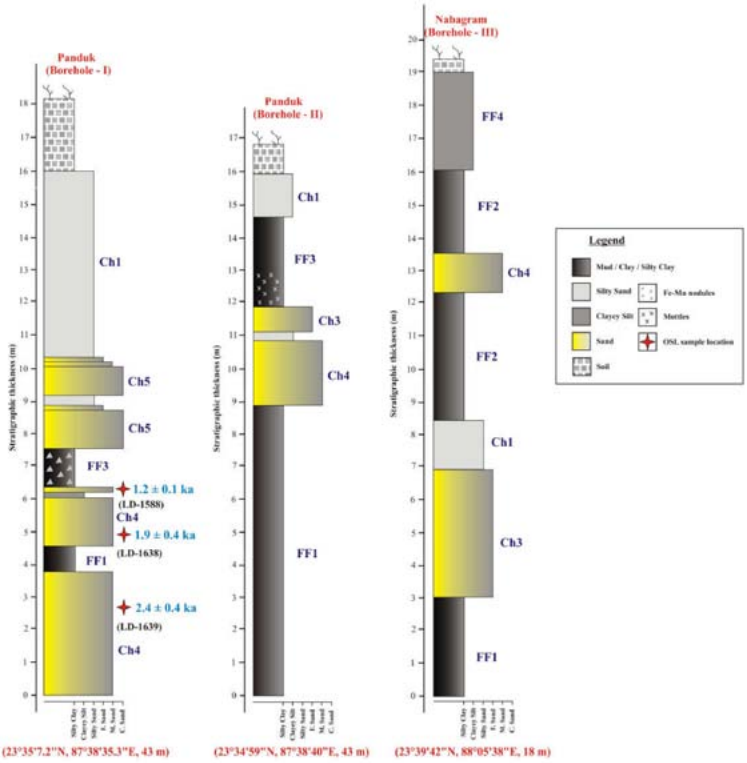


*Figure 8: Borehole facies logs in the Ajay Basin showing stratigraphic units. The available OSL data are shown (see Table 1 for details).*

region (Rarh) provide an integrated picture of the depositional environment over the last ~48 ka and beyond. The Quaternary depositional units suggest that the strength of the SWIM has varied significantly on a timescale of centuries to millennia. The trends in sedimentation, pedogenesis, and erosion in the study area preserve an archive of valuable information about complex climate-stream basin history. The valley boreholes record episodes of floodplain development and lateral migration of trunk river during MIS-1, especially around the Roman Warm period; and in the latest Holocene (after 1.2 ka). During LGM time, reduced fluvial activity observed, and no channel sediments have yet been identified that correspond with this period. There was modest accumulation of Unit Q3, punctuated by discontinuities, through to early MIS 2. The rivers probably varied in its degree of attachment to the floodplain, periodically inundating the adjoining, more elevated alluvial tract but at other times unable to flood this zone. There is the indication that the rivers has inundated during MIS-3. We infer that the rivers of the area experienced strong variation in its equilibrium profile over relatively short periods (centuries to thousands of years), linked to varied sediment and water discharge from the Chottanagpur and the lowland alluvial plain. Finally, the use of stratigraphy, sedimentology and OSL chronology in the Ajay basin and the adjacent region results in the following conclusions: (a) the preserved sequence

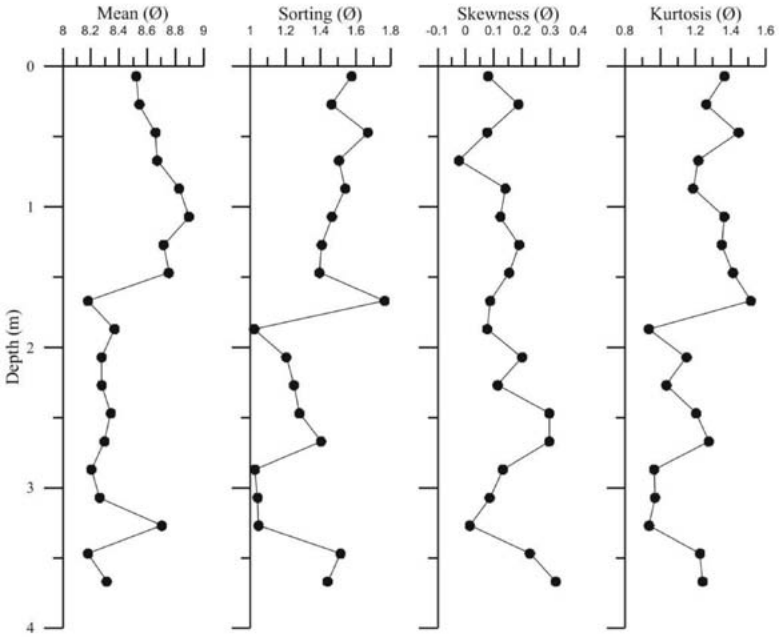


*Figure 9: Grain size characterization (Graphic mean, standard deviation, skewness and kurtosis) of the samples of Unit Q2 formation along Panduk borehole section (Borehole-II) in Ajay Basin (20 samples). All parameters are calculated following formulations of Folk and Ward (1957).*


*Figure 10: Field photographs showing units and facies in the cliff section of the study area. (a) Sampling location in litho-section-I in the Damodar valley. (b) Laterite formation as observed around Lalgarh in Kasai Basin. (c) Gravelly sediments observed in the litho-section-I near Barjora (base not exposed). (d) Ferricrete profile exposed around Illambazar, Ajay basin. (e) Calcrete exposure at Kopai River showing pedogenesis. (f) Recent flood deposits along the Ajay River representing depositional unit Q1 at Nelegarh.*

of laterite deposits (Unit Q4) within the study area are evidence of an evolving early Pleistocene sedimentary record but unknown environmental records, adding to the research potential; (b) aggradation and geomorphic stability (Unit Q3) and subsequent pedogenesis in the Late Pleistocene are likely responses to climate change and intrinsic mechanisms, as regional basins responded independently during this time; (c) the regional depositional record for Rarh region is sparse during early Holocene; (d) The Unit Q2 was initiated by a regionally identified warming trend within the Holocene, with major subsequent incision associated with a warm, dry climate; (e) deposition at Unit Q1 affected by intrinsic factors, with climate acting as a driving mechanism based on the integration of regional fluvial systems.

## 6. Budget justification

The present research benefited immensely from  1000 from the International Association of Sedimentologists (IAS) Postgraduate Grant Scheme, which partially funded the fieldwork activities in lower Gangetic plain (LGP) and laboratory activities at Wadia Institute of Himalayan Geology (WIHG), Dehradun and therefore, a significant portion of my Ph.D. study. The grant was also used for travel from Burdwan to Dehradun and return with samples. The data collected during the IAS supported field work synthesized in this report. The finding were partly presented in 6th International Association of Sedimentologists (IAS) International Summer School on “Sediments: from Land to Sea -Archives of global change -Mesozoic and Cenozoic” which held in Alghero (Sardinia, Italy) from 25th September -2nd October 2016 and 9th International Conference on Geomorphology: “Geomorphology and Society” which held in New Delhi (India) from 6 -11 November 2017.

## Acknowledgements

This study is part of my Ph.D. research at the University of Burdwan, India. SB gratefully acknowledges Prof. Anil K Gupta (Ex.-Director, WIHG) for providing facilities to carry out this work in a collaborative way. He also thanks Dr. Swapan Kr. Pan (Principal, Gushkara Mahavidyalaya) for the support extended in carrying out Ph.D. work. The West Bengal Mineral Development and Trading Corporation Limited (WBMDTC) is thankfully acknowledged for permitting us to conduct field survey in the Trans Damodar Open Cast Project. Thanks are accorded to Director, State Water Investigation Directorate (SWID), Government of West Bengal, Kolkata for providing available lithologs of boreholes of the Ajay Basin. Debika Chowdhury, Sourav Mukhopadhyay, Prasanta Ghosh, Samiran Dutta, Asraful Alam, Soumen Chatterjee, Surajit Kundu, Md. Intazar Alam Khan, Jhuman Ghosh, Dulali Kuiry and Monali Banerjee provided field assistance and discussed many aspects of the present study. The help received from Dr. Debasis Ghosh (Assistant Professor, University of Calcutta) for vibratory sieve shaker equipment and Dr. Anil Kumar (Scientist-C, WIHG) for the OSL dating work is invaluable.

## References

Agarwal R.P. and Mitra, D.S. (1991): Paleogeographic reconstruction of Bengal delta during quaternary period. In: Vaidyanadhan, R. (ed.), Quaternary deltas of India. Mem Geol Soc India, 22, pp. 13-24.

Bagchi, K. (1944): The Ganges Delta, Calcutta University, Calcutta, p. 120.

Bagchi, K. and Mukherjee, K.N. (1979): Diagnostic Survey of Rarh Bengal, Part-1 (Morphology, Drai-

nage and Flood: 1978), Dept. of Geog., University of Calcutta, Cal., p. 9.

Bandyopadhyay, S., Das, S. and Kar, N.S. (2015): Discussion: Changing river courses in the western part of the Ganga-Brahmaputra delta by Kalyan Rudra (2014), Geomorphology, 227, 87-100. Geomorphology, 250: 442-453.

Bandyopadhyay, S., Kar, N.S., Das, S. and Sen, J. (2014): River Systems and Water Resources of West Bengal: A Review. In: Vaidyanadhan, R. (ed.), Rejuvenation of Surface Water Resources of India: Potential, Problems and Prospects. Geol Soc India, Special Publication 3, pp. 63-84.

Basu, S.R. (1973): The decay and the associated problems of river dynamics of the Bhagirathi valley. (Unpublished Ph.D Thesis, University of Calcutta). Available in the Central Library of the University of Calcutta. (Accession No. 3202).

Biswas, A. (1987): Laterites and Lateritoids of Bengal. In: Datye, V.S., Diddee, J., Jog, S. R., Patil, C., (eds.), Exploration in the Tropics. Pune: Prof. K. R. Dikshit Felicitation Committee, pp. 157-167.

Chaudhuri, S.K. (1985): Characteristics of Soils and Evaluation of Land in the Southern Rarh plain, West Bengal. (Unpublished Ph.D. Thesis, University of Edinburg). Available in the Edinburgh Research Archive.

Das Gupta, A.B. and Mukherjee, B. (2006): Geology of NW Bengal Basin, Geological Society of India, Bangalore, pp. 5, 7, 57.

Deshmukh, D.S. and 13 others (1973): Geology and Groundwater Resources of the alluvial areas of West Bengal. Bulletins of the Geological Survey of India, Series B, 34: 23-24.

Folk, R.L. and Ward, W.C. (1957): Brazos river bar: a study in the significance of grain size parameters. Journal of Sedimentary Petrology, 27: 3-26.

Galbraith, R.F., Roberts, R.G., Laslett, G.M., Yoshida, H. and Olley, J.M. (1999): Optical dating of single and multiple grains of quartz from Jinmium rock shelter, Northern Australia: Part I, Experimental Design and Statistical Models. Archaeometry, 41: 339-364.

Ghosh, R.N. and Majumdar, S. (1981): Neogene-Quaternary Sequence of Kasai Basin, West Bengal, India. Proc. Neogene/Quaternary Boundary Field Conf., India, 1979: 63-73.

Jain, M. and Singhvi, A.K. (2001): Limits to depletion of blue-green light stimulated luminescence in feldspars: implications for quartz dating. Radiation Measurements, 33: 883-892.

Murray, A.S. and Wintle, A.G. (2000): Luminescence dating of quartz using an improved single aliquot regenerative-dose protocol. Radiation Measurements, 32: 57-73.

Niyogi, D. (1975): Quaternary Geology of the Coastal Plain in West Bengal and Orissa. Indian Journal of Earth Sciences, 2 (1): 51-61.

Prescott, J.R. and Stephan, L.G. (1982): Contribution of cosmic radiation to environmental dose. PACT, 6: 17-25.

Rudra, K. (2014): Changing river courses in the western part of the Ganga-Brahmaputra delta. Geomorphology, 227: 87-100.

Rudra, K. (2015): Ref: Changing river courses in the western part of the Ganga–Brahmaputra delta by Kalyan Rudra (2014), Geomorphology, 227, 87-100. Geomorphology, 250: 454-458.

Sarkar, A., Filley, T.R. and Bera, S. (2014): Carbon isotopic composition of lignin biomarkers: Evidence of grassland over the Gangetic plain during LGM. Quaternary International, 355: 194-201.

Sarkar, A., Sengupta, S., McArthur, J.M., Ravenscroft, P., Bera, M.K., Bhushan, R., Samanta, A. and Agrawal, S. (2009): Evolution of Ganges-Brahmaputra western delta plain: clues from sedimentology and carbon isotopes. Quaternary Science Reviews, 28, 2564-2581.

Sengupta, S. (1966): Geological and geophysical studies in the western part of the Bengal Basin, India. Am. Assoc. Pet. Geol., Bull., 50 (5): 1001-1017.

Shamsudduha, M. and Uddin, A. (2007): Quaternary shoreline shifting and hydrogeologic influence on the distribution of groundwater arsenic in aquifers of the Bengal Basin. Journal of Asian Earth Sciences, 31: 177-194.

Singh, R.L. (1994): India: A Regional Geography. National Geographical Society of India, Varanasi.

Sinha, R. and Sarkar, S. (2009): Climate-induced variability in the Late Pleistocene-Holocene fluvial and fluvio-deltaic successions in the Ganga plains, India: A synthesis. Geomorphology, 113: 173-188.

Srivastava, P., Brook, G.A., Marais, E., Morthekai, P. and Singhvi, A.K. (2006): Depositional environment and OSL chronology of the Homeb silt deposits, Kuiseb River, Namibia. Quaternary Research, 65: 478-491.

Strickland, C. (1940): Deltaic Formation, with Special Reference to the Hydrographic Processes of the Ganges and the Brahmaputra. Longmans, Green and Co. Ltd., Calcutta, pp. 1-10.

UNICEF (2009): Manual Drilling Techniques. Technical Note Series on Manual Drilling, 4. Available in UNICEF web (https://www.unicef.org/wash/index_54332.html).

# Using backscatter imagery for resolving tsunamigenic basin bottom features in Chilean coastal lakes

*Evelien Boes*
*Renard Centre of Marine Geology, Ghent University*

## INTRODUCTION

Our research focuses on the identification and characterisation of tsunami deposits in coastal lakes all around the world (i.e. Chile, Japan and Thailand). We want to assess whether lakes are better tsunami recorders than subaerial sites, and/or under which circumstances they are better recorders. We address a range of lacustrine case studies in different geomorphologic settings ("multi-lake approach") to gain a conceptual understanding of depositional mechanisms and influencing factors. Our research hypothesis dictates that tsunami inundation leads to the formation of a distinct stratigraphic unit at the bottom of the affected lake basin. Deposits in lakes are supposed to be not as fragmentary as subaerial sites thanks to their higher preservation potential and ability to accumulate sediment in between events.

Many bedforms and sedimentary structures/components have been attributed to tsunami deposits. In addition to sedimentology, we want to further explore geophysical methods for tracing tsunamigenic deposits ("multi-proxy approach"). Side-scan sonar (SSS) imagery has been proven useful to explore lake basin dynamics and the presence, sedimentology, thickness, lateral extent etc. of tsunami deposits (Kempf et al., 2015). With the awarded IAS grant money we conducted SSS surveys on three coastal lakes/lagoons, Vichuquén, Budi and Gemelas I, in south-central Chile.

## USE OF GRANT

IAS Grant money was used to cover costs of accommodation, meals and vessel fuel during the course of the SSS surveys, and airfreight of the SSS system (see Proof of expenses). We focused on the -for us- interesting parts of the lakes, i.e. areas that are most likely to have been affected by tsunami inundation in the past. These focus areas are located close to lake inlets and/or connections to the Pacific Ocean. SSS imagery was acquired using a Klein 3000 system (Fig. 1A) with a simultaneous dual-frequency (100 kHz and 500 kHz) operation and a swath width of 200 m in Vichuquén and Budi, and 150 m in Gemelas I. Swath widths were chosen in function of the available survey time, the area to be covered, and, in case of Gemelas I, battery lifetime of the electrical boat-motor. The SSS fish was towed below the vessel's bow (Fig. 1B). Shallow water (<1 m), dense vegetation and various obstacles (fishermen's nets, buoys etc.) were avoided in order to not damage the equipment. Coverage was achieved by navigating straight lines with overlaps of one swath width. SonarPro software (Klein Associates) was used for

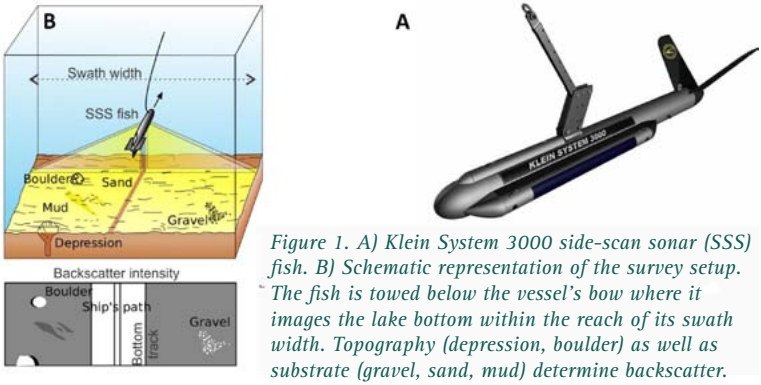


*Figure 1. A) Klein System 3000 side-scan sonar (SSS) fish. B) Schematic representation of the survey setup. The fish is towed below the vessel's bow where it images the lake bottom within the reach of its swath width. Topography (depression, boulder) as well as substrate (gravel, sand, mud) determine backscatter.*

sonar data acquisition and in-field visualisation of the acoustic backscatter.

Office and computer work involved visualising, processing and interpreting SSS data using the SonarWizMap software (Chesapeake Technology). Concrete steps consisted of: 1) creating projects for each lake in which all data tiles are combined; 2) cropping unusable data (e.g. test runs, gps errors, tortuous navigation), aggregating data tiles into lines and applying beam-angle corrections. The latter corrections compensate for the non-linear acoustic energy response characteristics of sonar transducers. All of these operations improve the overall quality of the combined imagery; 3) interpreting lake bottom features, knowing that the degree of SSS backscatter depends on topography as well as acoustic hardness of the substrate (Fig. 1B); 4) extracting water depths along bottom tracks from navigation lines in waterfall view in order to create detailed bathymetry maps of the surveyed lake areas.

## PRELIMINARY RESULTS

Preliminary observations and interpretations are discussed below, for each lake separately:

Vichuquén: SSS survey lines were navigated in the northern part of the lake basin, which stands in direct connection with Rio Vichuquén, the pathway towards the Pacific Ocean. Upon entering the lake basin, Rio Vichuquén builds out a high-backscatter, shallow water (<5 m) delta (Fig. 2). We relate the high-backscatter to the coarse-grained (sandy) nature of the delta deposits (confirmed by core samples) and its elevated topography. Gentle to moderate slopes separate the delta from the deeper basin (max. depth of 32 m), in which fine-grained deposits (low acoustic reflectance) prevail. Across the southern delta slopes, we observe a series of semi-parallel, bright streaks with a slightly negative topography. We interpret these streaks to be subaqueous channels that are preferentially used for transport of mainly coarse-grained sediment from delta to deeper basin, explaining the high backscatter (Fig. 2A). These channels reach down to the foot of the slope. They are the continuation of the subaerial Rio Vichuquén, however, most likely not all equally frequented throughout time. For example, in this 2016 backscatter image, the eastern channel is most prominent and characterised by clear channel features (central depression, levees, coarse-grained deposits, Fig. 2B) down to the 25 m

isobath. We also interpret these channels to be the most important pathways for transportation of sediment brought into the lake by tsunami waves. Other high-backscatter structures are the bulging lobes with pressure waves in front, observed along some of the basin slopes (Fig. 2C, D). These are most likely the product of slope failure-induced landslides following a sudden trigger, such as an earthquake

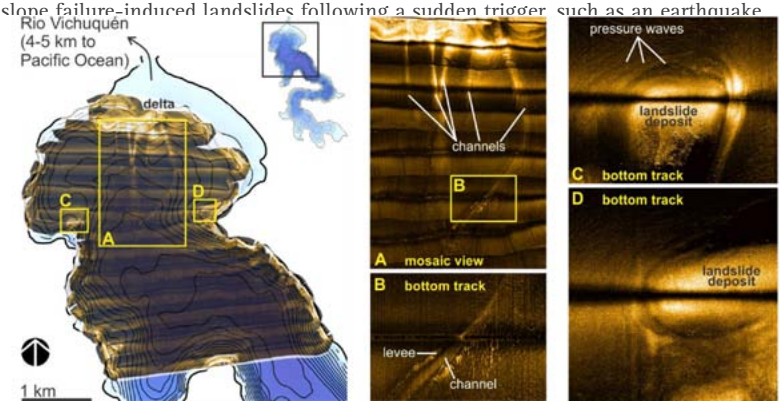


*Figure 2. Left: Bathymetry (isobaths every 5 m) with SSS mosaic overlay of the surveyed part of Vichuquén. A) Five channels along which delta sediment is transported downslope. B) Channel features. C)D) Landslide deposits with pressure waves.*

or an instant lake-level change.

Budi: Lago Budi has a very complex shape, which consists of many elongated arms, bays and sub-basins, related to its origin as a branch of uplifted river valleys. We focused our survey on the western extremities of two of the lake's arms that have most likely been connected to the Pacific Ocean in the past and/or display subaerial delta structures, which suggest sediment transport from the ocean to the lake during past tsunami inundation (Fig. 3). Subaqueous expressions of these delta deposits can be observed in both lake arms in the shape of defined high-backscatter fans, which spread out eastward, towards greater water depths. High backscatter is likely the result of the fans' coarser-grained nature, compared to the silty lacustrine deposits below. The relatively strong wipe-out of the high-reflectivity signal with greater swath angles (Fig. 3A, B), especially in the southern lake arm, could mean that the coarse-grained fan deposits are buried underneath a layer of low energy-absorbing, soft sediment.

Gemelas I: The connection between the ocean-proximal lagoon of the Lagunas Gemelas ("twin lagoons") consists of a narrow, winding channel between bedrock and massive dunes (Fig. 4). SSS imagery shows zones and patches of high backscatter close to the lagoon's inlet (Fig. 4), which are absent when moving towards the northern, more distal parts of the basin. High backscatter is again interpreted to be the result of coarser-grained deposits, transported from beach to lake by high-energy events, such as tsunamis, but also by the continuous supply of aeolian dune sands. The more discrete patches of high-reflectance with a positive morphology (Fig. 4) suggest the presence of relatively large, acoustically hard objects, e.g. bedrock fragments, logs and others, which must have been deposited in the lake basin by a high-energy event, a tsunami following an earthquake for example.

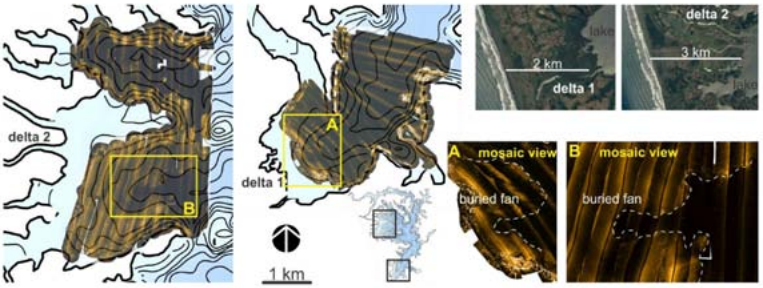


*Figure 3. Left: Bathymetry (isobaths every 1 m) with SSS mosaic overlay of the surveyed parts of Lago Budi. Connections between lake arms and the Pacific are characterised by delta structures, without topographic obstacles. A)B) Buried, coarse-grained fan deposits.*

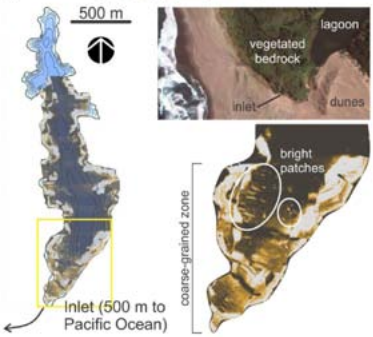


*Figure 4. Left: Bathymetry (isobaths every 2 m) with SSS mosaic overlay of Lagunas Gemelas I. Close to the inlet, lagoon deposits display a high backscatter.*

**PROOF OF EXPENSES (see attached)**

1 Chilean Peso (CLP) = 0.00130 euro (EUR)

| | Separate costs (CLP) | Total costs (CLP) | Total costs (EUR) |
|---|---|---|---|
| Lodge° | 150000+179800 | 329800/3* = 109933 | 143 |
| Meal° | 12200+1700+3180+1700+7250+ 11810+30000+22700+1400+4720+ 3520+2090+8550+1855 | 112675 | 146 |
| Fuel survey vessel° | 27400+17008+30000+28000+ 23000+21700+16504+30605+25800+ 61869+24000+24200 | 330086 | 429 |
| Air freight° | | | 451 |
| TOTAL | | | **1169** |
| REQUESTED | | | **1000** |

° receipts/invoices are attached and amounts indicated with red boxes
* 329800 CLP represents lodge costs for three people

# POSTGRADUATE STUDENT GRANT-1ST SESSION 2016

## Sedimentologic and Stratigraphic Investigation of Carboniferous Strata in Northern Utah and Central

*Justin Ahern*
*University of Nebraska-Lincoln, Lincoln USA*
*justin.ahern@huskers.unl.edu*

### *MONTANA: A RECORD OF LATE PALEOZOIC CLIMATE EVOLUTION AND EUSTACY*

**Background:**

The Late Paleozoic Ice Age (LPIA) was a ~76 myr icehouse when ice centers waxed and waned during asynchronous1 glaciations across Gondwana, resulting in complex glacio-eustatic sea-level oscillations2, 3,4. Initially the LPIA was considered a single period of ice sheet accumulation with orbitally controlled ice growth-decay cycles comparable to those of the Pleistocene5. Upon further investigation of near-field glacial deposits, this interpretation was later modified to two initial, temporally distinct episodes of alpine glaciation and one final episode of ice sheet accumulation6. Recent study of the near-field in Australia shows the LPIA to have entailed eight discrete intervals of glaciation, ~1 to 8 m.y. in duration, with intervening non-glacial episodes of comparable scale3, spanning the late Mississippian (330.5 mya)4 to the late Permian. The LPIA records the only transition of a vegetated Earth both into and out of a long-lived icehouse regime, and is considered an analog for the Quaternary ice age in which humans have evolved and currently reside7. Despite substantial progress made in documenting this event, the nature of initial LPIA ice cycles is not fully resolved.

**Motivation:**

Recent exploration drilling in the Heath (central MT) and Manning Canyon (northern UT) Formations yielded new cores in which the preserved paleoclimate record has been overlooked. These units are prospective unconventional hydrocarbon plays8,9 that preserve western Pangean paleotropical cyclothems that broadly coincide with the late Mississippian onset of the LPIA4. These units and encasing Carboniferous strata permit refined records of LPIA onset, as well as Carboniferous sea-level and paleoclimate change. Additionally, combined sedimentologic, stratigraphic and geochemical analysis utilized in this project will provide new insight into the controls LPIA ice cycles and persistent plate migration exert on low-latitude Carboniferous paleoclimate patterns through time.

**Methods:**

This study utilizes recently drilled cores with surface exposures in a sedimentologic and stratigraphic investigation of the Heath and Manning Canyon

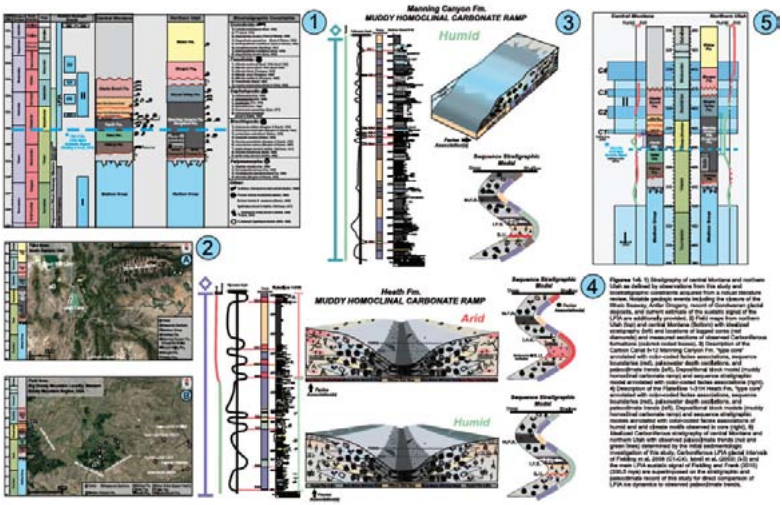


Formations in addition to their enclosing Carboniferous strata (Fig. 1). Stratigraphic relationships of studied formations are based on field observations from this study, whereas biostratigraphic constraints are solely a product of an extensive literature review (Fig. 1). Core descriptions and measured sections of observed units range from the Madison karst surface (Visean) to the Bashkirian Alaska Bench Fm. (central Montana) and the mid to latest Pennsylvanian portion of the Weber Fm. (northern Utah)-Fig. 1; Fig. 2A & 2B.

Core logging and fieldwork in central MT (Big Snowy Mountains) is complete and is currently underway in northern UT (Oquirrh & Uinta Mountains). Fieldwork entails logging detailed measured sections and sample collection for petrographic, carbonate isotope, X-ray diffraction (XRD) and X-ray fluorescence (XRF) analyses. Core, surface, and petrographic descriptions facilitate a detailed facies and diagenetic analysis from which facies associations are used to determine environments of deposition in observed units. Vertical stacking patterns of facies associations are used to document changes in stratigraphic style to evaluate the magnitude and frequency of sea-level fluctuations2 and produce sequence stratigraphic models for the target units. Physical climate indicators, carbonate isotopes, mudstone mineralogy, and chemical indexes of weathering (CIW)10 from marine and paleosol facies will provide a robust record of paleoclimate evolution for the target units. Determination of clay mineralogy and CIWs using XRD and a Bruker Tracer 5i XRF device is currently underway.

## Initial Results:

Stratigraphic records observed in this study shows that preserved high frequency sea-level oscillations, 10s of meters in magnitude, initiated in the Heath and Manning Canyon Formations and persisted at discrete intervals in younger formations. Presently, 8 (Heath) and 7 (Manning Canyon) 4th order depositional

sequences, bounded by sequence boundaries were identified in cored sections, in addition to at least 2 additional sequences in Manning Canyon surface exposures. This record informs an early Serpukhovian onset to the LIPA in central Montana and northern Utah that is in agreement with recent high-resolution estimates (330.5 mya)4.

Additionally, new depositional models for the Heath and Manning Canyon Formations, and new stratigraphic records of Carboniferous sea-level and paleoclimate variations for the study areas were produced. In the Heath and Manning Canyon Formations, the basin-ward progression of facies associations is partitioned by bathymetric controls. Paleoenvironments range from terrestrial to offshore locales, which is here interpreted within the context of a muddy, homoclinal carbonate ramp (Figs. 3&4). Paleosol and peritidal anhydrites are sequence boundaries, whereas offshore organic-rich, phosphate-bearing shales are flooding surfaces. These facies associations are the two end members from which paleowater-depths are inferred for the sequence stratigraphic frameworks of these units (Figs. 3&4).

Initial delineation of preserved Carboniferous paleoclimate patterns observed in this report are derived from sedimentological evidence alone (Figs. 5 & 6), incorporation of carbonate isotope, mudstone mineralogy and CIWs into these interpretations constitutes the next stage of this project.

In both central Montana and northern Utah the upper Madison contains silicified and brecciated limestones overprinted by karst, suggestive of restricted, potentially arid conditions, followed by increased humidity that fueled karst processes (Fig. 6 A&B).

## Central Montana:

The Kibbey Fm. contains channel-form clastics with internal silicified and breccia intervals, red beds and silicified and brecciated pedogenically-altered mudstones with carbonate nodules (Fig. 6C). These features support at least periodic aridity; however, poor outcrop preservation greatly inhibits investigation of this unit. The Otter Fm. preserves ooids, stratified peloid-rich grainstones, silicified carbonate-bearing paleosols, as well as silicified and brecciated stromatolites, indicating semi-arid tropical to sub-tropical conditions and partial hydrographic restriction (Fig. 6 D&E). Increasing humidity is inferred for the Lower Heath Fm. by the presence of mixed coal and paleo-entisol/vertisol bearing cyclothems (Fig. 4). Pronounced aridity is observed in the Upper Heath by the presence of thick evaporite and peritidal microbiolites that stratigraphically earlier paleosol and coal facies (Figs. 4 & 6F). Where preserved from erosion, the Bear Gulch is composed of monotonous, non-cyclothemic alterations of variably silicified, calcareous siltstone and micrite. Regionally extensive fluvial sandstone bodies of the Tyler Fm. incise into the Heath and locally contain basal conglomerates, iron accumulations and log casts. Intervening carbonaceous shale, iron carbonate-bearing paleosols, and minor ironstone (Fig. 6G) were also observed and are interpreted to indicate a shift to more humid conditions compared to the underlying upper Heath and Bear Gulch. The Heath-Tyler regional unconformity broadly coincides with the C1-C2 glacial events3 (Fig. 5) and is here interpreted to be glacio¬eustatic in origin. Tyler facies grade upward into alterations of marine limestones, microbialites, highly brecciated

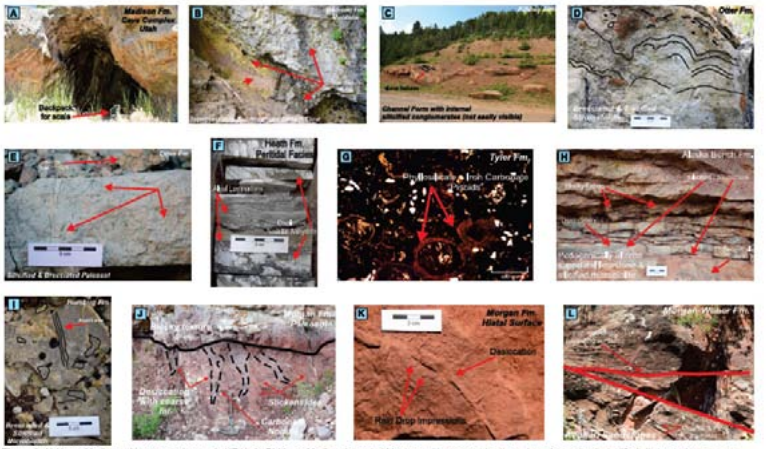


**Figure 6.** **A)** Upper Madison with preserved caves in NE Utah. **B)** Upper Madison in central Montana with preserved collapse breccias and red, stratified siltstones that support deposition in subterranean streams. **C)** Kibbey Fm. with preserved red beds in addition to channel-form clastics containing internal silicified and conglomeratic intervals and slump features. **D)** Brecciated and silicified stromatolitic facies present in the Otter Fm. **E)** Silicified and brecciated paleosol preserved in the Otter Fm. that contains well preserved rootlets and a blocky ped-structure with micritic carbonate nodules (background). **F)** Peritidal facies observed in the upper Heath Fm. that contains algal laminations and displacive, nodular anhydrite. **G)** Photomicrograph of "layered" pedogenic pisoids composed of phyllosilicates, iron, and iron carbonate that was extracted from an ironstone facies of the lower Tyler Fm. **H)** Pedogenically altered peritidal carbonates and silicified microbiolites that contain desiccation and fenestral pores, which are common facies in the Alaska Bench Fm. and typically preserve variable proportions of brecciation. **I)** Highly brecciated and silicified microbiolites preserved in the Humbug Fm., which occur as intervening intervals between cross-stratified quartz arenites. **J)** Paleo-vertisol/vertic-calcisol observed in the Morgan Fm. that preserves distinct horizon differentiation, deep desiccation with coarse fill, abundant slickensides, and carbonate nodules. **K)** Red bed hiatal surface preserved in the Upper Morgan Fm. that contains desiccation and raindrop impressions. **L)** Eolian sandstones observed in the upper Morgan and Weber Fm. that contain coarse and fine laminations, ripple cross-lamination, multi dm-scale cross-bedding, and 1st-3rd order bounding surfaces.

and silicified intervals, red beds, and calcretes of the Alaska Bench Fm. (Fig. 6H). These cyclic facies roughly coincide with the boundaries of the C2-C3 glacial events3, and suggest increased hydrographic restriction and aridity.

### Northern Utah:

The Humbug Fm. preserves alterations of peloidal limestone, micrite, brecciated and silicified microbiolites (Fig. 6I) and cross-bedded quartz arenites that are suggestive of moderate hydrographic restriction and aridity. The Great Blue Limestone is a monotonous accumulation of massive crystalline limestone with intervening black shales locally. The lower 1/3 of the Manning Canyon Fm. contains mixed limestone, carbonaceous shale and progradational packages of deltaic sandstones. The upper 2/3 of the Manning Canyon preserves mixed coal, and paleo-entisol/vertisol bearing cyclothems, indicative of humid conditions comparable to those recorded in the lower Heath (Fig. 3). In the Round Valley Fm., cyclic limestone-mudstone alterations and local channel forms plugged with dark mudstone roughly coincide with the C2 and initial C3 glacial intervals3. A regionally extensive, mature paleosol, locally bearing carbonate nodules and desiccation separates the Round Valley from the overlying Morgan Fm. and co-occurs with the initial C3 glacial interval3. Numerous cyclic alterations of marine limestone, microbial laminates, brecciated and silicified surfaces, fine eolian sands, paleo-vertisols/calcisols and red beds bearing desiccation and raindrop impressions are preserved in the Morgan (Figs 6 J-L). These features suggest variably arid conditions with seasonal humidity that coincide with the C4 glacial interval3. Terrestrial facies increase in abundance upward in the Morgan and grade into the eolian quartz arenites of the Weber Fm. (Fig. 6L), which records a pronounced arid paleoclimate shift.

## Discussion:

A Serpukhovian, paleotropical humid to arid climate shift is preserved in the Heath Fm. by an upward transition from paleosol-coal associations to limestone-evaporite associations. This paleoclimate shift is not observed in northern Utah until the Moscovian (Fig. 5). A ~15° difference in paleolatitude between the study areas, coupled with persistent northward plate migration into increasingly arid climate belts is a likely primary control on the observed paleoclimate patterns. A shift from semi-arid paleoclimate indicators preserved in adjacent, underlying formations, to coal and paleo-vertisol bearing cyclothems in the lower Heath and Manning Canyon, supports a shift to more humid paleoclimate conditions at the onset of the LPIA. Additionally, a shift from arid to humid climate indicators from the upper Heath to the lower Tyler may be related to C1/C2 ice accumulation. Furthermore, mixed alterations of eolian, paleo-vertisols/vertic-calcisols, and preserved raindrop impressions in the Morgan may be suggestive of seasonal humidity induced by ice growth during the C4 glacial event. During each of these occasions glacial ice accumulation may have caused northern Polar cells to expand southward, concentrating moist low pressure cells at paleo-low latitudes, inducing wetter than normal conditions and subsequent deposition of humid paleoclimate indicators at these times11. Considering this, a glacially induced LST coupled with increased humidity could have been a primary driver for the incision and subsequent deposition of the regionally extensive Tyler fluvial sandstone bodies. As such, its is plausible that the deposition of humid climate indicators in the Heath, Tyler and Morgan formations that are not explained by the overall humid to arid paleoclimate trend driven by northward plate migration, can be explained by periods of coeval Gondwanan ice growth. This study provides evidence that Carboniferous low-latitude paleo-climate patterns may have been influenced by both plate migration and Gondwanan ice cycles of the LPIA; however, more work is needed to more accurately elucidate the influence of these factors, in addition to others not disclosed in this report.

## Use of Funds:

Funds from this research grant were spent on vehicle rental charges ( 1000). An SUV rental was necessary in order to travel from Lincoln, NE to my field cites in central Montana and Northern Utah and complete all field and core data acquisition.

## References:

[1]Cagliari, J. et al. Journal of the Geological Society, 173(6), 2016.
[2] Birgenheier, L. P et al. Journal of Sedimentary Research, 79(2), 2009.
[3] Fielding, C. R et al., Journal of the Geological Society, 165(1), 129-140, 2008.
[4]Fielding, C. R., & Frank, T. D. 2015. Palaeo3, 426, 121-138, 2015.
[5] Crowley, T. J. & Baum, S. K., Geology, 19(10), 975-977, 1991.
[6] Isbell, J.L et al., Special Papers-Geological Society of America, 370, 5-24, 2003.
[7] Raymond, A., & Metz, C, The Journal of Geology, 112(6), 655-670, 2004.
[8]Bottjer, R.J et al. Search and Discovery Article # 51234, 2016.
[9]Schamel, S & Quick, J. Search and Discovery Article #10537, 2013.
[10]Harnois, L. Sedimentary Geology, 55 \(3-4), 1988.
[11] Miller, D.J., & Eriksson, K.A. Geology, 27(1), 1999.

# Pattern, dynamics and timing of glaciation on the Gaick Plateau, Central Grampian Highlands, Scotland

*Chandler Benjamin*
*School of Geography, Queen Mary University of London*
*b.m.p.chandler@qmul.ac.uk*

## 1. Introduction

The complex record of Quaternary sediment-landform assemblages in Britain provides an excellent opportunity to reconstruct the pattern, dynamics and timing of glacial events. Extensive research examining these well-preserved records over the last ~40 years has allowed the development of a significant inventory of evidence relating to (i) deglaciation of the last British-Irish Ice Sheet (e.g. Evans et al., 2005) and (ii) a less extensive period of glaciation during the Younger Dryas (YD; Golledge, 2010). Despite this, there remain areas where the pattern, dynamics and timing of events are poorly constrained. This is exemplified by the Gaick Plateau, Central Scottish Highlands (Figure 1). A number of contrasting conceptual models have been proposed for glacial events in this area: (i) an extensive Lateglacial readvance over central and southeast Grampian Highlands (e.g. Charlesworth, 1955); (ii) advance and retreat of a locally-sourced YD plateau icefield (e.g. Sissons, 1974); and (iii) retreat of the last ice-sheet (Lukas et al., 2004). Elucidating the pattern, dynamics and timing of glacial events in this region is of key importance as it has significant implications for understanding of palaeoclimate during the Last Glacial-Interglacial Transition (LGIT; c. 16–8 ka) in Scotland. The value of (re-)examining contentious areas has been demonstrated by recent (re-)appraisals elsewhere in Scotland (e.g. Boston et al., 2015). This PhD project seeks to resolve the issues outlined through applying a combination geomorphological, sedimentological and chronological techniques to arrive at a holistic understanding of events during the LGIT.

## 2. Methods

Funding from the IAS enabled a four-week field campaign to be undertaken involving sedimentological investigations and sampling for luminescence dating. Sedimentological analysis of available natural exposures, enlarged and cleaned with a trenching tool, was undertaken to provide key information on landform genesis and valuable insights into glacier dynamics. Investigations followed standard procedures, including section logging and description, lithofacies analysis, clast shape analysis and structural measurements (e.g. Evans and Benn, 2004; Lukas et al., 2013). Sampling for luminescence dating followed a lithofacies approach (e.g. Thrasher et al., 2009; Smedley et al., 2016), with glaciolacustrine sediments targeted as these have been shown to be particularly promising (e.g. Lukas et al., 2012; Wyshnytzky et al., 2015). Where possible, samples were obtained by hammering steel cylinders into cleaned sections, but particularly fine, consolidated sediments were sampled as blocks. In the latter case, ~1 cm of sediment has since been trimmed from all sides of the blocks in the QMUL Luminescence Laboratory to remove any ambiguities of light having penetrated the sides of blocks (cf. Lukas et al., 2012).

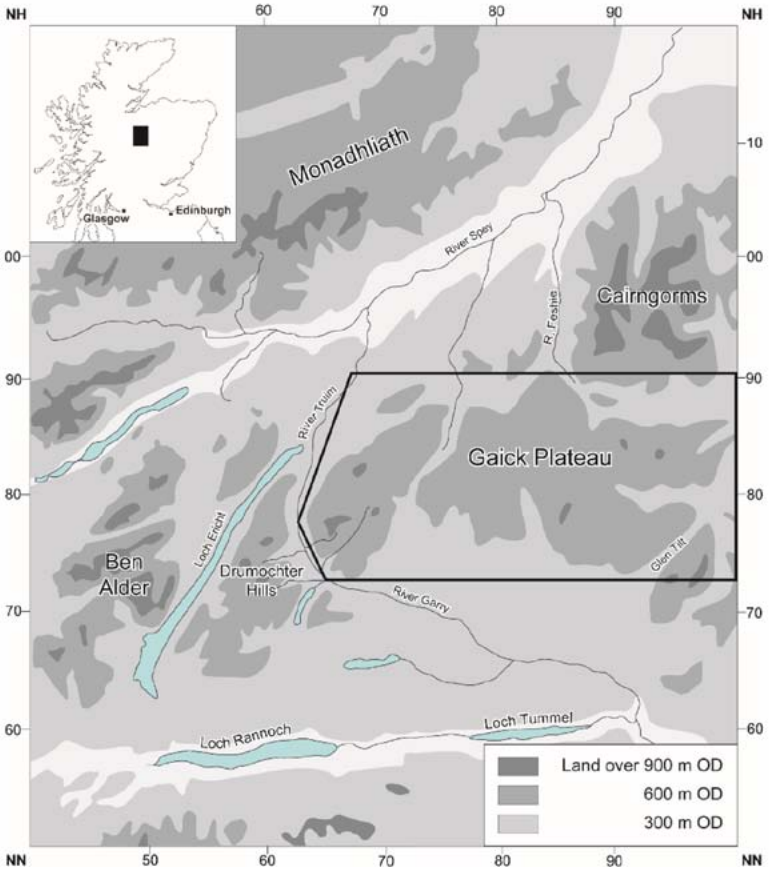


*Figure 1: Topographic map illustrating the location of the Gaick Plateau in Scotland, with the study area outlined by the black box. Scale and orientation is given by British National Grid Coordinates. Elevation data © Crown Copyright. Ordnance Survey an EDINA Digimap/JISC supplied service.*

## 3. Preliminary findings

Like many areas in the Scottish Highlands, good quality sediment exposures are limited in the Gaick area. Nevertheless, it was possible to examine and log eight exposures, including four exposures through moraines. The moraine exposures principally comprise diamicton units that typically vary from matrix-supported and stratified to clast-supported and stratified. Within the diamicton units occur lenses of laminated to bedded sand that display varying degrees of deformation. Stratification of the diamicton units and the dip of thin sand lenses commonly follow the dip and azimuth of the moraine surface slopes. These characteristics

indicate these lithofacies were deposited as debris flow units, with the sand lenses representative of periods of sheet wash (cf. Lukas, 2005, and references therein). This is consistent with sedimentation in terrestrial ice-contact fans which subsequently underwent varying degrees of deformation (cf. Lukas, 2005). In all cases, clast shape analysis indicates that clasts in the moraine samples were dominantly subglacially transported, as shown elsewhere (e.g. Benn, 1992; Lukas, 2005).

Aside from moraine sections, a particular impressive section was investigated at the northern end of Loch an Duin (NN 7254 8115). The left-hand side of the section comprises steeply dipping (26–34°) gravel and granule gravel clinoforms (Figure 2). Characteristics of individual beds are variable, with massive, sandy matrix-supported gravels and moderately sorted openwork granule gravels and gravels. The right-hand side of the section is dominated by couplets of massive to laminated silty fines and medium to fine sands (F/Sl; Figure 2), with sand laminae and beds displaying type S ripple cross-lamination (or draped lamination). Couplets fine upwards in section, with fine laminae and beds becoming increasingly dominant towards the top of the unit (Figure 2c). Occasionally, relatively thin,

discontinuous layers of matrix-supported diamicton occur within the F/Sl couplets. Numerous normal faults and graben structures are evident towards the right-hand side of the exposure, and measurements of the strike and dip of a number of the faults were undertaken to investigate these further. This exposure is interpreted as a Gilbert-type delta, with the gravel clinoforms representing the foreset component of the delta (cf. Benn and Evans, 1993, 2010; Brazier et al., 1998). Based on strong morphostratigraphic evidence (cf. Lukas, 2006), it is inferred that this delta formed during the YD in a lake dammed by ice at the northern and southern ends of the valley. To test this hypothesis and to provide age control, the F/Sl couplets have been sampled for OSL dating. Sediments in a nearby deformed grounding-line fan have also been sampled.

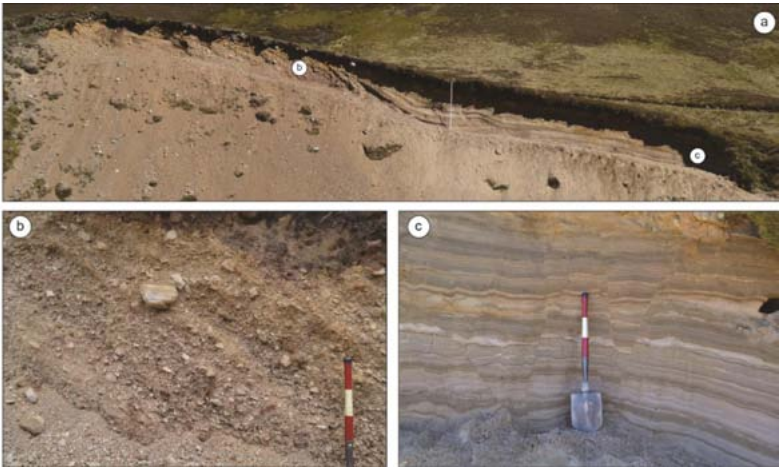


*Figure 2: (a) Overview of the Loch an Duin section described in the text, with a 2 m measuring staff for scale. Close-ups of the gravel clinoforms (b) and the faulted F/Sl couplets (c). Painted red and white intervals on the trenching tool are 10 cm.*

## 4. Significance

The morphological similarity of the sampled moraines with YD moraines elsewhere in the Gaick, combined with detailed studies of moraine sedimentology from elsewhere in Scotland (Benn, 1992; Lukas, 2005), strongly imply that the majority of YD moraines in the Gaick area formed as terrestrial ice-contact fans. The presence of terrestrial ice-contact fans, with varying degrees of post-depositional deformation, indicate YD ice masses in the Gaick area underwent incremental and oscillatory retreat. Meanwhile, the section described from Loch an Duin provides evidence for a hitherto-unrecognised YD ice-dammed lake (cf. Sissons, 1974). Combined with geomorphological evidence from the valley and neighbouring valleys, there is strong evidence indicating that this valley was ice free during the YD and that the YD ice coverage was, therefore, less extensive than proposed by Sissons (1974).

## References

Benn, D.I., 1992. The genesis and significance of 'hummocky moraine': evidence from the Isle of Skye, Scotland. Quaternary Science Reviews 11, 781–799.

Benn, D.I., Evans, D.J.A., 1993. Glaciomarine deltaic deposition and ice-marginal tectonics: The 'Loch Don Sand Moraine', Isle of Mull, Scotland. Journal of Quaternary Science 8, 279–291.

Benn, D.I., Evans, D.J.A., 2010. Glaciers and Glaciation (2nd Edition). Hodder Education, London, 802 pp.

Boston, C.M., Lukas, S., Carr, S.J. 2015. A Younger Dryas plateau icefield in the Monadhliath, Scotland, and implications for regional palaeoclimate. Quaternary Science Reviews 108, 139–162.

Brazier, V., Kirkbride, M.P., Gordon, J.E., 1998. Active ice-sheet deglaciation and ice-dammed lakes in the northern Cairngorm Mountains, Scotland. Boreas 27, 297–310.

Charlesworth, J.K., 1955. Late-glacial history of the Highlands and Islands of Scotland. Transactions of the Royal Society of Edinburgh 62, 769–928.

Evans, D.J.A., Benn, D.I. (eds.), 2004. A Practical Guide to the Study of Glacial Sediments. Arnold, London, 266 pp.

Evans, D.J.A., Clark, C.D., Mitchell, W.A., 2005. The last British Ice Sheet: a review of the evidence utilised in the compilation of the Glacial Map of Britain. Earth-Science Reviews 70, 253–312.

Golledge N.R., 2010. Glaciation of Scotland during the Younger Dryas stadial: a review. Journal of Quaternary Science 25, 550–566.

Lukas, S., 2005. A test of the englacial thrusting hypothesis of 'hummocky' moraine formation: case studies from the northwest Highlands, Scotland. Boreas 34, 287–307.

Lukas, S., 2006. Morphostratigraphic principles in glacier reconstruction: a perspective from the British Younger Dryas. Progress in Physical Geography 30, 719-736. Lukas, S., Merritt, J.W., Mitchell, W.A. (eds.), 2004. The Quaternary of the central Grampian Highlands: Field Guide. Quaternary Research Association, London, 227 pp.

Lukas, S., Benn, D.I., Boston, C.M., Brook, M.S., Coray, S., Evans, D.J.A., Graf, A., Kellerer-Pirklbauer-Eulenstein, A., Kirkbride, M.P., Krabbendam, M., Lovell, H., Machiedo, M., Mills, S.C., Nye, K., Reinardy, B.T.I., Ross, F.H., Signer, M., 2013. Clast shape analysis and clast transport paths in glacial environments: A critical review of methods and the role of lithology. Earth-Science Reviews 121, 96–116.

Lukas, S., Preusser, F., Anselmetti, F.S., Tinner, W., 2012. Testing the potential of luminescence dating of high-alpine lake sediments. Quaternary Geochronology 8, 23–32.

Sissons, J.B., 1974. A lateglacial ice cap in the central Grampians, Scotland. Transactions of the Institute of British Geographers 62, 95–114.

Smedley, R.K., Glasser, N.F., Duller, G.A.T., 2016. Luminescence dating of glacial advances at Lago Buenos Aires ( 46 °S), Patagonia. Quaternary Science Reviews 134, 59–73.

Thrasher, I.M., Mauz, B., Chiverrell, R.C., Lang, A., 2009. Luminescence dating of glaciofluvial deposits: A review. Earth-Science Reviews 97, 133–146.

Wyshnytzky, C.E., Rittenour, T.M., Nelson, M.S., Thackray, G., 2015. Luminescence dating of late Pleistocene proximal glacial sediments in the Olympic Mountains, Washington. Quaternary International 362, 116–123.

# Role of Cretaceous volcanogenic sedimentation in development of Neotethys in the E Mediterranean region (N Cyprus)

*Guohui Chen*
*School of GeoSciences, University of Edinburgh, Edinburgh EH9 3FE, UK*
*guohui.chen@ed.ac.uk*

Volcanogenic rocks can provide critical information concerning island arc genesis, either in an oceanic or a continental margin setting. As part of the PhD research by the first author, two contrasting units were studied in the Kyrenia Range, N Cyprus: a lower silicic sequence, termed the Fourkovouno (Selvilitepe) Formation of presumed Late Cretaceous age, and a separate basaltic sequence of well-dated Late Cretaceous and Eocene age. Although the basaltic sequence has been studied previously (Baroz, 1979; Robertson et al., 2012), the genesis and emplacement of the silicic sequence in relation to adjacent units has, until now, remained unclear. Also, the age of the silicic volcanism was only loosely constrained, and detailed geochemical evidence on its origin was lacking. Despite this, a good understanding of the siliceous rocks is critical to help interpret the

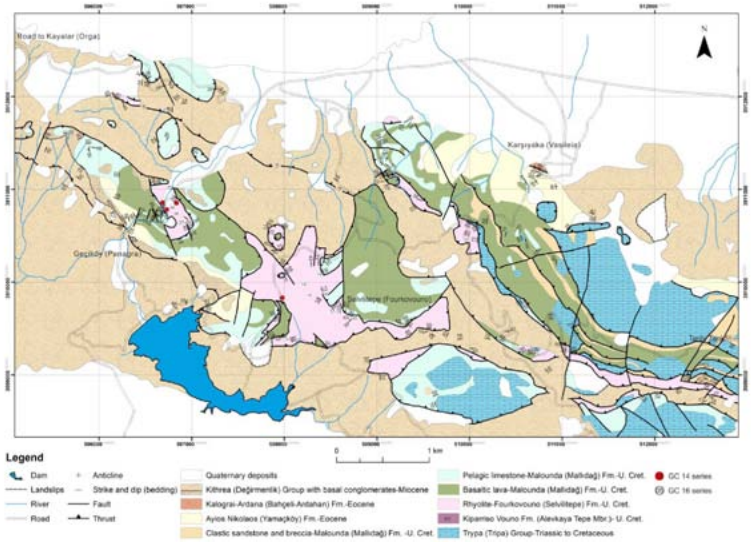


*Fig. 1 Geological map and sampling locations in the western Kyrenia Range, N Cyprus (based on previous mapping by Baroz (1979) with numerous changes and additions.*

Eastern Mediterranean Neotethys.

In April 2017, with the support of the International Association of Sedimentologists, fieldwork was carried in the northern part of Cyprus (9 days), with the main objective of studying tuffaceous and volcaniclastic lithologies of the Fourkovouno (Selvilitepe) Formation. The specific aims were to understand the field relations, sedimentology and structure of these rocks in relation to other units exposed in the Kyrenia Range (Fig. 1). (1): Sequences of Upper Cretaceous volcanic and sedimentary rocks are well exposed near Geçiköy (Panagra) Gorge in the western Kyrenia Range. Detailed re-mapping shows that a thrust contact separates contrasting silicic and basaltic sequences (e.g. SE of the gorge; Fig. 2). (2): Comparable lithologies crop out in the Selvilitepe (Fourkovouno) area further east, with the occurrence of weakly-bedded silicic tuff (beds <0.5 m thick), passing upwards into a sequence made up of interbedded lenticular rhyolitic lava and occasional debris flows (up to 90 m thick). Mapping indicates that the silicic sequence takes the form of a thrust slice which is located between siliciclastic sediments of Oligocene-Early Miocene Bellapais (Beylerbey) Formation below, and pelagic chalk/basalt sequence of the Lapithos (Lapta Group) above (3): Further east (south of the 'tank locality'), the silicic lava/tuff sequence forms a east-southeast-trending slice within a thrust stack made up of Mesozoic platform carbonates belonging to the Trypa (Tripa) Group and also Upper Cretaceous sandstone, breccia and pillow lavas of the Malounda (Mallıda ) Formation. (4): In a coastal exposure situated west of Kayalar (Orga) village (far west of the study area) the overall succession is strongly folded. Siliceous tuff and pelagic chalk are exposed in an anticline, whereas Eocene debris-flow deposits make up a syncline.

*Fig. 2 Thrust contact between silicic and basaltic sequences*

In summary, our field observations allow us to recognise the original Upper Cretaceous stratigraphic sequence in the western Kyrenia Range. This begins with a thickening- and coarsening-upward sequence of siliceous tuff and rhyolitic debris-flows and culminated in thick-bedded, to massive silicic lava flows. The above succession is structurally overlain by a sequence of pelagic chalk/pillow basalt of Maastrichtian age, based on previous dating of the pelagic sediments using

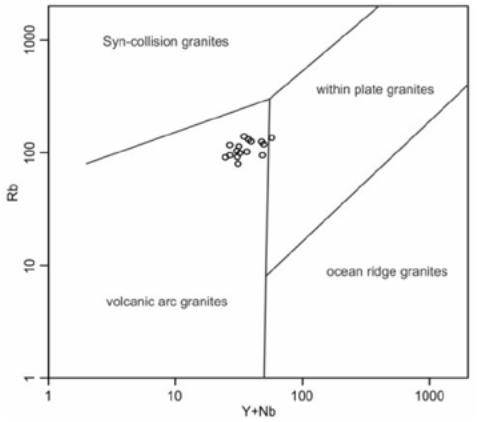


*Fig. 3 Rb versus Y+Nb diagram (after Pearce et al., 1984)*

planktonic foraminifera. The sequence is unconformably overlain by the basal conglomerates of the Bellapais (Beylerbey) Formation (e.g. Geçiköy (Panagra) Gorge area). The Miocene siliciclastic sediments of Kithrea (De irmenlik) Group are folded and truncated, probable related to reactivation of the Kithrea (De irmenlik) Fault.

With a view to gaining a better understanding of the conditions of formation, 16 samples of the silicic tuffaceous rocks were analysed geochemically by XRF and ICP-MS (partly funded by IAS). Compared to oceanic ridge granites, the rhyolitic rocks are enriched in LILEs, with pronounced depletion in Zr, Hf, Y and Yb. They are similar to volcanic arc granites of oceanic calc-alkaline arcs and active continental margin settings (Pearce et al., 1984). On discrimination diagrams, e.g. Rb versus Y+Nb (Fig. 3) and Th/Yb versus Ta/Yb, the silicic tuffaceous rocks and rhyolites are comparable with arc granites (Pearce et al., 1984; Harris et al., 1986; Gorton and Schandl, 2000). In contrast, the structurally overlying basaltic sequence is chemically of within-plate type, with a small subduction-related signature (e.g. negative Nb anomaly) that may be inherited (rather than contemporaneous). It appears therefore that the two volcanic sequences erupted adjacent to each other, with different geochemical signatures; i.e. an active continental margin setting for the silicic sequence, and a within-plate setting for the basaltic sequence. Both sequences experienced southwards thrusting during the Early-Mid Eocene to form large slices within a regional-scale thrust stack. This was part of a south-verging accretionary prism related to closure of the Southern Neotethys. Further S-directed thrusting took place during the Late Miocene with the thrusting the entire Late Mesozoic volcanogenic sequences over Oligocene-Early Miocene marine siliciclastic sandstones (Kithrea (De irmenlik) Flysch).

On-going research (funded separately) has included successful SIMS U-Pb dating of zircons from the silicic sequence which yielded ages of 73.5±1.4 Ma.

## Acknowledgements

The first author would like to thank the International Association of Sedimentologists for awarding this Postgraduate Grant, which made this fieldwork possible.

## References

Baroz, F., 1979. Etude géologique dans le Pentadaktylos et la Mesaoria (Chypre Septentrionale). Université de Nancy.

Gorton, M.P., Schandl, E.S., 2000. From continents to island arcs: a geochemical index of tectonic setting for arc-related and within-plate felsic to intermediate volcanic rocks. The Canadian Mineralogist 38, 1065-1073.

Harris, N.B., Pearce, J.A., Tindle, A.G., 1986. Geochemical characteristics of collision-zone magmatism. Geological Society, London, Special Publications 19, 67-81.

Pearce, J.A., Harris, N.B., Tindle, A.G., 1984. Trace element discrimination diagrams for the tectonic interpretation of granitic rocks. Journal of petrology 25, 956-983.

Robertson, A.H.F., Tasli, K., nan, N., 2012. Evidence from the Kyrenia Range, Cyprus, of the northerly active margin of the Southern Neotethys during Late Cretaceous–Early Cenozoic time. Geological Magazine 149, 264-290.

# Provenance of late Quaternary loess along the middle and lower Danube River, Europe

*Kaya Fenn*
*University of Oxford Oxford UK*
*kaja.fenn@hertford.ox.ac.uk*

## 1. Introduction

Loess represents a key terrestrial climate archive and provides an unparalleled opportunity to investigate the past dust cycle, a major component of the past climate system. It preserves evidence of its origins, critical to deciphering climatic signals in proxies, sediment transport and dynamics, as well as factors controlling dust emission. Palaeoenvironmental interpretations rely on climate proxies (e.g. grain-size), the interpretation of which requires an understanding of sediment source change.

Quaternary loess is found across Europe, with Central-Eastern sequences along the mid/lower reaches of the Danube River being particularly extensive, thick, well preserved, and providing robust geochronologies (Markovi et al., 2015) of sedimentary deposition. Previously proposed source(s) of Danubian loess have been mainly theoretical or inconclusive. The Fennoscandinavian Ice-Sheet and Alpine glaciers were considered the main sediment producers, with transport occurring via melt waters, through the Moravian depression and Danube River. Others suggested Miocene–Pliocene sands from the Carpathian Basin (Smith et al., 1991). Smalley et al. (2009) proposed the Alps, Carpathians and Sudeten as sources and argued for no glacial component in production. Bulk geochemical work in the Lower Danube (Buggle et al., 2008) supported the Alps and Carpathians, but argued for no dominant source, showing substantial homogeneity between sites along the Danube. Conversely, a study using U-Pb zircon dating and Sr-Nd isotopes showed that Hungarian loess is derived from Danubian alluvial fans and local geologies (Újvári et al., 2012). Furthermore, due to methodological differences, the investigations at the Austrian, Bulgarian and Romanian sites, have failed to connect data with sites across the basin to achieve regional overview of controls on sediment production and transport along the Danube.

## 2. Methods

The funding from the IAS Postgraduate Research Scheme allowed for a fieldwork visit to be undertaken along the Bulgarian side of the Danube River. The trip included final site selection as well as sample collection for sedimentological analysis, luminescence dating and provenance. The loess cliffs near the village of Slivata were selected. Sample collection followed standard

procedures including cleaning exposures followed by detailed logging and description. Samples for luminescence and provenance were taken at the same depths at ~50cm resolution throughout the profile. Luminescence samples were collected by hammering black plastic tubes into the cleaned sections. Care was taken to minimise the sunlight exposure to just the ends of the tubes. Once

luminescence samples have been taken gamma spectroscopy was also measured in the field to provide more accurate dose rates for luminescence dating. As this site has not been previously investigated additional samples were collected to provide a palaeoenvironmental record for the site. The samples for particles size and magnetics susceptibility were collected at 2cm resolution throughout the profile.

Particle size, magnetic susceptibility were measured at the School of Geography and Environment, University of Oxford. Magnetic susceptibility was analysed using a Bartington MS2 Magnetic Susceptibility System with a MS2B dual frequency sensor. Prior to analysis samples were dried in the oven (up to 40°C) overnight, gently crushed to homogenise sediment and secured with cotton wool to minimise sediment movement. Samples were measured at a stable temperature, and the results were converted to mass corrected values.

The remaining dried material from the magnetic susceptibility analysis was used for the particle size measurements using a Malvern Laser Particle Sizer Mastersizer 2000 with Hydro 2000MU. 30 second ultrasonic pre-treatment was applied to each sample to disperse sample in the deionised water.

3. Preliminary results

Currently the literature is split as to whether loess samples should be treated prior to the particle size analysis. Some studies argue that no treatment needs to be carried out, others claim that both hydrogen peroxide (to remove organic matter) and hydrochloric acid (to remove carbonates) should be administered. Others suggest that only one of the two treatments is sufficient.

To determine if all samples had to be "cleaned" with hydrochloric acid and hydrogen peroxide prior to particle size analysis, we assessed a series of samples pre- and post- treatment. For comparison each sample was also analysed multiple times to create true replicates, rather than standardly accepted three pseudo-replicates conducted by the machine itself. Our tests showed some variability can be

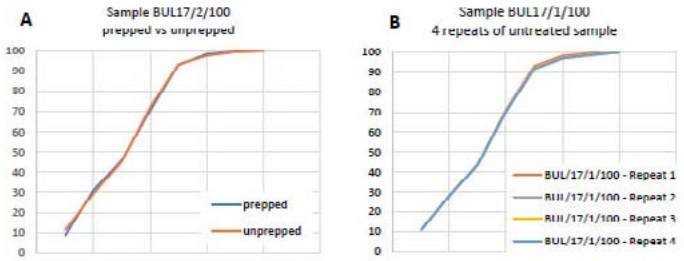


*Figure 1. A) Cumulative frequency diagram for a typical sample showing the difference samples fully treated prior to analysis and sample without treatment. B) Cumulative frequency diagrams for the true replicates of the sample shown in diagram A.*

recorded between samples pre- and post- treatment (Fig. 1). However, this change was comparable to the variability registered when "true – replicates" were measured. This showed that the samples did not require pre-treatment.

The preliminary particle size results (D50) and low frequency mass magnetic

susceptibility (Xlf) for one of the subsections are shown in the Figure 2.

This site shows multiple palaesol horizons, the thickest of which is picked up in the Xlf data. In all cases the peaks in MS correlate with increased proportions of clay and fine silt particles in the section. The Holocene soil is recorded as a thick (1.1 m) unit with the highest proportion of clay and fine silt, and therefore the lowest D50 values in the whole section. This also corresponds with the highest values of MS which gradually decrease to reach average loess values. We note here the previously unseen variability between palaeosols and loess units with multiple pedogenetic horizons, most of which also correspond with an increase in magnetic susceptibility values and a drop in the median grain size. This work will in the future be supported by the luminescence ages to help us understand the timing of

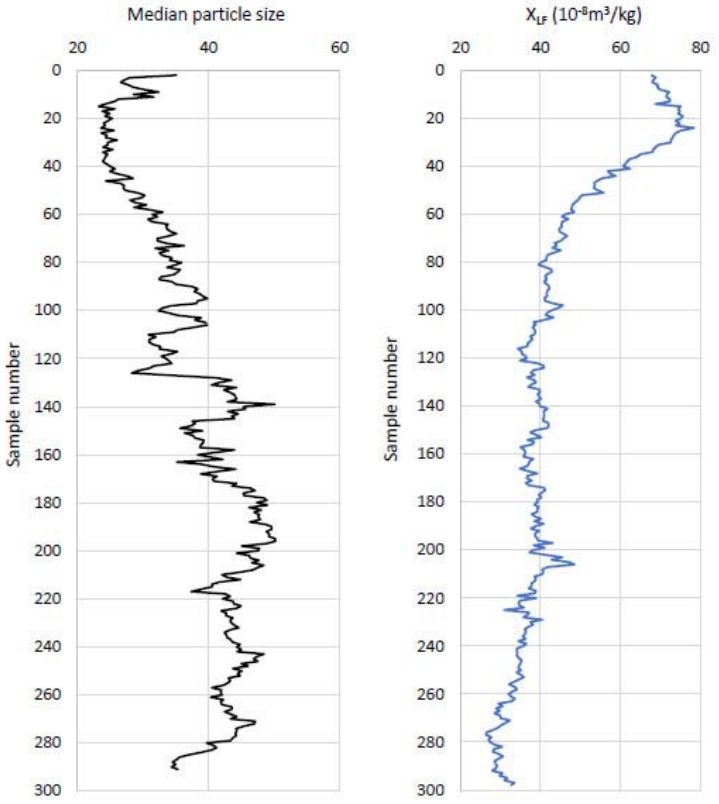


*Figure 2. Particle size and low frequency magnetic susceptibility variation at Slivata 1 loess profile.*

the loess deposition and soil development.

Samples collected for the OSL and provenance analyses are still in a preparation and measurement stages, as they are more time intensive techniques.

The grant money was used to fund a return flight from Romania, car hire accommodation and subsistence costs during the field visit. The sedimentological data and optically stimulated luminescence ages will be presented at the EGU 2018 conference in Vienna.

## References

Buggle, B., Glaser, B., Zöller, L., Hambach, U., Markovi , S.B., Glaser, I., Gerasimenko, N.P., 2008. Geochemical characterization and origin of Southeastern and Eastern European loesses (Serbia, Romania, Ukraine). Quat. Sci. Rev. 27, 1058–1075. doi:10.1016/j.quascirev.2008.01.018

Markovi , S.B., Stevens, T., Kukla, G.J., Hambach, U., Fitzsimmons, K.E., Gibbard, P., Buggle, B., Zech, M., Guo, Z., Hao, Q., Wu, H., O'Hara Dhand, K., Smalley, I.J., Újvári, G., Sümegi, P., Timar-Gabor, A., Veres, D., Sirocko, F., Vasiljevi , D.A., Jary, Z., Svensson, A., Jovi , V., Lehmkuhl, F., Kovács, J., Svir ev, Z., 2015. Danube loess stratigraphy - Towards a pan-European loess stratigraphic model. Earth-Science Rev. 148, 228–258. doi:10.1016/j.earscirev.2015.06.005

Smalley, I.J., O'Hara-Dhand, K., Wint, J., Machalett, B., Jary, Z., Jefferson, I., 2009. Rivers and loess: The significance of long river transportation in the complex event-sequence approach to loess deposit formation. Quat. Int. 198, 7–18. doi:10.1016/j.quaint.2008.06.009

Smith, B.J., Wright, J.S., Whalley, W.B., 1991. Simulated aeolian abrasion of Pannonian sands and its implications for the orgins of Hungarian loess. Earth Surf. Process. Landforms 16, 745–752.

Újvári, G., Varga, A., Ramos, F.C., Kovács, J., Németh, T., Stevens, T., 2012. Evaluating the use of clay mineralogy, Sr-Nd isotopes and zircon U-Pb ages in tracking dust provenance: An example from loess of the Carpathian Basin. Chem. Geol. 304–305, 83–96. doi:10.1016/j.chemgeo.2012.02.007

# Environmental controls on trace fossil distribution from the Ediacaran-Cambrian GSSP of Burin Peninsula, Newfoundland, Canada: integrating ichnologic and sedimentologic datasets to unravel early metazoan evolution.

*Romain C. Gougeon*
*University of Saskatchewan, Saskatoon (Canada)*
*gougeon.romain@gmail.com*

## 1. Introduction

The appearance of complex life in the fossil record is a fascinating and highly debated topic. In his classic book On the Origin of Species, Darwin recognized a weakness in his theory of evolution: if species gradually change through time by the process of natural selection, how is it that no fossil record of simpler bilaterian organisms than the "Silurian" trilobites (i.e. the trilobites of the Cambrian in the modern geological scale) has been found? Where are the missing pieces of this gradual complexification of life? He concluded that this crucial absence of data in the evolutionary puzzle may be the result of the dearth of paleontological findings at that time. When in the mid-fifties enigmatic and unconventionally shaped fossils from the Ediacaran biota were discovered, Darwin inquiry came back to mind. Following up, the missing pieces were bit by bit recovered in the shape of the first bacterial colonies (stromatolites from 3.5 Ga), large, diverse acritarch microfossils appearing after the Marinoan glaciation (i.e. at the base of the Ediacaran period, 635 Ma) and small shelly fossils (SSF) from the base of the Cambrian.

Additionally to these lines of evidence, the record of traces of activity from higher grade metazoans provides unique evidence of the presence of animals. Indeed, by being at the interface between organisms and the sea-floor, trace fossils unveil behaviors of benthic organisms. Consequently, the base of the Phanerozoic eon and its first geological time period, the Cambrian, are situated at the first evidence of complex animal behavior at Fortune Head, Burin Peninsula, Newfoundland, in Canada (Narbonne et al., 1987).

## 2. The Chapel Island Formation and evidence for behavioral innovations

The Cambrian Global boundary Stratotype Section and Point (GSSP) was defined by the first appearance of the trace fossil Treptichnus pedum in the Chapel Island Formation (CIF) at Fortune Head in 1992 (Brasier et al., 1994). The CIF is a continuous, dominantly siliciclastic section of more than 1000 m spanning the late Ediacaran to the Cambrian Stage 2, the latter being located at the first appearance of the SSF Watsonella crosbyi (Myrow, 1987; Landing et al., 2013; Fig. 2). This section is composed of five informal members based on lithological arguments, mainly recorded in three outcrops along the south-western part of the Burin Peninsula: Fortune Head, Grand Bank Head and Little Dantzic Cove (Bengtson and Fletcher, 1983; Figs. 1, 2). Member 1 is best exposed at Grand Bank

Head, and record green and red siltstones to fine-grained sandstones characteristic of a perital environment. Member 2 is recorded at Fortune Head and Grand Bank Head and corresponds to hetetolithic siltstones and fine-grained sandstones (Fig. 3A) deposited in shallow marine, wave influenced settings. Member 3, 4 and 5 are exposed at Little Dantzic Cove. Member 3 represents the deepest part of the section with a higher amount of siltstone beds associated with many carbonate concretions. Member 4 is bounded by two limestone beds (a third bed is also present in the middle of the member; Fig. 2) and corresponds to red, green and grey mudstones deposited in a nearshore, low-energy environment. Finally, member 5 records a typical progradational sequence going from offshore to shoreface marine settings (Myrow, 1987).

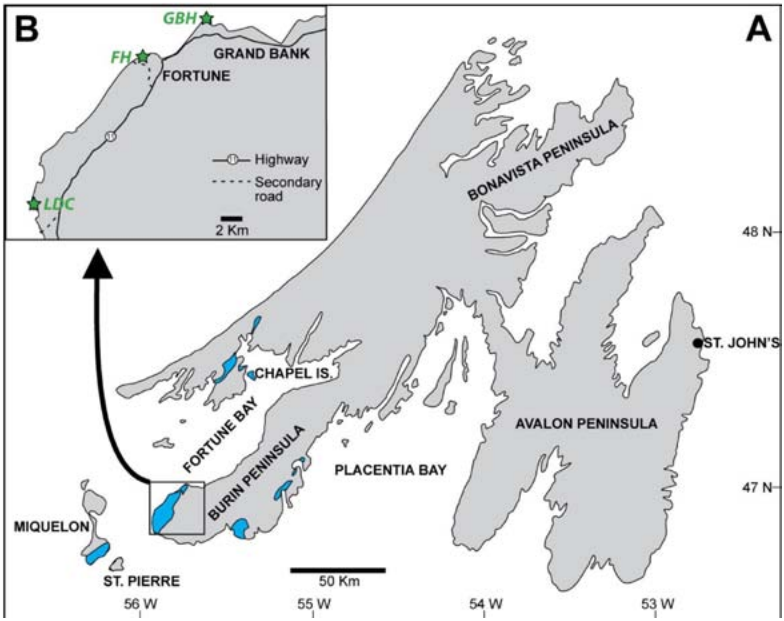


*Figure 1 | Location of the study in Newfoundland, eastern Canada. (A) Map of eastern Newfoundland, showing the location of the Burin Peninsula and the Cambrian outcrops (in purple). (B) Close up to the south-western part of the Burin Peninsula, with the three main outcrops of the study. GBH = Grand Bank Head; FH = Fortune Head; LDC = Little Dantzic Cove.*

Defining a GSSP from a trace fossil appearance is an unorthodox approach, other periods being usually placed at the first appearance of body fossils (e.g. graptolites, trilobites, ammonites). What makes T. pedum ichnofossil unique is its complex structure, recording horizontal to vertical, shallow infaunal probes of a possible priapulid worm (Vannier et al., 2010). Associated with treptichnids, an important set of ichnofossils characterize behavioral innovations. The helicoidal Gyrolithes, the plug-shaped Conichnus, the scratch marks Monomorphichnus or

the tri-lobate Curvolithus are some examples of this diversification in trace fossils reported since the base of the Cambrian (Narbonne et al., 1987; Laing et al. 2018). Conversely, Ediacaran strata only record simple horizontal trails associated with surficial microbial mats that typify an Ediacaran matground ecology (Fig. 3C). Thus, member 2 shows the first evidence for penetrative behaviors within the sediment, slightly destroying the sedimentary fabric, but maintaining an Ediacaran style ecology in the basal Fortunian part of the section (Buatois et al., 2014; Fig. 3A, 3C). Moreover, burrows from member 2 are characterized by sharp outlines without any reinforcement feature as well as insights of passive infill of open structures arguing for firmground seafloor condition (Droser et al., 2002). Uncontroversial evidence for arthropod-like organisms is displayed by the extremely shallow, delicate resting trace Rusophycus avalonensis that appears higher up in member 2 (Fig. 3D). In addition, first steps of more intense sediment reworking are revealed by the record of Psammichnites, a backfilled burrow produced by a shallow infaunal bulldozing organism (Fig. 3F). Deeper infaunal activity is also exposed by the presence of Teichichnus rectus, a vertical spreiten burrow found in abundance in the middle of member 3 (Fig. 3E). This diversification in trace fossils through the section is well known since the mid-eighties, but the changes in bioturbation levels and the influence of facies control has not been debated so far.

## 3. Objectives and preliminary results from the 2017 Summer Field Trip

In order to precisely decipher the changes in animal-sediment interaction trough the section, a careful bed-by-bed analysis of the three main outcrops is required. The 2017 Summer Field Trip objectives were threefold: (1) logging the sedimentary facies of the three main outcrops, by carefully looking at the bedding, architecture and sedimentary structures; (2) careful identification of trace fossils through the section, focusing on specific morphological features; and (3) recording the general change in bioturbation. Each of these three points will be detailed below.

For this field trip, facies logging was focused on Grand Bank Head and member 5 of Little Dantzic Cove sections. Grand Bank Head is located in the north-western point of the town of Grand Bank, by following the Admiral Cove walking trail. The outcrop is perfectly and continuously exposed from the top of the first red beds of member 2 to the top of the member (Fig. 2). Facies is dominantly composed of siltstone and very-fine to fine grained sandstone, ranging in thickness from millimeters to few decimeters (Fig. 3A). Gutter and pot casts are common, as well as many erosive bases. Thicker sandy beds show undulating to wavy tops, and lateral variation in thickness typifies hummocky-cross stratification bedding. Top of member 2 is marked by the development of carbonate concretions in a more silt-dominated facies reminiscent of member 3 facies (Fig. 2). Little Dantzic Cove represents a beautifully exposed but difficult to access outcrop, located at the westernmost point of the Burin Peninsula. After a 1.5 km hike, member 5 of the CIF is revealing a shallow marine progradational sequence on top of the last member 4 limestone bed (Fig. 2). Facies is represented at the base by green siltstone, being more and more intercalated by very-fine to medium-bedded, sometime highly bioturbated sandstones (Fig. 2, 3B). Top of member 5 is mostly represented by thick packages of fine red sandstone, ending up with few conglomeratic beds at the uppermost part of the section.

Secondly, trace fossils were carefully identified following a precise set of

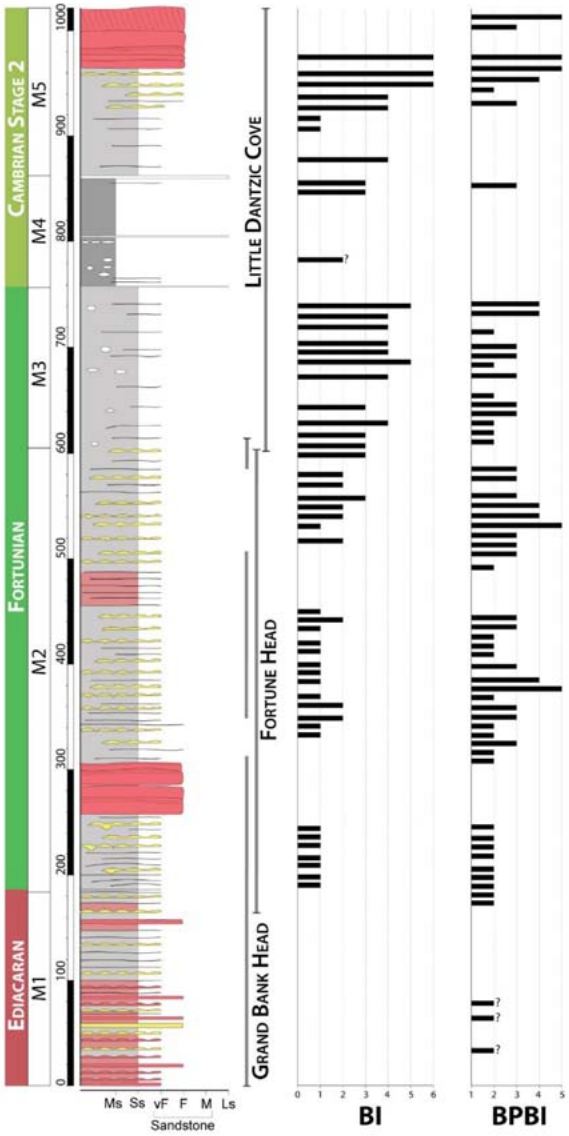


*Figure 2 | The Chapel Island Formation lithofacies and preliminary results. On the left side, a stratigraphic column (modified from Myrow, 1987) shows the five informal members of the formation, encompassing the Ediacaran to Cambrian Stage 2. On the right side, preliminary results on Bioturbation Index (BI, sensu Taylor and Goldring, 1993) and Bedding Plane Bioturbation Index (BPBI, sensu Miller and Smail, 1997) display the increase in animal-sediment interaction through the succession.*

morphological features. Ichnotaxobases permit to ascribe correctly a trace to its taxonomic name, by looking at the general form, the wall and lining, the branching pattern, the fill and additionally the presence of spreite (Bromley, 1996). Skolithos annulatus, a vertical burrow found in abundance in member 2 has been recently the topic of taxonomic reassessment, the general morphology showing evidence

of an affinity with spiral burrows Gyrolithes (Laing et al., 2018). In the same vein, careful examination of structures traditionally assigned to Taphrhelminthopsis and Helminthoida argues in favor of an affinity with Psammichnites. Notably, the presence of backfill (Fig. 3F) is the end result of bulldozing activity by a shallow infaunal organism. Originally, more than fifty different ichnotaxon were described by authors (Crimes and Anderson, 1985; Narbonne et al., 1987; Landing et al., 1988), but our first results tend to argue for a lower ichnodiversity. A correct and consistent taxonomic work is mandatory in order to track the changes in ichnodiversity and ichnodisparity through the succession, and thus unravel the accurate magnitude of behavioral innovations.

The general change in bioturbation intensity can be tracked by the use of two methods: the Bioturabation Index and the Bedding Plane Bioturbation Index. A Bioturbation Index (sensu Taylor and Goldring, 1993) focusses on the vertical reworking of sediment sea-floor by evaluating the intensity of disturbance of the original sedimentary fabric. Seven categories, from 0 to 100% of disturbance, typify this index. A critical point is to discriminate correctly the two extremes (0 and 100% disturbance) which can look closely similar and could lead to totally opposite conclusions. The Bedding Plane Bioturbation Index (sensu Miller and Smail, 1997) evaluates the degree of disturbance of base and top surfaces of well exposed beds in five discrete levels. By carefully collecting data following these two proxies, the seafloor turnover from Ediacaran matground to Phanerozoic mixground ecology known as the Agronomic Revolution (Seilacher, 1999) can be tracked through the section. Moreover, sampling of about 60 rock specimens along the CIF provides further data on the matter. Preliminary results (Fig. 2) reveal a general increase in both bioturbation indexes through the succession. Additional work remains to be done in order to carefully decipher the changes in ecospace utilization by organisms (i.e. by looking at the tiering patterns) in order to understand the major changes taking place in the benthos and affecting biogeochemical cycles during the early Cambrian.

## 4. Ongoing debate and future work

The definition of a GSSP on the first appearance of a trace fossil is the topic of controversy. Notably, the facies control observed during the Phanerozoic (at the base of the ichnofacies model of Seilacher, 1967) and the record of Treptichnus pedum below the boundary in the CIF (Gehling et al., 2001) are some of the main inquiries. About the latter issue, modern approaches on ichnostratigraphy argue for the use of a whole set of trace fossils that record major behavioral innovations at the base of the Cambrian and define a Treptichnus pedum Ichnological Zone (Landing et al., 2013; Laing et al., 2017). To solve the issue of facies control on trace fossil distribution, a comprehensive understanding of the sedimentary basin architecture aided by a sequence stratigraphic model is required in the CIF. Successful results on other Ediacaran-Cambrian sections (MacNaughton and Narbonne, 1999; Shahkarami et al., 2017) unraveled evolutionary changes as the first order control on ichnological diversity, and a similar approach on the CIF is the next step to this project.

## References

Brasier M., Cowie J. & Taylor M. 1994. Decision on the Precambrian-Cambrian boundary stratotype.

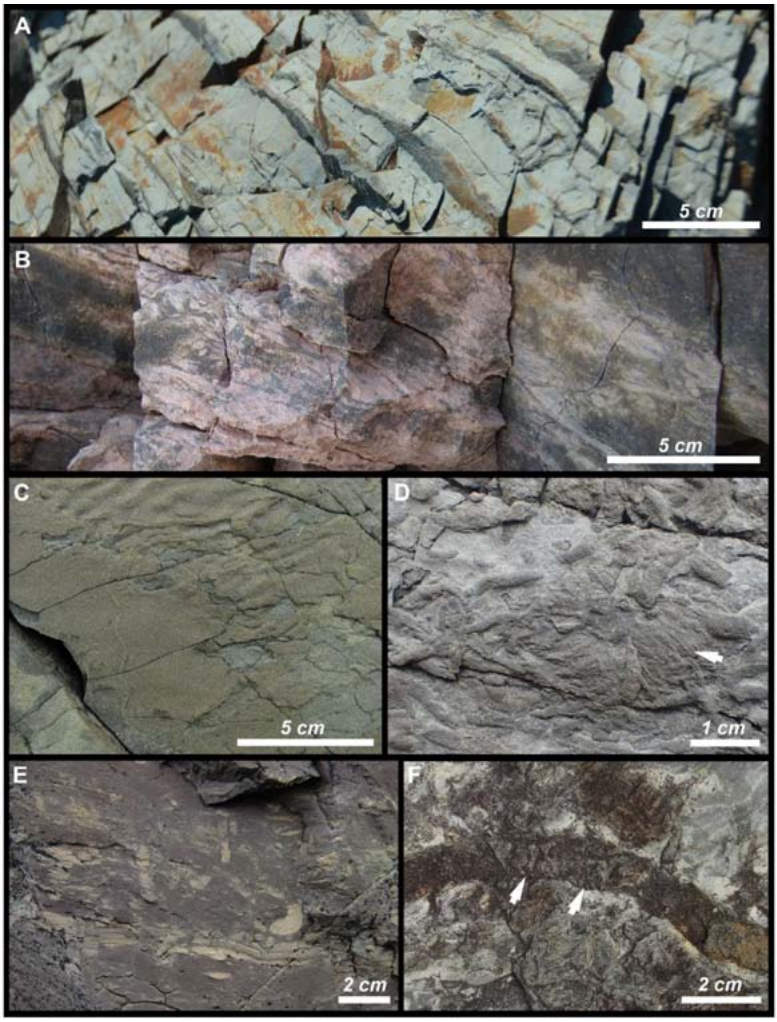


*Figure 3 | Facies, bioturbation and trace fossils from the Chapel Island Formation. (A) Heterolithic facies from member 2, Grand Bank Head, with well-preserved sanstone laminae and discrete trace fossils. BI = 1. (B) Highly bioturbated facies from middle of member 5, Little Dantzic Cove. BI = 5. (C) Ediacaran-style ecology, with horizontal grazing trail (Cochlichnus) and microbial mats from member 2, Fortune Head. BPBI = 2. (D) Delicate Rusophycus avalonsensis (arrow) overprinted with shallow infaunal burrows (treptichnids?). BPBI = 4. (E) Vertical spreiten burrow Teichichnus disturbing the sedimentary fabric from member 3, Little Dantzic Cove. BI = 3. (F) Bulldozing shallow infaunal burrow Psammichnites showing evidence of backfill (arrows) from member 3, Little Dantzic Cove. BPBI = 2.*

Episodes 17, 3-8.
Bromley R. G. 1996. Trace fossils: Biology, taphonomy and applications. London, Chapman and Hall, 361 pp.
Buatois L. A., Narbonne G. M., Mángano M. G., Carmona N. B. & Myrow, P. 2014. Ediacaran matground ecology persisted into the earliest Cambrian. Nature Communications 5, 1-5.
Buatois L. A., Wisshak M., Wilson M. A. & Mángano M. G. 2017. Categories of architectural designs in trace fossils: A measure of ichnodisparity. Earth-Science Reviews 164, 102-181.
Crimes T. P. & Anderson M. M. 1985. Trace fossils from Late Precambrian-Early Cambrian strata of southeastern Newfoundland (Canada): temporal and environmental implications. Journal of Paleontology 59, 310-343.
Droser M. L., Jensen S., Gehling J. G., Myrow P. M. & Narbonne G. M. 2002. Lowermost Cambrian ichnofabrics from the Chapel Island formation, Newfoundland: implications for Cambrian substrates. Palaios 17, 3-15.
Gehling J. G., Jensen S., Droser M. L., Myrow P. M. & Narbonne, G. M. 2001. Burrowing below the basal Cambrian GSSP, Fortune Head, Newfoundland. Geological Magazine 138, 213-218.
Laing B. A., Buatois L. A., Mángano G. M., Narbonne G. M. & Gougeon R. C. 2017. Trace fossil zonation at the Ediacaran-Cambrian GSSP. International Symposium on the Ediacaran-Cambrian Transition, Abstracts, p. 58.
Laing B. A., Buatois L. A., Mángano M. G., Narbonne G. M. & Gougeon R. C. 2018. Gyrolithes from the Ediacaran-Cambrian boundary section in Fortune Head, Newfoundland, Canada: Exploring the onset of complex burrowing. Palaeogeography, Palaeoclimatology, Palaeoecology 495, 171-185.
Landing E., Geyer G., Brasier M. D. & Bowring S. A. 2013. Cambrian evolutionary radiation: context, correlation, and chronostratigraphy - overcoming deficiencies of the first appearance datum (FAD) concept. Earth-Science Reviews 123, 133-172.
Landing E., Narbonne G. M., Myrow P., Benus A. P. & Anderson M. M. 1988. Faunas and depositional environments of the Upper Precambrian through Lower Cambrian, southeastern Newfoundland. New York State Museum Bulletin 462, 18-52.
MacNaughton R. B. & Narbonne G. M. 1999. Evolution and ecology of Neoproterozoic-Lower Cambrian trace fossils, NW Canada. Palaios 14, 97-115.
Miller M. F. & Smail S. E. 1997. A semiquantitative field method for evaluating bioturbation on bedding planes. Palaios 12, 391-396.
Myrow P. M. 1987. Sedimentology and depositional history of the Chapel Island Formation (Late Precambrian-Early Cambrian), southeast Newfoundland. Unpublished PhD thesis, St. John's, Newfoundland, Memorial University of Newfoundland, 512 p.
Narbonne G. M., Myrow P. M., Landing E. & Anderson M. M. 1987. A candidate stratotype for the Precambrian–Cambrian boundary, Fortune head, Burin Peninsula, southeastern Newfoundland. Canadian Journal of Earth Sciences 24, 1277-1293.
Seilacher A. 1967. Bathymetry of trace fossils. Marine Geology 5, 413-428.
Seilacher A. 1999. Biomat-related lifestyles in the Precambrian. Palaios 14, 86-93.
Shahkarami S., Mángano M. G. & Buatois L. A. 2017. Discriminating ecological and evolutionary controls during the Ediacaran–Cambrian transition: trace fossils from the Soltanieh Formation of northern Iran. Palaeogeography, Palaeoclimatology, Palaeoecology 476, 15-27.
Taylor A. M. & Goldring R. 1993. Description and analysis of bioturbation and ichnofabric. Journal of the Geological Society 150, 141-148.
Vannier J., Calandra I., Gaillard C. & yli ska A. 2010. Priapulid worms: Pioneer horizontal burrowers at the Precambrian-Cambrian boundary. Geology 38, 711-714.

# Facies and sedimentary evolution of the Upper Jurassic-Lower Cretaceous limestones from Piatra Craiului Massif, South Carpathians, Romania

*Cristian Victor Mircescu, Department of Geology, Babeş-Bolyai University, Cluj Napoca, Romania, mircescu_cristian2005@yahoo.com*

## 1. Background research

Piatra Craiului Massif is located in the easternmost part of the Southern Carpathians, Romania. The carbonate succession from this area forms a 20 km long, NE-SW oriented calcareous ridge. It consists of an Upper Jurassic-Lower Cretaceous prograding megasequence which has an average thickness of 800 m. Kimmeridgian-Tithonian limestones are forming the basal part of the carbonate succession. They are defined mainly by the presence of coral-microbial-microencruster boundstones. By contrast, the middle and upper part of the megasequence comprises peritidal deposits (internal platform subtidal, intertidal and supratidal carbonates) (Ple et al., 2013; Mircescu et al., 2014).

## 2. Preliminary findings

Several fieldwork campains were deployed in the summer of 2017 in order to study properly the peritidal component comprising the middle and upper part of the succession (Fig. 1).

*Fig. 1 Peritidal limestones from the upper part of the carbonate succession from the Piatra Craiului Massif (photo: Mircescu Cristian Victor) (scale: 1 m)*

However, a previous study involved the analysis and reinterpretation of an additional 800 thin sections which were collected from this area in the past five years. Detailed microfacies analysis indicates the presence of three distinct litostratigraphic intervals (Fig. 2). Litostratigraphic interval I is defined by alternating coral-microbial boundstones and bioclastic intraclastic rudstones. Corals are encrusted by different associations of encrusting organisms (Lithocodium/Bacinella type structures), worm tubes and calcareous sponges (Calcistella jachenhausenensis Reitner). The sedimentology of this lithostratigraphic interval is documented in detail by Ple et al., (2013).

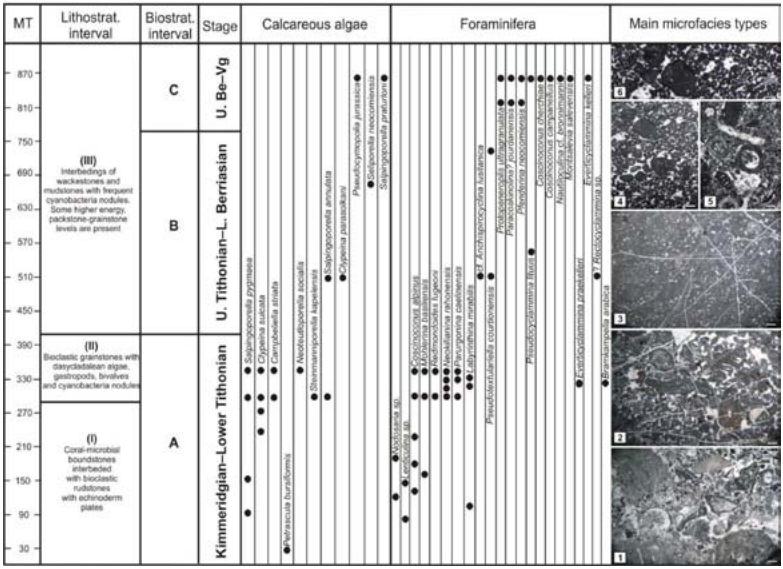


*Fig. 2 Lithostratigraphic and micropaleontological characteristics of the carbonate succession from the Piatra Craiului Massif [1-Bioclastic rudstone with coral fragments, echinoderm spines, dasycladalean algae (Salpingoporella pygmaea) and encrusting organisms (Crescentiella morronensis); 2-Coarse bioclastic intraclastic grainstone with cyanobacteria nodules, dasycladalean algae (Neoteutloporella socialis; Campbeliella striata) and gastropods. Black pebbles consist of blackened cyanobacteria nodules; 3-Peloidal fenestral packstone with cyanobacteria nodules; 4-Peloidal intraclastic grainstone with cyanobacteria nodules and angular/subangular micritic intraclasts; 5-Peloidal bioclastic intraclastic grainstone. Bioclasts: foraminifera (Bramkampella arabica), dasycladalean algae (Pseudocymopolia jurassica); 6-Peloidal grainstone with cyanobacteria nodules] (Scale bar: 1 mm).*

Litostratigraphic interval II includes the entire package of carbonate deposits between 290 and 408 meters of stratigraphic thickness (Fig. 2). The main facies type is coarse biontraclastic grainstones with gastropods, dasycladalean algae, sponges, echinoderm fragments and foraminifera (Fig. 2). Intraclasts are represented at some levels by various-sized black pebbles (mm to cm). Some have a brecciated structure consisting of blackened bioclasts encased in a muddy matrix which is pigmented with organic matter. In some cases they consist of darkened bioclasts (cyanobacteria nodules, dasycladalean algae). Litostratigraphic interval III comprises the middle and upper parts of the carbonate deposits from the Piatra Craiului Massif (between 408 and 880 m) (Fig. 2). Peloidal wackestone-packstone facies alternate with homogeneous mudstones with cyanobacteria. However, some levels of of bioclastic packstone/grainstone with dasycladalean algae and foraminifera were also identified in the uppermost part of this interval (Fig. 2). Several biostratigraphic intervals were defined by interpreting a micropaleontological association which consists of foraminifera and dasycladalean algae (Fig. 2).

Approximately 950 samples were collected from two type sections (Ciorânga-Vf. Ascu it-Padinile Frumoase; Upper Vl du ca) in the summer of 2017 (Fig. 3) by carefully sampling each carbonate bed. Key features such as bed thickness, macrofacies characteristics and vertical stacking patterns were taken into account in order to reconstruct the evolution of the peritidal component from the upper part of the carbonate succession. Bed thickness usually changes from centimeter thick beds (approx. 10-20 cm) to decimeter thick beds (80-90 cm). Bed contacts are sharp. In both sections, the reefal limestones belonging to litostratigraphic interval I are overlain by 30 m of coarse bioclastic grainstones belonging to litostratigraphic interval II. They contain frequent black pebbles which are sometimes encased in a muddy, red matrix with abbundant iron oxides. The base of the peritidal succession is formed by this level which can be traced through all the studied sections. Microfacies analysis suggests that the limestones belonging to litostratigraphic interval II were subaerially exposed. This hypothesis is strengthened by the presence of micritic mensiscus cements, vadous silt and dog-tooth type cements within the black pebbles bearing limestones.

IAS funding was required to perform isotope analysis on 50 powders extracted from samples of the Ciorânga-Vf. Ascu it and Zaplaz-Lan uri sections (Fig. 4). By integrating microfacies analysis results and geochemistry one could infer that a possible exposure event occured accross the entire carbonate platform, at the top of litostratigraphic interval I.

Powders were produced either from red sediment consisting of iron oxide pigmented grainstone carbonate or from black pebble type intraclasts (Table 1). Few exceptions included sampling from micritic oncoids and undifferentiated carbonate

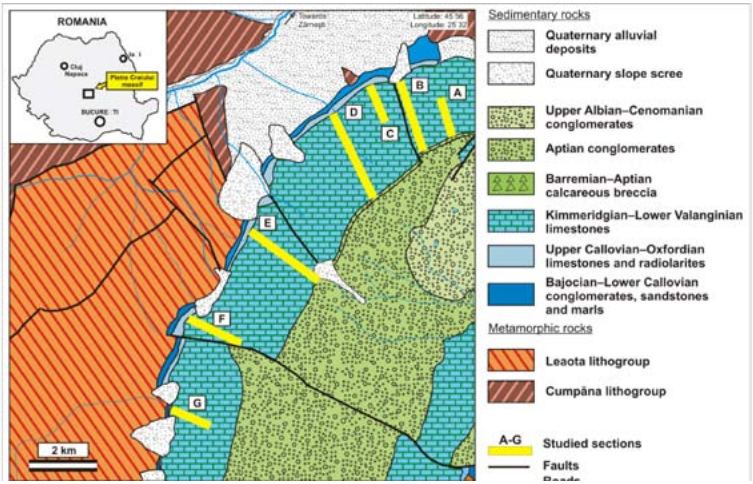


Fig. 3 Location of studied sections on the geological map of the Piatra Craiului Massif (modified from Dimitrescu et al. 1971; 1974; Patrulius et al. 1971; S ndulescu et al. 1972) (A-Curm tura-Turnu; B-Padina Închis -Drumul lui Lehmann; C-Padina Popii; D-Ciorânga Mare-Vf. Ascu it-Padinile Frumoase; E-Vl du ca de Vest-Vl du ca de Est; F-Zaplaz-Lan uri; G-Padina L ncii).

material. By integrating microfacies analysis results and geochemistry one could infer that a possible exposure event occured accross the entire carbonate platform, at the top of litostratigraphic interval I.

In terms of values, two distinct trends were recorded. All the samples from the Ciorânga-Vf. Ascu it section record positive -13C values, between 0.61 ‰ and 2.40 ‰ with several variation tendencies. These values show an abrupt increase from 0.92 ‰ to 2.58 ‰ followed by an important decrease to 0.61 ‰. They increase again to 2.05 ‰ just to remain relatively constant until 2.32 ‰. Another decreasing trend is recorded (1.21 ‰) which is followed by relatively constant values (1.47 ‰). A last significant decrease to 0.97 ‰ is followed by an increase to 2.05 ‰. By contrast, the samples from the Zaplaz-Lan uri section have negative -13C values. They range between -0.62 ‰ and -1.92 ‰. Only the first two samples record positive values of 1.92 ‰ and 1.95 ‰ (Table 1).

-18O values show negative tendencies in both studied sections. They range between -1.51 ‰ and -3.80 ‰ in the Zaplaz-Lan uri section, with similar values for the Ciorânga-Vf. Ascu it section (minimum of -4.03 ‰ and maximum of -1.07 ‰) (Table 1).

## 3. Significance

Three informal litostratigraphic intervals are defining the overal regresive carbonate megasequence from the Piatra Craiului Massif. The existing micropaleontological assemblage provides additional paleoenvironmental data regarding the associated depositional environments. Several chronostratigraphic units were defined by interpreting this microfossil association. Thus, biostratigraphic interval A corresponds to the Kimmeridgian-Tithonian, biostratigraphic interval B characterises the late Tithonian-early Berriasian while biostratigraphic interval C indicates the upper Berriasian-? early Valanginian.

In terms of geochemistry, the negative -13C values suggest a Lower Tithonian subaerial exposure event. This hypothesis is strengthened also by the available microfacies and microfossil data. A negative -13C value may indicate an increase of the organic carbon content (Saltzmann and Thomas, 2012). Primary and diagenetic factors have a strong impact on such depleted -13C values (Colombié et al. 2012). A primary control on the depletion of -13C could be associated with vital effects such as respiration and photosynthesis (Colombié et al. 2012 sensu Auclair et al., 2004; Patterson and Walker, 1994). Organic matter oxidation represents another factor which contributes substantially to the depletion of the -13C (Joachimski, 1994). Depleted -13C values may be associated with freshwater input and early meteoric diagenesis (Allan and Matthews, 1982; Moore, 2001; Patterson and Walter, 1994). Durring subaerial exposure marine carbonates are placed in the vadose zone where they react with meteoric water. An important effect of this interaction is represented by the carbon isotope exchange between -13C enriched sediments and the -13C depleted vadose water. This process generates the -13C depletion of the sediments (Yang, 2001). A certain degree of -13C variability may be observed in the Zaplaz-Lan uri section. The first two samples have positive values while the rest of them show negative trends. In addition, the transition from positive to negative values is relatively abrupt (1.95 ‰ to – 1.11) and even the negative values record some fluctuations. By contrast, the -18O curve has constant

values, only with some minor exceptions. Highly variable -13C associated with relatively constant -18O are key features which define meteoric systems were depleted CO2 is common in soil areas (Allan and Mathews, 1982; Lohmann, 1988; Immenhauser et al., 2003)

Further research requires the integration of isotope chemostratigraphy, biostratigraphy and sequence stratigraphy data in order to reconstruct the geological evolution of the Upper Jurassic-Lower Cretaceous carbonate succession from the Piatra Craiului Massif.

| Section | Sample number | Result $\delta$-$^{13}C_{V\text{-}PDB}$ (‰) | Result $\delta$-$^{18}O_{V\text{-}PDB}$ (‰) | Sample description |
|---|---|---|---|---|
| ZL | 11718 | 1.95 | -1.51 | Carbonate sediment |
| ZL | 11719 | 1.92 | -3.80 | Micritic oncoids |
| ZL | 11722 | -1.11 | -2.48 | Black pebbles |
| ZL | 11722 | -0.71 | -2.71 | Red sediment |
| ZL | 11723 | -1.07 | -1.84 | Red sediment |
| ZL | 11723 | -1.26 | -2.54 | Black pebbles |
| ZL | 11724 | -1.11 | -1.73 | Red sediment |
| ZL | 11726 | -1.19 | -2.22 | Black pebbles |
| ZL | 11726 | -0.62 | -1.46 | Red sediment |
| ZL | 11727 | -1.43 | -1.87 | Red sediment |
| ZL | 11727 | -1.37 | -1.65 | Black pebbles |
| ZL | 11728 | -0.69 | -1.20 | Black pebbles |
| ZL | 11728 | -1.41 | -1.50 | Red sediment |
| ZL | 11729 | -1.45 | -2.10 | Red sediment |
| ZL | 11729 | -1.29 | -1.91 | Black pebbles |
| ZL | 11730 | -1.92 | -1.77 | Red sediment |
| ZL | 11731 | -1.85 | -1.76 | Red sediment |
| ZL | 11732 | -0.92 | -1.74 | Grey-greenish silt |
| ZL | 11733 | 0.01 | -3.36 | Red sediment |
| CM-VA | 1082 | 0.92 | -3.93 | Oncoids |
| CM-VA | 1083 | 0.66 | -4.03 | Oncoids |
| CM-VA | 1084 | 1.00 | -3.17 | Undif. sediment |
| CM-VA | 1086 | 1.52 | -2.50 | Brown-red sediment |
| CM-VA | 1086 | 2.40 | -1.07 | Undif. sediment |
| CM-VA | 1087 | 2.58 | -1.26 | Undif. sediment |
| CM-VA | 1089 | 1.07 | -3.62 | Undif. sediment |
| CM-VA | 1090 | 1.17 | -3.56 | Oncoids |
| CM-VA | 1093 | 0.61 | -3.03 | Oncoids |
| CM-VA | 1094 | 2.05 | -1.33 | Green silt |
| CM-VA | 1095 | 1.99 | -1.68 | Black pebbles |
| CM-VA | 1095 | 2.32 | -1.14 | Undif. sediment |
| CM-VA | 1096 | 1.78 | -1.77 | Green silt |
| CM-VA | 1097 A6 | 1.57 | -1.89 | Red sediment |
| CM-VA | 1097 C1 | 1.61 | -1.42 | Red sediment |
| CM-VA | 1097 B | 1.45 | -2.10 | Red sediment |
| CM-VA | 1098 C1 | 1.21 | -1.80 | Black pebbles |
| CM-VA | 1098 C1 | 1.91 | -1.47 | Undif. sediment |
| CM-VA | 1098 B | 1.47 | -1.66 | Black pebbles |
| CM-VA | 1098 B | 0.97 | -1.98 | Undif. sediment |
| CM-VA | 1097 A1 | 2.05 | -1.68 | Red sediment |
| CM-VA | 1101 | 1.35 | -1.99 | Black pebbles |
| CM-VA | 1102 | 1.37 | -1.84 | Undif. sediment |

*Table 1. Ş13C and Ş18O data. Carbonate powders are extracted from samples belonging to the Ciorânga Mare-Vf. Ascuşit and Zaplaz-Lanşuri sections (ZL-Zaplaz-Lanşuri section. CM-VA-Ciorânga Mare-Vf. Ascuşit section).*

## References

Allan, J. R., Matthews, R. K. (1982). Isotope signatures associated with early meteoric diagenesis. Sedimentology, 29, 797-817.

Auclair, A. C., Lecuyer, C., Bucher, H., Sheppard, S. M. F. (2004). Carbon and oxygen isotope composition of Nautilus macromphalus: a record of thermocline waters off New Caledonia. Chemical Geology, 207, 91-100.

Colombié, C., Lécuyer, C., Strasser, A. (2012). Carbon-and oxygen-isotope records of palaeoenvironmental and carbonate production changes in shallow-marine carbonates (Kimmeridgian, Swiss Jura). Geological Magazine, 148(1), 133-153.

Dimitrescu, R., Patrulius, D., Popescu, I. (1971). Geological map of Romania, 1:50.000, sheet 110c. Institutul Geologic i Geofizic al României, Bucure ti (in Romanian).

Dimitrescu, R., Popescu, I., Schuster, C.A. (1974). Geological map of Romania, 1:50.000, sheet 110a. Institutul Geologic i Geofizic al României, Bucure ti (in Romanian).

Immenhauser, A., Della Porta, G., Kenter, J. A. M., Bahamonde, J. R. (2003). An alternative model for positive shifts in shallow-marine carbonate -13C and -18O. Sedimentology, 50, 953-959.

Lohmann, K. C. (1988). Geochemical Patterns of Meteoric Diagenetic Systems and Their Application to Studies of Paleokarst. In: N. P., James et al. (eds.), Paleokarst, 58-80.

Mircescu, C. V., Bucur, I. I., S s ran E. (2014). Dasycladalean algae from Upper Jurassic-Lower Cretaceous limestones of Piatra Craiului Massif (South Carpathians, Romania) and their relationship to paleoenvironment. Studia UBB Geologia, 59(1) (for 2013), 5-27.

Moore, C. H. (2001). Carbonate Reservoirs: Porosity evolution and diagenesis in a sequence stratigraphic framework. Elsevier, 460 p.

Patterson, W. P., Walter, L. M. (1994). Depletion of 13C in seawater ∑CO2 on modern carbonate platforms: Significance for the carbon isotopic record of carbonates. Geology, 85, 885-888.

Patrulius, D., Dimitrescu, R., Popescu, I. (1971). Geological map of Romania, 1:50.000, sheet 110d. Institutul Geologic i Geofizic al României, Bucure ti (in Romanian).

Ple , G., Mircescu C. V., Bucur I. I., S s ran, E. (2013). Encrusting micro-organisms and microbial structures in Upper Jurassic limestones from the Southern Carpathians (Romania). Facies, 59, 19-48.

Saltzmann, M. R., Thomas, E. (2012). Carbon Isotope Stratigraphy. In: Gradstein, F., Ogg, J., Schmitz, M., Ogg, G. (eds.), The Geologic Time Scale, 1144 p.

S ndulescu, M., Popescu, I., S ndulescu, J., Mih il , N., Schuster, C. A. (1972). Geological map of Romania, 1:50.000, sheet 110b. Institutul Geologic i Geofizic al României, Bucure ti (in Romanian).

Yang, W. (2001). Estimation of duration of subaerial exposure in shallow-marine limestones-an isotopic approach. Journal of Sedimentary Research, 71(5), 778-789.

# TRACE ELEMENTS AND STABLE ISOTOPES WITHIN RECENT AND MODERN TRAVERTINES AND ASSOCIATED MICROBIAL MATS IN THE "LOS HORNOS" HOT SPRING, CATAMARCA, ARGENTINA: ORGANO-MINERAL INTERACTIONS AND TEXTURES DEVELOPMENT

*R.A. Mors*
*Centro de Investigaciones en Ciencias de la Tierra, Facultad de Ciencias Exactas, Físicas y Naturales,*
*CONICET, Universidad Nacional de Córdoba, Córdoba, Argentina,*
*ragustinmors@gmail.com*

## INTRODUCTION

The "Los Hornos" hot spring, located at the southern Puna of Catamarca, Argentina, is an active hydrothermal complex characterized by temperatures up to 65 Celsius degrees and pH average 6.5. Where hydrothermal upwelling systems or vents are developed, ponds with microterracettes, pisolitic acumulations and staggered fluvial travertines are distinguished. The vents are colonized by different groups of extremophile microorganisms (photo- and chemo-trophos), controlled by local changes in pH and temperature. These microbial communities are associated with precipitated carbonate minerals, salts and iron oxides. Laterally, to the present day hot spring, lies a fossil travertine body up to 40m thick. This important travertinic-tuffaceous fossil record will be used as a fossil analogue of the currently active system.

The main objective of our project is to conduct a detailed and high-resolution sedimentological, geomicrobiological, petrographic-petrophysical and geochemical study of active travertine and tufa systems to understand mineral precipitation processes and biogeochemical signatures there preserved. This is intended to build a model for the development of the different textures and fabrics. Geochemical and isotopic signals preserved in recent/ancient carbonates and from the present hydrothermal/tufaceous waters, are essential to achieve this goal, because they could help on the better understanding of the microbiological and physico-chemical controls.

### *METHODS*

Water samples for the determination of cations, anions, 13C of DIC, 2H and 18O were taken within the "Los Hornos" active carbonate system, at different locations: pristine "Los Hornos" river (point 66 in table 1 and figure 1), "Los Hornos" hot spring field one (point 67 in table 1 and figure 1), "Los Hornos" hot spring field one prime (point 68 of table 1), "Los Hornos" hot spring field two (points 69-A1 to 69-A4 in table 1 and figure 1), "Los Hornos" hot spring field

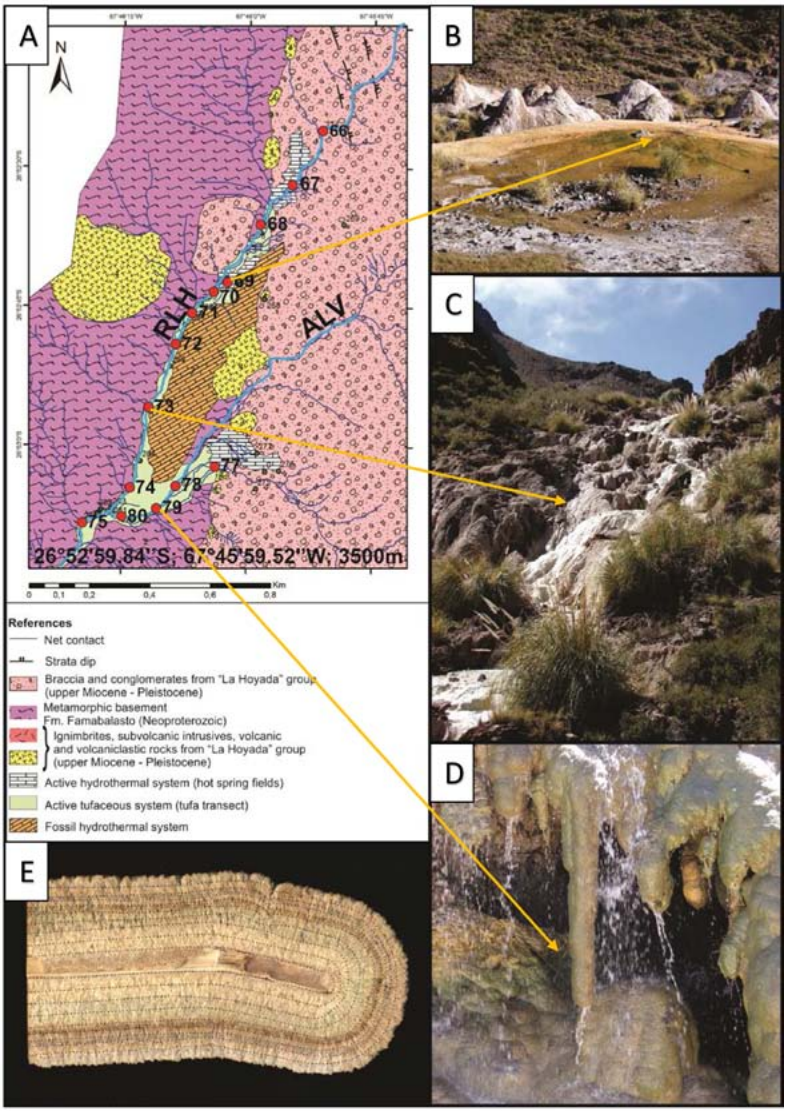


*Figure 1 - A. Shows a detailed map of the "Terma Los Hornos" study area. Red points are indicating the sampling locations; B. "Los Hornos" active hot spring (field two); C. "Los Hornos" tufaceous river; D. Stalactites developed in a waterfall at "Las Vizcachas" tufaceous creek; E. Longitudinal section of the sampled stalactite.*

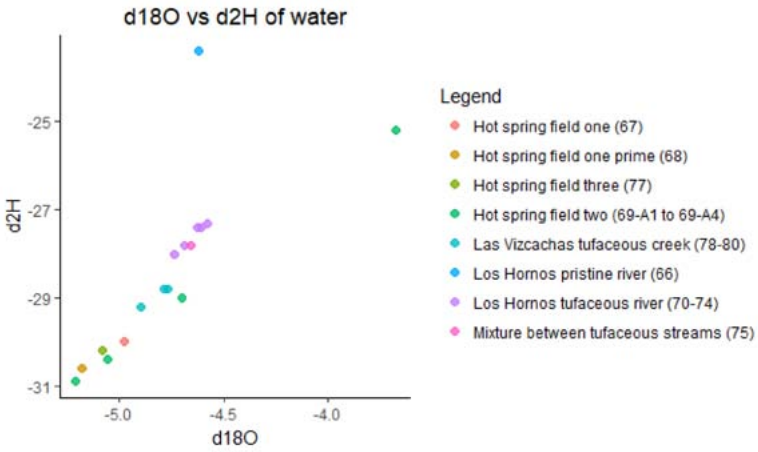


*Figure 2 - Stable hydrogen and oxygen isotope ratios of water samples took from every different water source detected in the active system.*

three (point 77 in table 1 and figure 1), transect realized at "Los Hornos" tufaceous river (points 70-74 in table 1 and figure 1), transect realized at "Las Vizcachas" tufaceous creek (points 78-80 in table 1 and figure 1) and at the mixture between tufaceous streams (point 75 in table 1 and figure 1). At same points, samples of carbonates, developed in chemical equilibrium with water, were taken for cations, anions, mineralogy, petrography, 13C and 18O determination, in order to perform a complete geochemical modeling of the carbonate system. Stalactites developed below waterfalls at the "Las Vizcachas" tufaceos creek (point 79 in table 1 and figure 1), were also sampled to examine their potential as paleoclimatic archives. At every point of water collection, pH and temperature values were measured with Oakton Acorn Series pH 5/6 & Ion 5/6 probe. Alcalinity and dissolved CO2 were also measured at each site using a test kit Hach FF-3 model.

Water samples for measurements of cations and anions were collected via syringe and passed through a 0.4µm filter to fill 50ml sterilized falcon tubes with no headspace. Samples for metal analysis were acidified with four drops of ultrapure nitric acid. On the other hand, water samples for 13C of DIC, 2H and 18O were collected via syringe and passed through a 0.4µm to fill 30ml sterilized glass tubes with no headspace. Rubber caps were sealed with parafilm tape to avoid gaseous exchange with the atmosphere. Using microdrilling technics, carbonate powders were performed from recent carbonate samples that were taken from every water sampling point and from several sheets of the stalactite.

Cations and anions concentrations are still being analized at the LABGEO – CICTERRA – CONICET – UNC laboratory, using inductively coupled plasma mass spectroscopy (ICP-MS, Agilent 7500CX, gas He y Ar) and ion chromatography with coupled anion separation column (Thermoscientific Constametric 3500, Dionex Ion Pack522, suppressor ARS-300 4mm), respectively. Due to quantification limits of the devices, samples were diluted.

The δ13C of DIC, δ2H - δ18O and δ13C - δ18O determination were performed

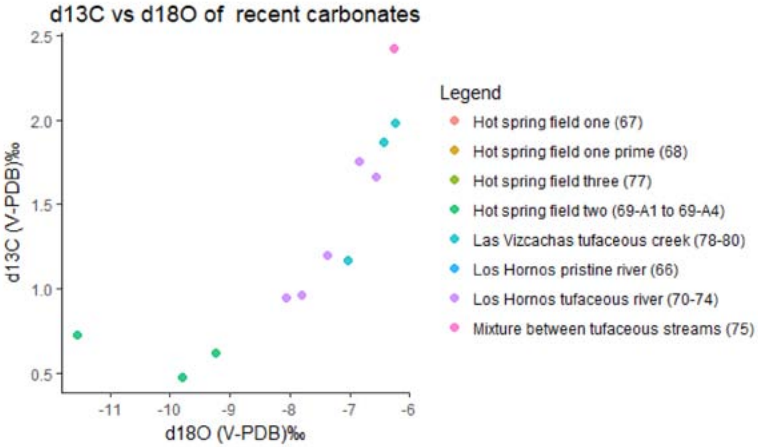


*Figure 3 - Stable carbon and oxygen isotope ratios of carbonate minerals took at every water sampling point.*

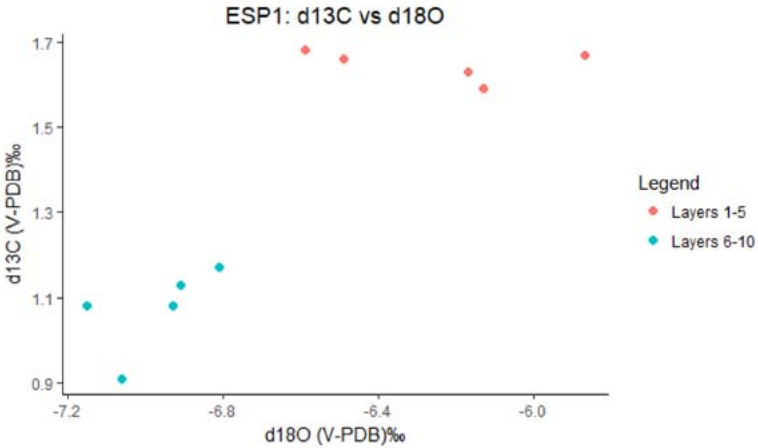


*Figure 4 - Stable carbon and oxygen isotope ratios of carbonate minerals took from every layer of the stalactite (see figure 1).*

at Centro de Pesquisas Geocronológicas CPGeo – USP. For determination of δ2H and δ18O, samples were analized with a cavity ringdown laser spectrometer (PICARRO – L2130i), and the data set was processed by a LIMS software, following "A Laboratory Information Management System for Stable Hydrogen and Oxygen Isotopes in Water Samples by Laser Absorption Spectroscopy: User Manual & Tutorial - Revision 2.0 2015/09/11" manual instructions. All

| ID | CARBONATES STABLE ISOTOPES RESULTS | | | | WATER STABLE ISOTOPES RESULTS | | | | DISTANCIA |
|---|---|---|---|---|---|---|---|---|---|
| | d $^{13}$C (V-PDB)‰ | SD d$^{13}$C‰ | d $^{18}$O (V-PDB)‰ | SD d$^{18}$O‰ | d$^{18}$O | SD d$^{18}$O | d$^{2}$H | SD d$^{2}$H | |
| 66 | NA | NA | NA | NA | -4,62 | 0,09 | -23,40 | 0,90 | 7.58 |
| 67 | NA | NA | NA | NA | -4,98 | 0,09 | -30,00 | 0,90 | 224.1 |
| 68 | NA | NA | NA | NA | -5,18 | 0,09 | -30,60 | 0,90 | 454.91 |
| 69 | NA | NA | NA | NA | -5,21 | 0,09 | -30,90 | 0,90 | 630.73 |
| 069-A2 | 0,73 | 0,04 | -11,55 | 0,06 | -5,06 | 0,09 | -30,40 | 0,90 | 633.73 |
| 069-A3 | 0,48 | 0,05 | -9,80 | 0,06 | -4,70 | 0,09 | -29,00 | 0,90 | 637.73 |
| 069-A4 | 0,62 | 0,04 | -9,25 | 0,02 | -3,68 | 0,09 | -25,20 | 0,90 | 645.73 |
| 070 | 0,96 | 0,04 | -7,81 | 0,05 | -4,74 | 0,09 | -28,00 | 0,90 | 727.84 |
| 071 | 0,95 | 0,04 | -8,06 | 0,04 | -4,69 | 0,09 | -27,80 | 0,90 | 830.22 |
| 072 | 1,20 | 0,05 | -7,37 | 0,06 | -4,58 | 0,09 | -27,30 | 0,90 | 986.32 |
| 073 | 1,75 | 0,04 | -6,85 | 0,05 | -4,63 | 0,09 | -27,40 | 0,90 | 1191.3 |
| 074 | 1,66 | 0,03 | -6,56 | 0,04 | -4,61 | 0,09 | -27,40 | 0,90 | 1434.81 |
| 075 | 2,42 | 0,04 | -6,27 | 0,06 | -4,66 | 0,09 | -27,80 | 0,90 | 1585.32 |
| 77 | NA | NA | NA | NA | -5,08 | 0,09 | -30,20 | 0,90 | 1108.44 |
| 078 | 1,17 | 0,04 | -7,03 | 0,07 | -4,90 | 0,09 | -29,20 | 0,90 | 1231.35 |
| 079 | 1,87 | 0,03 | -6,43 | 0,05 | -4,79 | 0,09 | -28,80 | 0,90 | 1316.79 |
| 080 | 1,98 | 0,03 | -6,25 | 0,04 | -4,77 | 0,09 | -28,80 | 0,90 | 1499.62 |
| ESP1-1 | 1,67 | 0,04 | -5,87 | 0,06 | NA | NA | NA | NA | NA |
| ESP1-2 | 1,59 | 0,04 | -6,13 | 0,06 | NA | NA | NA | NA | NA |
| ESP1-3 | 1,63 | 0,04 | -6,17 | 0,04 | NA | NA | NA | NA | NA |
| ESP1-4 | 1,66 | 0,03 | -6,49 | 0,04 | NA | NA | NA | NA | NA |
| ESP1-5 | 1,68 | 0,03 | -6,59 | 0,05 | NA | NA | NA | NA | NA |
| ESP1-6 | 1,13 | 0,04 | -6,91 | 0,05 | NA | NA | NA | NA | NA |
| ESP1-7 | 0,91 | 0,04 | -7,06 | 0,04 | NA | NA | NA | NA | NA |
| ESP1-8 | 1,08 | 0,04 | -7,15 | 0,04 | NA | NA | NA | NA | NA |
| ESP1-9 | 1,08 | 0,04 | -6,93 | 0,04 | NA | NA | NA | NA | NA |
| ESP1-10 | 1,17 | 0,04 | -6,81 | 0,05 | NA | NA | NA | NA | NA |

*Table 1 - Preliminary stable isotopes results: δ13C & δ18O for carbonates samples and δ2H & δ18O for water samples.*

samples were corrected using IAEA international standards and/or internal standards calibrated by the IAEA (SD: ±0.09 for δ18O and ±0.9 for δ2H. The δ13C of dissolved inorganic carbon (DIC) determination was performed using a ThermoFinnigan Delta Plus Advantage mass spectroscopy device (IRMS) coupled with a ThemoFinnigan Gas-Bench-II online preparation system. The δ13C - δ18O from recent carbonates minerals were determined in a continuous flow mode using a Thermo Finnigan GasBench II coupled to a Delta V Advantage IRMS. Ratios were determined on evolved CO2 gas released from carbonate minerals by reaction with orthophosphoric acid at 72°C for the carbonate rock. Results are reported in conventional per mil notation (‰) relative to Vienna Pee-Dee Belemnite (VPDB) standard for carbon and oxygen. Accuracy of the analysis was ±0.02‰ for δ18O and ±0.03‰ for δ13C, and the analytical precision was better than ±0.08‰ for δ18O and ±0.07‰ for δ13C average of last three years 2014/2015/2016/SN=206.

## RESULTS

Preliminary stable isotopes results (δ13C and δ18O of carbonates samples, δ13C of dissolved inorganic carbon, and δ2H and δ18O for water samples) are shown at table 1. Although data set has not yet been analyzed in depth, some preliminary results catch on sight when it is plot.

Stable hydrogen and oxygen isotope ratios of water samples are showing

values near to those shown in global meteoric water line graphics (Figure 2). This conclusion allows to despise a juvenile water spring associated with an active magmatic chamber hypothesis. Although pristine river and hydrothermal/tufaceous system isotope ratios values are plotted near the global meteoric water line, they aren't isotopically the same (Figure 2). So, assuming that the "Los Hornos" pristine river is the source of the hot spring waters related to the active travertine/tufa system, the isotopic differences could be related to: a) long transfer time from the sink point to the different hot spring vents, allowing the surge of past meteoric waters; or b) a rapid change of water isotopic due to the transmission of hot meteoric water through a highly fractured/weathered basement.

Stable carbon and oxygen isotope ratios of carbonate minerals took at every water sampling point (hydrothermal/tufaceous system) are showing a progressively enrichment in $^{13}C$ and $^{18}O$ as it increases the distance from the hot spring source (Figure 3). This is probably related to constant evaporation/degasification of water. Once the $^{13}C$ of DIC results are ready, an isotopic comparison between water and recent carbonate deposits will be done, and the evaporation/degasification hypothesis will be tested, if so, a normal Rayleigh fractionation behavior is expected.

Stable carbon and oxygen isotope ratios of carbonate minerals took from every layer of the stalactite (see figure 1) are showing two different groups (figure 4). This grouping could be explained by a climate change, impacting in the isotopic of the water source and consequently in the stable carbon and oxygen isotopic signal of carbonates. Even that, when stalactite data set is plotted with the rest of the carbonate deposits along the hydrothermal/tufaceous system (figure 5), the two different groups now are coinciding with different degasification states in the active system. So, maybe the isotopic differences between the first and the second five sheets inside the slactite is not only showing a climate change, but also an increase in the distance of the hot spring source, or a change in the topography that could impact in the turbulence of the creek, and with that, in the degasification and the final isotopic signal. This last hypothesis should not be despised, especially considering the rapid geomorphological changes that these systems suffer due to the high precipitation rate.

# Incorporation of atmospheric radiocarbon into coral during laboratory preparation

*Philip Staudigel, RSMAS, Miami, USA*
*pstaudigel@rsmas.miami.edu*

## Introduction:

At elevated temperatures, aragonite will spontaneously convert to calcite. This transition has been demonstrated to facilitate isotopic exchange with available CO2 (Staudigel and Swart, 2016). This exchange is sufficient to cause a significant covariance between the 13C and mineralogy of the material (Figure 1). The heat produced during drilling can be sufficient to facilitate these reactions (Figure 2), and thus may present a vector for contaminating isotopic analyses. If, during drilling, isotopically "young" atmospheric carbon is exchanged with an isotopically "older" aragonite archive, radiocarbon dating may yield an erroneously young age estimate.

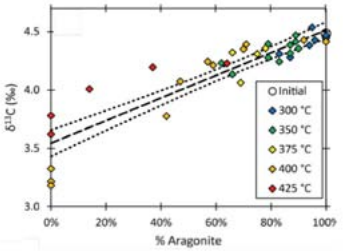


*Figure 1: Sclerosponge aragonite incorporating atmospheric ş13C values as it converts to calcite in direct heating experiments. Modified from Staudigel and Swart (2016).*

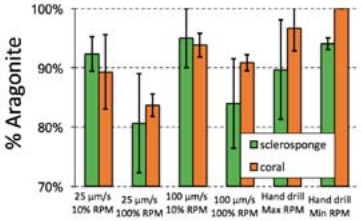


*Figure 2: Mineralogy of powder liberated from initially aragonite sclerosponge and coral using a Micromill and handheld drill. Data from Staudigel and Swart (2016).*

## Methods:

In this study, a Pleistocene-aged (~130 ka) coral was sampled using a variety of techniques to determine the effect this atmospheric contamination has on radiocarbon dates. Powder was liberated using a handheld drill, a micromill and a mortar and pestle. One sample from the mortar and pestle was heated to 400°C for 90 minutes, which was predicted to convert a significant fraection of the carbonate to calcite. Each sample yielded approximately 50 mg of carbonate, which was split into two aliquots, one for isotopic analysis and one for XRD analysis for mineralogy. After the powders were liberated, 9-10 mg were immediately transferred to copper boat and stored in vacuum. This powder was reacted with concentrated phosphoric acid at 90°C for 30 minutes. These samples were frozen into an evacuated Pyrex™ using liquid nitrogen. The tube was sealed using a propane torch and stored at room temperature prior to being shipped to

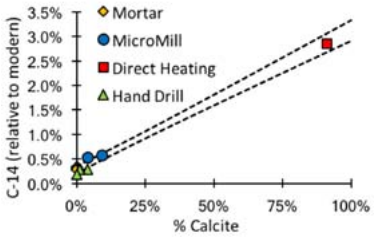


*Figure 3: Radiocarbon abundance of samples collected using different sample preparation techniques plotted relative to mineralogy. Dashed lines display ±95% uncertainty for linear regression.*

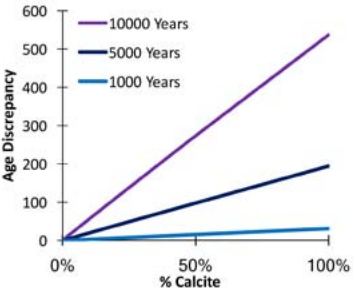


*Figure 4: Modeled C-14 age discrepancy expected from atmospheric carbon exchange during the aragonite-calcite transition of corals of variable age.*

NOSAMS. The remaining powder was analyzed using X-Ray Diffractometry to determine the relative fraction of aragonite and calcite.

## Results/Discussion:

Samples incorporated up to 3% atmospheric radiocarbon and different sampling methods resulted in significantly different incorporation of radiocarbon. In total, 9 samples were analyzed, the results being displayed in table 1. There is a highly significant co-variance between the relative conversion to calcite and the abundance of atmospheric radiocarbon ($p = 2 \times 10^{-8}$) shown in figure 3, although this relationship is heavily biased by the sample heated in an oven prior to analysis. With this sample removed, there still exists a linear relationship, although it is less significant ($p = 0.015$).

Micromilling incorporated significantly more atmospheric radiocarbon that hand drilling ($p = 1.3 \times 10^{-4}$, Student's T-Test). Drilling samples by hand did not result in significnatly different incorporation compared to using a mortar and pestle ($p = 0.19$, Student's T-Test). The degree of conversion to calcite in these experiments was relatively minor, compared to other similar experiments (e.g. Figure 2), thus the contamination in other similar experiments may have been higher.

Because of the relative scarceness of radiocarbon in the sample used for this study, even a relatively small degree of radiocarbon contamination (e.g. 0.4% rather than 0.2%) would result in potentially halving the estimated age.

The extent of radiocarbon contamination, as well as the significance of its effect, would be diminished in younger samples. In order to demonstrate this, we model the incorporation of radiocarbon using the linear relationship derived in our experiments. This linear relationship diminishes such that if age = 0, slope = 0. Using this method, the deviation in estimated age can be calculated for any degree of conversion to calcite for a sample of any age, the output of this model shows results for 1000, 5000 and 10,000 year old samples. If, during sampleing, a sample is converted by 10% from aragonite to calcite, these models predict an offset in age of 3 years for a 1000 year old specimin, a 20 year offset for a 5000 year old

| Preparation Method | %Calcite | Radiocarbon abundance (%Modern) |
|---|---|---|
| Mortar + Pestle | 0 | 0.33% |
| Mortar + Pestle | 0 | 0.29% |
| Micromill | 9% | 0.57% |
| Micromill | 4% | 0.53% |
| Hand Drill | 4% | 0.28% |
| Hand Drill | 1% | 0.29% |
| Hand Drill | 1% | 0.29% |
| Hand Drill | 0% | 0.18% |
| Direct heating 400°C | 91% | 2.86% |

specimin and a 55 year offset for a 10,000 year old specimin. These offsets are relatively minor for small degrees of conversion, although the discrepancy increases roughly linearly with greater conversion to calcite.

## Conclusions/future work:

The results of this study are promising, atmospheric radiocarbon is incorporated into aragonite samples when heated during normal sample preparation techniques, the extent of which varies in relation to the degree of conversion to calcite. Therefore, the mineralogy can be used as a "canary in the coalmine" for atmospheric carbon contamination. We therefore propose that aragonite mineralogy should be confirmed prior to radiocarbon analysis, to confirm that atmospheric contamination has been minimized.

Future work on this subject should evaluate this behavior in other aragonite materials, which may be more, or less, susceptible to conversion to calcite. Denser materials may result in greater drill heating, and thus more significant conversion.

We are grateful to the IAS for providing funding for these analyses, and to the laboratory staff at NOSAMS/WHOI.

# The stratigraphy and sedimentary provenance of late Mesozoic strata in the Great Artesian Basin, Australia, and the reconstruction of the tectonic history and palaeodrainage evolution of eastern Australia

*Christopher N. Todd*
*Geosciences Department, James Cook University, Townsville, QLD, Australia*
*christopher.todd@my.jcu.edu.au*

## Introduction

The Jurassic to Early Cretaceous in northeastern Australia remains a poorly understood time in geologic history. The tectonic setting of the northeastern margin is not known due to a lack of contemporaneous deposits, sedimentary or igneous, preserved on the present-day coastline. However, significant intracratonic basins were forming with vast quantities of sediment, including volcanogenic sediments, being deposited from the margin towards depocentres in the continental interior; sediments which we can study. Previous investigations have resulted in two dominant hypotheses regarding the tectonic setting and source of these sediments: a volcanic arc that spread along the entire eastern margin throughout the Mesozoic (Veevers, 2006) or numerous failed rifts off the eastern margin that preceded the opening of the Coral Sea Basin in the Cenozoic (Fielding, 1996).

Additionally, the final depocentre of these sediments is also undetermined. Some suggestions include the Ceduna Delta off the coast of South Australia, consisting of Permian to Cretaceous aged sediments from across eastern Australia (Lloyd et al., 2016). This is disputed by other authors who instead suggest that sediments in the delta were derived from a more proximal location (MacDonald et al., 2013).

By studying the sedimentary rock record from Australia's eastern basin system, a better understanding of palaeodrainage evolution can be determined (sensu Shaanan and Rosenbaum, 2016). Indeed, coupling sedimentary studies with advanced provenance approaches, including U-Pb geochronology, Lu-Hf isotope geochemistry and trace element geochemistry of glass melt inclusions in detrital zircons, a more holistic understanding of the timing, tectonic processes, and palaeogeography can be achieved for the late Mesozoic of eastern Australia.

## Methodology

This project utilises a previously untested method of sedimentary provenance called sedimentary petrochronology. Based on a metamorphic geology approach, this technique involves the combination of LA-ICP-MS U-Pb detrital zircon geochronology, LA-MC-ICP-MS Lu-Hf isotopic analysis, and microprobe analysis of melt inclusions in detrital zircons. In association with sandstone petrography, palaeocurrent analysis, palynology and fieldwork methods, this technique will aid in the determination of sedimentary provenance, in particular the origin and sources of previously unknown Mesozoic volcanic sediments in the Great Artesian Basin.

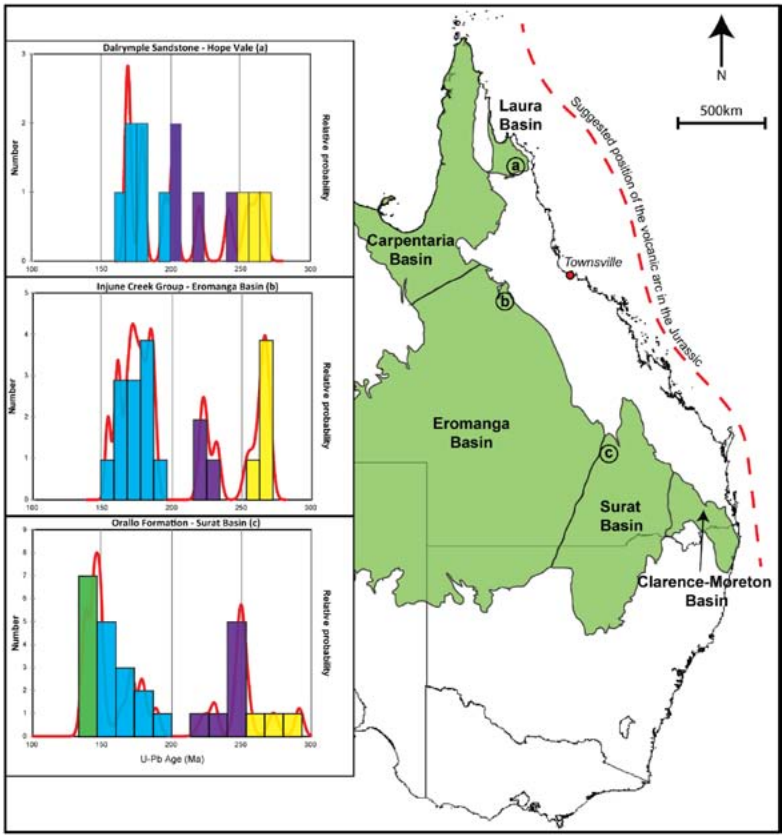


*Figure 1. U-Pb detrital zircon geochronology frequency distribution diagrams and spatial positions for the Dalrymple Sandstone, Injune Creek Group and Orallo Formation.*

## Results

The results herein are strictly related to those collected through the allocation of the 1000 Post-Graduate Research Grant Scheme funding provided by the IAS. This funding was put towards a single day of U-Pb detrital zircon geochronology using LA-ICP-MS at the Advanced Analytical Centre facilities at James Cook University in Townsville, Australia. This time equates to three samples analysed.

The analysed detrital zircon samples for this report were collected from the Late Jurassic Dalrymple Sandstone near Hope Vale, Far North Queensland, the Middle Jurassic Injune Creek Group of the Hughenden region of northern Queensland, and the Early Cretaceous Orallo Formation of south central Queensland (Figure 1). These fluvial units were selected because they are suggested to represent the time periods most likely to yield the Jurassic aged grains that have been missing from the record so far, and so these Jurassic ages and their implications will be the only things discussed here.

The Dalrymple Sandstone contained some Jurassic zircons, with the youngest population at ~169 ± 2.3 Ma, the next population at ~179 Ma, and the final population at ~200 Ma. The Injune Creek Group has a single concordant grain age at ~155 Ma, but an older population at ~162 Ma, followed by populations at ~173 Ma, ~179 Ma and ~185 Ma. The Orallo Formation contained a significant number of Jurassic grains, with major populations at ~145 Ma, ~150 Ma, ~170 Ma and ~180 Ma.

## Discussion

The ages of the populations in these samples suggest that Jurassic volcanogenic sediments were indeed being deposited into continental sedimentary basins, albeit discontinuously and in smaller amounts. This trend is different from the Cretaceous, Triassic, and even Permian periods in northeastern Australia which contain continuous signals of grains in vast quantities over a significant length of time (Tucker et al, 2016).

Palaeocurrent data that has been collected previously indicates that these sample sites were fed by sediments flowing in an overall westerly direction. This suggests that the sources of these detrital zircons must be from the eastern Australian continental margin. When the eastern continental margin rifted away in the Late Cretaceous, the remaining coastline was uplifted (R.A. Henderson, pers. comm.). This may have led to a lack of preservation of Jurassic aged sediments east of these continental basins, meaning their exact source is still undetermined. Further work with Lu-Hf isotopic analysis and glass melt inclusions in Jurassic zircons will provide a better understanding of the composition of the parent magma and may answer the question regarding the main tectonic driver of this volcanism.

## References

Fielding, C.R. 2001. Mesozoic sedimentary basins and resources in eastern Australia – a review of current understanding, IN: Mesozoic Geology of the Eastern Australian Plate Conference Book, pp. 180-185.

Lloyd, J., Collins, A.S., Payen, J.L., Glorie, S., Holford, S. & Reid, A.J. 2016. Tracking the Cretaceous transcontinental Ceduna River through Australia: The hafnium isotope record of detrital zircons from offshore southern Australia. Geoscience Frontiers, 7, pp. 237-244.

MacDonald, J.D., Holford, S.P., Green, P.F., Duddy, I.R., King, R.C. & Backe, G. 2013. Detrital zircon data reveal the origin of Australia's largest delta system. Journal of the Geological Society, London, 170, pp. 3-6.

Shaanan, U. & Rosenbaum, G. 2016. Detrital zircons as palaeodrainage indicators: insights into southeastern Gondwana from Permian basins in eastern Australia. Basin Research, doi:10.1111/bre.12204

Tucker, R.T, Roberts, E.M., Henderson, R.A., Kemp, A.I.S. 2016. Large igneous province of long-lived magmatic arc along the eastern margin of Australia during the Cretaceous? Insights from the sedimentary record. Geological Society of America Bulletin. Doi:10.1130/B31337.1

Veevers, J.J. 2006. Updated Gondwana (Permian-Cretaceous) earth history of Australia. Gondwana Research, 9, pp. 231-260.

# Geochemical characterization of eolian sediments of the Pampean Plain, Argentina.

*Gabriela Torre*
*Universidad Nacional de Córdoba, Cordoba Argentina*
*gabrielatorre@unc.edu.ar*

## Introduction

Rocks and minerals have different isotope ratios depending, among other things, on their geological origin and age of formation. As the same time, the isotopic compositions are also significantly different in the rocks that derive from the mantle and the crust, allowing as a first step, a distinction between lithologies with extreme origins. Many authors (e.g., Gousset et al., 1992; Basile et al., 1997; Walter et al., 2000; Delmonte et al., 2004; Gaiero et al., 2007; Grousset et al., 2005; Biscaye and Grousset, 2008) have demonstrated the importance of the use of radiogenic isotopes (e.g., Sr, Nd and Pb) when dealing with studies of origin or traceability of sediments, since they maintain and inherit the isotopic composition of the source area of the which they derive. For example, sediments that are deflated or removed by the wind from continental areas become excellent natural tracer of atmospheric circulation because they are: a) are transported great distances, b) suffer little chemical modifications during transport and, c) endure in complete climate cycles.

Among the isotopes in sediments, there are some that are used as a diagnostic of the provenance of the material from a particular rock source (i.e., Sr, Nd, Pb, Hf, etc). Strontium (Sr) is a divalent alkaline earth element having four naturally occurring isotopes: 84Sr, 86Sr, 87Sr, 88Sr. Only 87Sr is radiogenic and it is produced by radioactive decay of 87Rb. The isotopic ratio 87Sr/86Sr is used to obtain information about the origin and the geological processes that affected a rock from the moment of its formation. During the Earth's geological history the amount of 87Sr has increased since the initial 87Sr present at the time of the formation of the first earth crust has been added 87Sr-radiogenic produced by the radioactive decay of 87Rb. As a consequence, the 87Sr/ 86Sr ratio in the cortex is higher and proportional to age. Therefore, those rocks formed by fusion or assimilation of cortical materials will have higher 87Sr/86Sr ratios than those derived from the mantle. Thus, the utility of the Rb/Sr isotopic system is important because different rocks or minerals from a given geological environment may have different 87Sr/86Sr ratios depending on the age and the original Rb/Sr ratio of that rock or mineral.

Neodymium (Nd) is an element of the rare earth group that belongs to the lanthanide series and is never found in nature in the free state. The Nd has seven natural isotopes: 142Nd, 143Nd, 144Nd, 145Nd, 146Nd, 148Nd and 150Nd. Among them, 142Nd and 143Nd are radiogenic isotopes produced by the decay of 146Sm and 147Sm respectively. During partial melting processes, Nd tends to concentrate in the liquid phase, while the Sm is concentrated in the residual phase. This preferential fractionation of Nd in the molten phase is responsible for the relative enrichment of the rocks of cortical origin of this element with respect to Sm. The

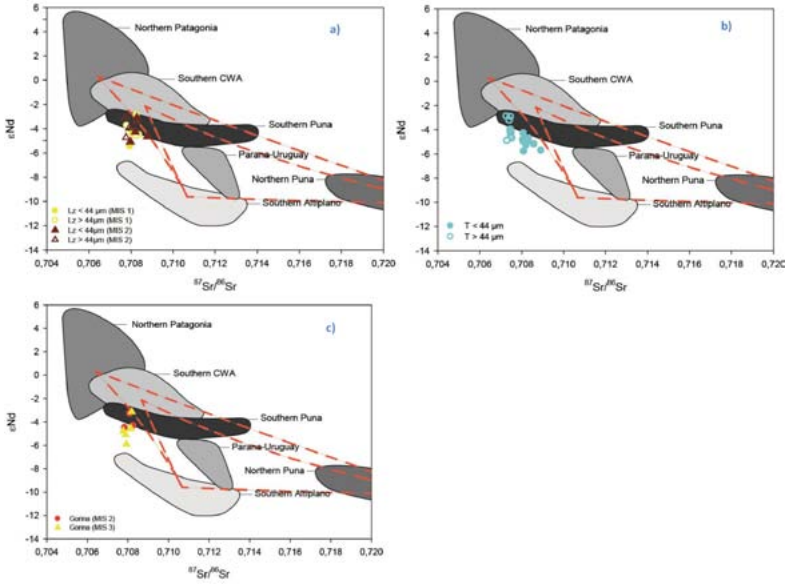


*Figure 1. Isotopic composition of loess samples in terms of 87Sr/86Sr vs εNd compared with previous data of the potential source areas of southern South America (Gili et al., 2016) a) Data from Lozada section, b)data from Tortugas profile and c) is the data from Gorina's quarry. Discontinuous red lines represent the mixing lines between the different potential source areas. Loess samples have been dated by OSL and are represented according to which MIS (Marine Isotope Stage) correspond.*

isotopic composition of Nd is expressed by the 143Nd/144Nd ratio of the rock to the current value of CHUR (Chondritic Uniform Reservoir).

By analyzing the isotopic compositions expressed in terms of 87Sr/86Sr and 143Nd/144Nd ratios of the Pampean loess sediments in three different sections (i.d. Lozada, Tortugas and Gorina), this study aims to determine the isotopic signal of the eolian sediments. Comparing this result with the geochemical signals of the potential source areas of southern South America we can obtain an approach of the provenance of the windblown material and determine the atmospheric paleocirculation.

Materials and Methods The isotopic composition of the sediments, measured in terms of 87Sr/86Sr and 143Nd/144Nd ratios of 50 loess samples (20 = >63 µm, 20 = <63 µm and 10 total samples) were analyzed in external laboratories (EcoLab and GET Institute, Toulouse, France).

100 mg of loess sample were brought into solution by tri-acid attack (HF-HNO3-HCl) using Teflon Savillex containers. Once in solution, the Sr and Nd atoms of the samples were chemically separated from the rest of the elements through chromatographic columns following standard techniques (Richard et al., 1976; Pin et al., 1994; Goldstein et al. 2003). For Sr separation, the samples were purified

on 30 µL columns using Eichrom Sr Spec resin and HNO3 3N. For the separation of Nd, 100 µL columns were first used with TRU-Spec resin and HNO3 1,6N to separate the rare earth elements (ETR) from other cations and then in columns of 800 µL pure Nd was obtained.

Isotopic ratios were then analyzed by Thermal Ionization Mass Spectrometry (i.e. Sr and Nd isotopes, TIMS - Thermal Ionisation Multicollector Mass Spectrometry -).

Results

The Nd isotopic data was reported as Nd (0):

$$\varepsilon Nd = \left[ \frac{\left(^{143}Nd/^{144}Nd\right)}{\left(^{143}Nd/^{144}Nd\right)_{CHUR}} - 1 \right] * 10^4$$

The CHUR (Chondritic Uniform Reservoir) has a value of 0,512638 (Jacobsen y Wasserburg, 1980). Samples from Lozada and Tortugas were analyzed in two fractions in order to separate in the two granulometric populations that are observed in the grain size distribution. The purpose of analyzing the geochemical signal for each population is to see if both correspond to the same source. For the Gorina section, the measurement of Sr and Nd was performed with the total of the sample.

## References

Basile, I., Grousset, F.E., Petit J.R., Biscaye, P.E. and Barkov, N.I. (1997) Patagonian origin of glacial dust deposited in E. Antarctica (Vostok and Dome C) during glacial stages 2, 4 and 6. EPLS. 146, 573-589.

Delmonte, B., et al. (2004).Comparing the Epica and Vostok dust records during the last 220,000 years: stratigraphical correlation and provenance in glacial periods. Earth Planetary Science Letters 66, 63-87. Faure, M., Monié, P., Pin, C., Maluski, H., & Leloix, C. (2002). Late Visean thermal event in the northern part of the French Massif Central: new 40Ar/39Ar and Rb–Sr isotopic constraints on the Hercynian syn-orogenic extension.International Journal of Earth Sciences, 91(1), 53-75.

Gaiero DM, Depetris PJ, Probst JL, Bidart SM and Leleyter L, (2004). The signature of river- and wind-borne materials exported from Patagonia to the southern latitudes: A view from REEs and implications for paleoclimatic interpretations. Earth Planet Sci Lett. 219, 3-4, 357-376. Gili, S., & Gaiero, D. M. (2015). south American dust signature in geological archives of the southern Hemisphere. DUST, 24, 78. Goldstein, S. L., & Hemming, S. R. (2003). Long-lived isotopic tracers in oceanography, paleoceanography, and ice-sheet dynamics. Treatise on geochemistry, 6(6), 453-489.

Grousset F.E., Biscaye P. E., 2005. Tracing dust sources and transport patterns using Sr, Nd and Pb isotopes. Chem. Geol. 222, 149-167. Jacobsen, S. B., & Wasserburg, G. J. (1980). Sm-Nd isotopic evolution of chondrites. Earth and Planetary Science Letters, 50(1), 139-155. Pin, C., Briot, D., Bassin, C., & Poitrasson, F. (1994). Concomitant separation of strontium and samarium-neodymium for isotopic analysis in silicate samples, based on specific extraction chromatography. Analytica Chimica Acta, 298(2), 209-217. Walter, M. R., Veevers, J. J., Calver, C. R., Gorjan, P., & Hill, A. C. (2000). Dating the 840–544 Ma Neoproterozoic interval by isotopes of strontium, carbon, and sulfur in seawater, and some interpretative models. Precambrian Research, 100(1), 371-433. Wegner, A., P. Gabrielli, D. Wilhelms-Dick, U. Ruth, M. Kriews, P. De Deckker, C. Barbante, G. Cozzi, B. Delmonte, and H. Fischer (2012), Change in dust variability in the Atlantic sector of Antarctica at the end of the last deglaciation, Clim. Past, 8, 135–147, doi:10.5194/cp-8-135-2012.

# AN INVESTIGATION OF THE EFFECT OF IMPACT PROCESSES IN SUBSEQUENT ROCK BREAKDOWN

*Ankit K. Verma*
*Department of Geography,*
*Trinity College Dublin*
*vermaan@tcd.ie*

## Introduction

Impact cratering is one of the catastrophic geologic processes that have modified the surfaces of all terrestrial bodies. Impacts are instantaneous events and the process has aneffect on the target geology and lithology. While several studies have investigated the morphology, structure, erosion and degradation of the crater landform on Earth and Mars (Kenkmann et al., 2014), relatively few have examined the effect of inheritance on subsequent rock breakdown. As rock breakdown is an important process that contributes to the evolution of landforms and sediments on many planetary bodies, it is important to assess the role of inheritance on the subsequent breakdown style and rate of impacted rocks.

A spherical shock wave generated during an impact event travels radially in all directions, but the amplitude of the shock decays exponentially with distance due to the consumption of energy (Kenkmann et al., 2014). This suggests that rocks closer to the point of impact have experienced more shock related deformation than rocks at a far distance. In the case of porous rocks like sandstone this effect would be more pronounced (Kenkmann et al., 2014).

The interaction of shock pressure of several gigapascals can exceed the effective strength of target lithology by three to four orders of magnitude and is responsible for melting, vaporisation, shock metamorphism, fracturing and fragmentation of rocks, deformation features, and high-pressure mineral phase transformations (Melosh, 1989). Many researchers have identified distinct diagnostic features of impact shock such as shatter cones, shock metamorphism, planar deformation features, and high-pressure mineral phase transformations (Kieffer, 1971, Ferrière and Osinski, 2013, Kenkmann et al., 2014). However, a large portion of rocks in impact craters shows no sign of shock metamorphism and plastic deformation, but are deformed at the sub-shock level by brittle fracturing mechanisms (Kowitz et al., 2013, Kenkmann et al., 2014). The resultant rock characteristics are influenced by a complex set of processes that involve shock, temperature, pressure and initial target rock properties. During impact, the rock porosity and permeability can change (Cockell and Lim, 2005). However, the shock environment and the target lithology are important influences on the effects. Low shock pressures (<5 GPa) cause pore collapse whereas high shock pressures (>10, <25 GPa) can cause vesiculation (Kieffer, 1971). If impacted rocks are subject to longer-term heating and annealing during crater cooling, the porosity and permeability will be further affected. For highly porous substrates (such as sandstones), more of the impact energy is taken up in pore collapse. Earlier studies have demonstrated that pore geometry affects rock susceptibility to

breakdown and controls the intensity of breakdown (Tu rul, 2004 and references therein).

Once emplaced erosional processes gradually rework ejecta material, breaking down larger debris and reducing vertical relief (Chapman, 2007). Similar to other subaerial rocks, impacted rocks and ejecta are affected by mechanical, thermal and chemical processes. Environmental conditions and heterogeneities in rock properties exert an important control in rock breakdown. The focus of this study is to understand how the inheritance from the impact process affects the subsequent breakdown of rocks at impact sites.

## Study Site

### *Meteor Crater*

Meteor Crater, Arizona is a classic simple impact crater and one of the best-preserved impact craters on Earth. It is selected for this study because the target was sedimentary rocks. Of the 184 known impact structures on Earth, approximately 70% occur full or partly on sedimentary rocks which possess a varying degree of porosity (Earth impact database). Other planetary surfaces are covered widely by porous regolith, breccias, rubbly material, and some even exhibit porous aeolian or fluvial sediments. Meteor Crater is located in a relatively low-relief portion of the southern part of the Colorado Plateau near the town of Winslow in north-central Arizona (Shoemaker, 1987). This 50,000-year-old impact crater was formed by hypervelocity impact of an iron meteorite in nearly flat-lying Paleozoic and Mesozoic sedimentary rocks of Colorado Plateau, underlain by Precambrian crystalline basement (Chapman, 2007, Newsom et al., 2013). Three principal formations: The Coconino Formation (Permian), the Kaibab Formation (Permian) and the Moenkopi Formation (Triassic), comprise 99% of the target lithology and ejecta (Kring, 2007). Additional details of these lithologies can be found elsewhere (chapter 2 of Kring (2007), and references therein). Meteor Crater provides an excellent opportunity to study the effect of rock breakdown processes on impacted rocks. What is key to this field site is that there are good exposures of the same formation (e.g., Moenkopi) that were not affected by the impact process nearby. Therefore, we have the potential to isolate unique and accelerated rock breakdown states that are specific to the impact process.

*Fig 1. Meteor Crater in Arizona (looking toward East crater wall).*

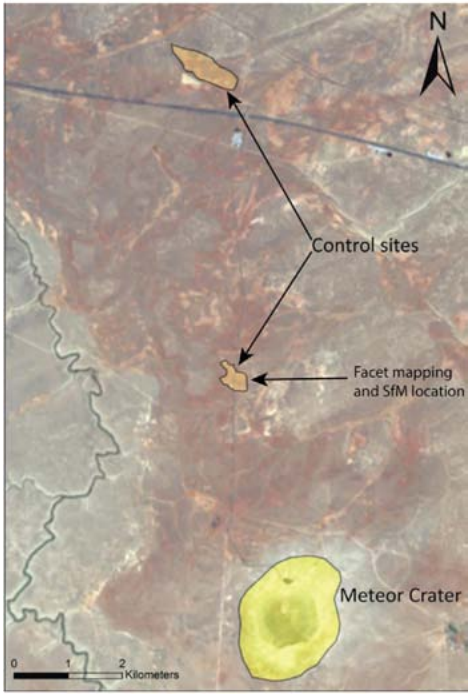


*Fig 2. This map shows the location of the Meteor Crater and control sites.*

### *Control sites*

The Moenkopi formation is extensively exposed at the surface of the Mogollon Slope surrounding Meteor Crater. We selected two sites of Moenkopi formation that were not affected by impact shock outside Meteor Crater as control sites (see Fig 2). At these sites Moenkopi formation bedrocks/boulders are well exposed. These sites are easily accessible by road. The first control site is approximately 9 kilometres to the north of Meteor Crater. The second control site is located along the Meteor Crater road, 4-5 kilometres from the Meteor Crater.

## Methodology

A combination of field and laboratory approaches were used to examine the effect of impact processes on rock breakdown.

## Field work

Traditional field mapping and extensive sampling techniques were used to characterise study site geology. Specific meso to micro-scale (meter to mm) rock breakdown features were recorded and classified using facet mapping (Heslop 2003) at Meteor Crater site in Arizona. Structure from Motion (SfM) photogrammetry (Micheletti et al., 2015) was used to generate sub-mm Digital Elevation Models of weathered rock surfaces. These data were used to classify

morphometric rock surface features and to establish relative style of development

of rock breakdown between impacted and non-impacted sites. Rock hardness was measured at Meteor Crater using the Schmidt hammer (Viles et al., 2011). During our field work at Meteor Crater, we collected data at 4 Moenkopi Sandstone exposures on NW crater wall at the Meteor Crater. We also collected similar data on 100 Moenkopi boulders and bedrock at the two control site areas (see Fig 2).

## Laboratory work

A number of Laboratory analysis were performed on impacted and non-impacted rock samples that were collected from Meteor Crater site in Arizona. Quantitative X-ray Diffraction(XRD) analysis was used to describe the mineral composition and to measure silica polymorph abundances in 4 Moenkopi Sandstone samples from Meteor Crater (Kieffer, 1971). This is necessary to classify rock samples into various shock pressure classes. Petrographic microscope and Scanning Electron Microscope (SEM) analysis was used to identify the composition (mineral composition, grain size, grain size distribution, grain contact, porosity, grain shape, matrix, sorting, and matrix-grain-ratio), weathering (secondary alteration minerals, grain disintegration, grain shape, secondary porosity, fracture patterns), and impact associated deformation of the rock (Krinsley et al., 2005, Hamers and Drury, 2011).

## Preliminary Results

A range of rock breakdown features observed at both the Meteor Crater and the control site include flaking, granular disintegration, cracks, alveoli, grus, exfoliation, splitting, tafoni, pachydermal weathering, spalling, crumbling, multiple splits, aeolian etching, and lichen-associated breakdown.

The preliminary findings from laboratory analysis has indicated that Moenkopi Sandstone exposed at Meteor Crater and control sites are similar in terms of mineral composition and physical properties (e.g. grain size and sorting). However, we have detected that the impact process has caused grain compaction and reduced the porosity in Moenkopi Sandstone at Meteor Crater. Field data has revealed differences in breakdown features in Moenkopi Sandstone at Meteor Crater and control sites. This may be due to change in porosity of Moenkopi sandstone caused during impact at Meteor Crater.

Facet mapping of breakdown features revealed difference in occurrence of some breakdown features on Moenkopi Sandstone boulders at Meteor Crater and control sites. Alveolar weathering, rounding/notching, lichen colonization, were not observed on boulders from Meteor Crater (see Fig 5). Dependent fissures were not observed on boulders outside Meteor Crater (control site) (see Fig 5). This analysis has revealed differences in breakdown features present on Moenkopi Sandstone boulders at Meteor Crater and control site. Previous weathering studies have shown that porosity plays a major role in the breakdown of Sandstone (Tu rul, 2004 and references therein). Our analysis has revealed that porosity of Moenkopi Sandstone at Meteor Crater is less compared to control sites. This could suggest that reduced porosity in Moenkopi Sandstone at Meteor Crater may be responsible for difference in style and intensity of breakdown compared to control sites.

Rock hardness data suggests that the average Schmidt hammer results are similar but the distribution of this data is different. It may mean that rocks at one site may be more weathered.

In percent area of morphometric classes, at 1×1 cm and all classes, there


*Fig 3. Rock breakdown features observed at control sites (a) Exfoliation and flaking in Moenkopi Sandstone. (b) Intense spalling in Moenkopi Sandstone. (c) Alveoli and granular disintegration in Moenkopi Sandstone. Granular disintegration produced loose, coarse-grained debris inside the alveoli. (d) Split Moenkopi Sandstone boulder. Grus or debris apron dominant in the sand and gravel-sized material at the base of the block. (e) Very well developed alveoli in Moenkopi Sandstone. Top of this rock is covered with black, yellow and white colored lichens. A 30 cm ruler has been used for scale.*

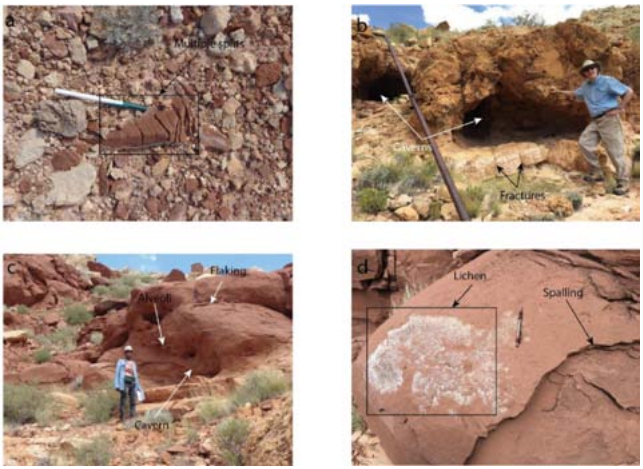


*Fig 4. Rock breakdown features observed at Meteor Crater (a) Multiple splits in the Moenkopi sandstone. A pen is used for scale. (b) Cavernous weathering in Kaibab dolomitic limestone. (c) Cavernous weathering in Moenkopi Sandstone. Alveoli and flaking were seen on the walls and the base of the cavern. (d) Beside the cavernous weathered Moenkopi Sandstone, spalling and white-coloured lichens seen on the top of the sandstone. A pen is used for scale.*

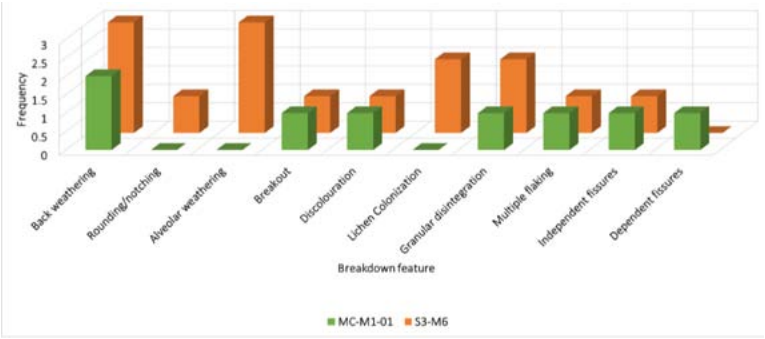


*Fig 5. This figure shows the comparison of breakdown feature occurrence on boulder MC-M1-01 (green colour; from Meteor Crater) and boulder S3-M6 (orange colour; from control site).*

were differences between Moenkopi Sandstone boulders at Meteor Crater and control sites. Moenkopi Sandstone boulder at control site had more channel features (39.55%), ridge features (36.79%) than boulder at Meteor Crater (27.1% and 29.65%) (see Fig 6). Whereas, Moenkopi Sandstone boulder at Meteor Crater had more pit features (1.48%), pass features (5.05%), peak features (1.68%), planar features (34.42%) than at control site (0.55%, 1.68%, 0.53%, and 20.91% respectively) (see Fig 6). The fact that the Moenkopi Sandstone boulder at Meteor Crater has more planar feature than the boulder at control site is due to lack of breakdown features on the boulders at Meteor Crater. The increased number of ridges on Moenkopi Sandstone boulder compared to boulders at the Meteor Crater at 1 cm scale may be due to the fact that there are sharply outlined centimetre-size alveoli walls. This also agrees with our visual observation that fewer breakdown features were observed on the Moenkopi Sandstone boulder at Meteor Crater compared to the boulder at the control site which has an alveoli weathered surface. In addition, the average Schmidt hammer rebound value (for rock hardness) for the boulder at the control site (28.80) was lower than the boulder at Meteor Crater (39.39). In the field, the boulder at the control sites had rougher texture than the boulder at Meteor Crater. The difference in breakdown features observed at the Meteor Crater and control site may be due the fact that porosity in Moenkopi Sandstone at Meteor Crater is reduced due to the impact event.

Petrographic microscope data revealed that Moenkopi Sandstone at Meteor Crater and the control site have similar chemical composition. In general, the Moenkopi Sandstone is very fine grained and well sorted. Grain size analysis has shown that the mean grain size and sorting of Moenkopi sandstone at Meteor Crater is similar to the Moenkopi sandstone at control sites and this rock property is not affected by the impact event or subsequent weathering processes. Petrographic and grain size analysis suggest that Moenkopi Sandstone at Meteor Crater and Control site had the same lithologic provenance. Kaolinite which is a product of chemical weathering was observed in rock thin sections from both the sites. Grain fracturing and iron oxidation are the most obvious signs of weathering. Iron oxidation and fracturing

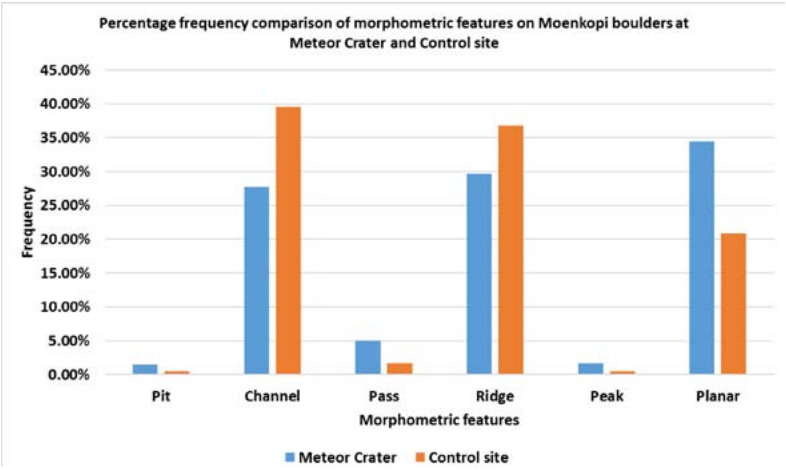


*Fig 6. Morphometric feature frequency comparison between boulders at Meteor Crater and Control site. This analysis reveals a difference in morphometric forms on boulder surface at both sites.*

in quartz grain was present in Moenkopi Sandstone from Meteor Crater and control sites.

X-ray Diffraction reveals no high-pressure polymorphs of quartz in the Moenkopi Sandstone from Meteor Crater and shows that it was identical to unshocked Moenkopi Sandstone at the control site. Porosity estimation from SEM BSE images has shown that porosity was found to be less in Moenkopi Sandstone from Meteor Crater (4.62% and 4.36%) than at Control site (10.47%). This suggests that the grains were compacted and pores were collapsed due to impact in Moenkopi Sandstone at Meteor Crater. SEM CL images revealed deformed quartz grains in Moenkopi Sandstone from Meteor Crater but no Planar Deformation Features were identified. Since none of the characteristic features (e.g. PDFs, high pressure polymorph of quartz, and diaplectic glass) of high pressure shock metamorphism was found, it is suggested that Moenkopi Sandstone have experienced low shock pressure regime (<5 GPa) during impact which has compacted the grains and reduced the porosity.

## Conference Presentation

We have presented papers on our work at 2 conferences

1. Verma, A., Bourke, M.C., (2016). A photogrammetry-based method for morphometric analysis of rock breakdown forms near Meteor Crater, Arizona, Geological Remote Sensing Group, London (Abstract attached in the end of this document).
2. Verma, A., Bourke, M.C., (2016). A photogrammetry based approach to generate sub-millimetre resolution Digital Elevation Models for investigating rock breakdown in the field. Irish Geomorphology Group annual workshop, University College Cork.

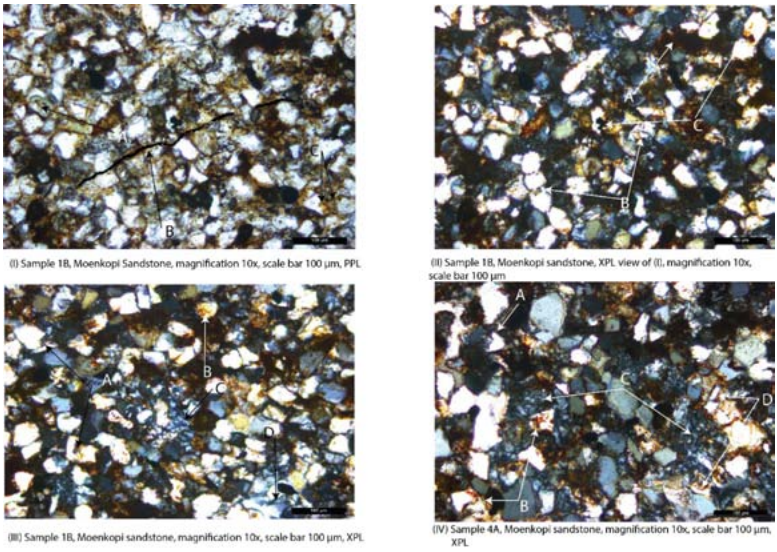


*Fig 7. Petrographic thin section 1: (I) Most of the grains are coated with thin rim of brown iron-oxide cement; B shows crack (traced) filled with iron-oxide; C shows calcite is typically coarser than the quartz. It has enveloped quartz and has anhedral margin, indicating a secondary origin. (II) A shows iron-oxide matrix; B shows dissolved quartz grain, one quartz grain penetrating another grain (concavo-convex contact); C shows dissolved quartz grain space occupied by opaque minerals. (III) A shows dissolved quartz grains; B indicates calcite grain; C shows kaolinite; D indicates crack within quartz grain. (IV) A shows dissolved quartz grain coated with the rim of brown iron oxide; B shows strongly weathered quartz grains; C shows kaolinite; D shows remaining fragments of quartz grain after dissolution*

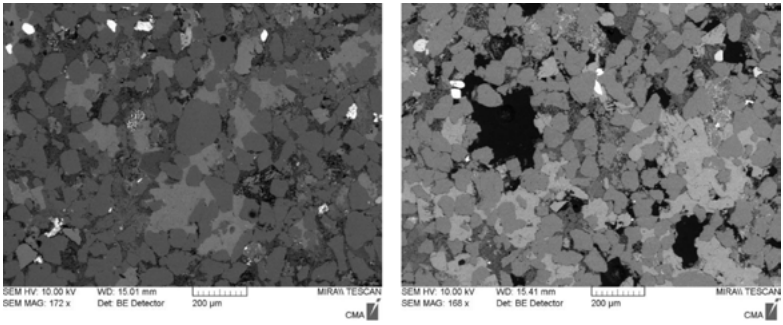


*Fig 8. BE images of shocked (left) and unshocked (right) Moenkopi sandstone. First image shows a shocked Moenkopi sandstone (left) in which grains are compacted and porosity is reduced compared to unshocked Moenkopi sandstone (right). Black areas are pore spaces.*

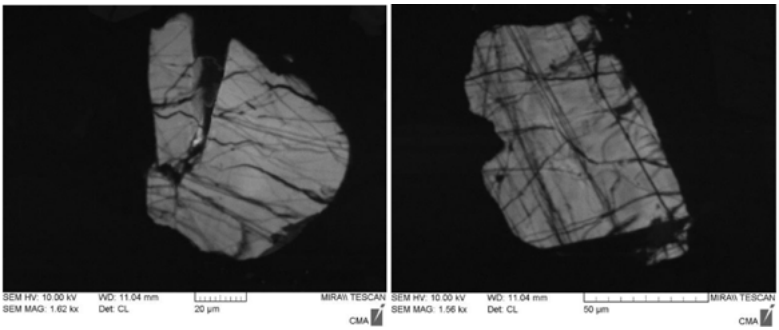


*Fig 9. CL images of shocked Moenkopi sandstone. Quartz grains in shocked Moenkopi sandstone is deformed and fractured due to impact.*

## References

CHAPMAN, M. 2007. The geology of Mars: evidence from earth-based analogs, Cambridge University Press.

COCKELL, C. S. & LIM, D. S. 2005. 11 Impact Craters, Water and Microbial Life. Water on Mars and life. Springer.

FERRIÈRE, L. & OSINSKI, G. R. 2013. Shock metamorphism. In: OSINSKI, G. R. & PIERAZZO, E. (eds.) Impact cratering: Processes and products. John Wiley & Sons.

HAMERS, M. & DRURY, M. 2011. Scanning electron microscope cathodoluminescence (SEM CL) imaging of planar deformation features and tectonic deformation lamellae in quartz. Meteoritics & Planetary Science, 46, 1814-1831.

HESLOP , E. E. M. 2003. Clast breakdown in the Atacama Desert, Chile :An intergrated field and laboratory approach. D.Phil, University of Oxford.

KENKMANN, T., POELCHAU, M. H. & WULF, G. 2014. Structural geology of impact craters. Journal of Structural Geology, 62, 156-182.

KIEFFER, S. W. 1971. Shock Metamorphism of the Coconino Sandstone. Journal of Geophysical Research.

KOWITZ, A., GÜLDEMEISTER, N., REIMOLD, W., SCHMITT, R. & WÜNNEMANN, K. 2013. Diaplectic quartz glass and SiO 2 melt experimentally generated at only 5 GPa shock pressure in porous sandstone: Laboratory observations and meso-scale numerical modeling. Earth and Planetary Science Letters, 384, 17-26.

KRING, D. A. 2007. Guidebook to the geology of barringer meteorite crater, arizona (aka Meteor Crater), Lunar and Planetary Institute Houston.

KRINSLEY, D. H., PYE, K., BOGGS JR, S. & TOVEY, N. K. 2005. Backscattered scanning electron microscopy and image analysis of sediments and sedimentary rocks, Cambridge University Press.

MELOSH, H. J. 1989. Impact cratering: A geologic process. Research supported by NASA. New York, Oxford University Press (Oxford Monographs on Geology and Geophysics, No. 11), 1989, 253 p., 1.

MICHELETTI, N., CHANDLER, J. H. & LANE, S. N. 2015. Structure from Motion (SfM) Photogrammetry.

NEWSOM, H. E., WRIGHT, S. P., MISRA, S. & HAGERTY, J. J. 2013. Comparison of simple impact craters: A case study of Meteor and Lonar Craters. Impact Cratering: Processes and Products, 271-289.

SHOEMAKER, E. M. 1987. Meteor Crater, Arizona. Centennial Field Guide, 2, 399-404.

TU RUL, A. 2004. The effect of weathering on pore geometry and compressive strength of selected

rock types from Turkey. Engineering Geology, 75, 215-227.
VILES, H., GOUDIE, A., GRAB, S. & LALLEY, J. 2011. The use of the Schmidt Hammer and Equotip for rock hardness assessment in geomorphology and heritage science: a comparative analysis. Earth Surface Processes and Landforms, 36, 320-333.

## Fieldwork expenses

The IAS PG grant ( 990) awarded was spent to cover transportation cost to the field. The fieldwork was undertaken from June 21 – July 06, 2016. Below is the breakdown of travel expenses –

| | |
|---|---|
| Return flights (Phoenix, Arizona to Dublin, Ireland) | € 697 |
| Extra luggage for equipment (charged by airlines) | €75 |
| Extra luggage for equipment and rock samples (charged by airlines) | €159 |
| Taxi (Uber) to travel to accommodation from airport | €60 |
| **Total costs** | **€991** |

# Understanding the Holocene paleoenvironmental changes in Madagascar using stalagmites

*Ny Riavo Voarintsoa, Department of Geology, University of Georgia, USA*
*Current: Postdoctoral Fellow, Institute of Earth Sciences, The Hebrew University of Jerusalem in Israel*
*nv1@uga.edu*

## General Overview of the project

Stalagmites have become one of the most reliable and useful paleoclimate archives, besides ice cores and tree rings, because they can be accurately dated [1]. The use of stable isotopes of O and C and other proxies from stalagmites has become very powerful in understanding the paleoclimate in several locations in the world [2].

Our understanding of past climate change depends on linking together paleoclimate records from locations all over the world. However, we have been challenged by the uneven distribution of the records [3], obviously leaving gaps in paleoclimate reconstruction. Madagascar is a location where such records are needed. It holds a key position in the Indian Ocean, seasonally visited by the ITCZ (Intertropical Convergence Zone) with a karst region crossing latitudinal belts along its western part.

This research has aimed to develop multi-proxy records from stalagmites from Anjohibe

and Anjokipoty Cave to a provide comprehensive data set to better understand the Holocene climate change in northwestern Madagascar. I specifically tested the following hypothesis: wetter/drier climate during colder/drier intervals when the ITCZ migrates south/north [4–5]. One of the driving factors to climate change in Madagascar is the ITCZ. It is responsible for the summer rainfall between November and April in the tropical savanna climate of northwestern Madagascar. The ITCZ migrates seasonally, and several studies (paleoclimate, models, reconstruction) have also shown that the ITCZ shifted further north or south at longer time scale depending on global conditions. Those conditions specifically reflect the cooling or warming of the Earth. During globally cooler conditions, the ITCZ shifted further South, and during globally warmer conditions, the ITCZ moved north, thus regions in one of the two hemispheres received more rainfall when the ITCZ stays longer there. For example, regions visited by the ITCZ in the Southern Hemisphere become wetter when the NH is cooler than the SH.

Holocene climate change in Madagascar is not well understood, simply because of the lack of long-term paleoclimate records. The two stalagmites supported by this IAS-PGS fund have yielded dates ranging from ca. 9kyr to ca. 0 yr. BP, thus covering the Holocene. The results have been published (e.g., Voarintsoa et al., 2017, Climate of the Past [6]) and presented at scholarly conferences (see details below). Another manuscript that will focus around the 8.2 ka event is in preparation.

## References:

[1] Edwards et al., Earth and Planetary Science Letters, 81, 2-3, 175-192, 1987; [2] Wong and Breecker,

Quaternary Science Reviews, 127, 1-18, 2015; [3] Wanner et al., Journal of the Geological Society, 172, 2, 254-263, 2015; [4] Chiang and Friedman, Annual Review of Earth and Planetary Sciences, 40, 383-412, 2012; [5] Schneider et al., Nature, 513, 7516, 45-53, 2014. [6] Voarintsoa et al., Climate of the Past, 13, 1771-1790, 2017.

## Relevant outcomes from this grant:

### Dissertation thesis

Voarintsoa, N. R. G. 2017. Investigating stalagmites from northeastern Namibia and northwestern Madagascar as a key to better understand local paleoenvironmental changes and implications for ITCZ dynamics. Jan 2017, University of Georgia, USA. 300p.

### Published to Climate of the Past (Special issue: SHAPE):

Voarintsoa, N. R. G., Railsback, L. B., Brook, G. A., Wang, L., Kathayat, G., Cheng, H., Li, X., Edwards, R. L., Rakotondrazafy, A. F. M., and Madison Razanatseheno, M. O.: Three distinct Holocene intervals of stalagmite deposition and nondeposition revealed in NW Madagascar, and their paleoclimate implications, Clim. Past, 13, 1771-1790, https://doi.org/10.5194/cp-13-1771-2017, 2017.

Voarintsoa, N. R. G., Railsback, L. B., Brook, G. A., Wang, L., Kathayat, G., Cheng, H., Li, X., Edwards, R. L., Rakotondrazafy, A. F. M., and Madison Razanatseheno, M. O., 2017. Three distinct Holocene intervals of stalagmite deposition and non-deposition revealed in NW Madagascar, and their paleoclimate implications, Clim. Past Discuss. doi:10.5194/cp-2016- 137. Special Issue: Southern Hemisphere Assessment of PalaeoEnvironment (SHAPE).

### Manuscript to be submitted to Quaternary Science Reviews:

Voarintsoa, N. R. G., Matero, Ilkka S.O., Gregoire, L., Railsback, L. B., Tindall, J., Sime, L., Cheng, H., Edwards, R. L., Brook, G. A., Kathayat, G., Li, X., Rakotondrazafy, A. F. M., and Madison Razanatseheno, M. O. Stalagmite records and model simulation indicating wet conditions in northwestern Madagascar during the 8.2 ka event.

### Conference presentations:

Voarintsoa, N. R. G., Railsback, L. B., Brook, G. A., Wang, L., Kathayat, G., Cheng, H., Li, X., Edwards, R. L., Rakotondrazafy, A. F. M., and Madison Razanatseheno, M. O., 2017. Mutiproxy evidence of a wet 8.2 ka event revealed in NW Madagascar: Linkage to latitudinal shifts of the Inter-Tropical Convergence Zone and the Atlantic Meridional Overturning Circulation. Climate Change: The Karst Record 8. University of Texas in Austin, USA (oral)

Voarintsoa, N.R. G., Wang, L., Railsback, L.B., Brook, G.A., Liang, F., Cheng, H., Edwards, R.L., 2017, Stalagmites and their uses in paleoenvironmental reconstruction, Interdisciplinary Research and Ideas Symposium (IRIS), Session Period 3: Pre-Fabricated Environment, University of Georgia. USA (oral)

Voarintsoa, N. R. G., Railsback, L. B., Brook, G. A., Wang, L., Kathayat, G., Cheng, H., Li, X., Edwards, R. L., Rakotondrazafy, A. F. M., and Madison Razanatseheno, M. O., 2016, Distinct early-, mid-, and late-Holocene climate in NW Madagascar: evidence from two stalagmites, Southern Hemisphere Assessment of PalaeoEnvironments (SHAPE) International Focus Group Workshop: Southern Hemisphere climate of the present and past, Universidad de Chile, Santiago. (oral)

# 1st Announcement

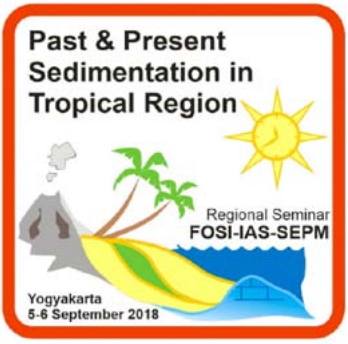


The Indonesian Sedimentologists Forum (FOSI) together with the International Association of Sedimetologists (IAS) and the Society of Sedimentary Geology (SEPM) are going to organize a regional seminar in Yogyakarta, Central Java, Indonesia, from 5 to 6 September 2018.

The seminar is titled "Past and Present Sedimentation in Tropical Region". Pre and post seminar field trip will be arranged. The committee is inviting potential speakers to participate in both oral and poster sessions.

E-mail address: iagifosi@gmail.com
Website: iagi.or.id/fosi/

Co-convenors:
Hendra Amijaya (University of Gajah Mada) &
Herman Darman (Indogeo Social Enterprise)

# EARLY CAREER SCIENTISTS RESEARCH GRANTS

Post-Doctoral Research Grants are intended as a seed to assist early-career post-doctoral researchers in either establishing a proof of concept, in order to support applications to national research funding bodies, or to fund areas of a project that were not included in the original project scope.

Up to 4 grants, each to a maximum of 2,500, are awarded twice per year to Early Career IAS members – those that have secured their Ph.D. within the previous 7 years.

Applicants should apply for a Post-Doctoral Research Grant via the IAS website. The application requires submission of a research proposal with budget and CV (template provided on the submission webpage), and a letter of support from the researcher's supervisor, line manager or Head of School.

## Eligibility:

- Applicants must be full members of the IAS.
- Applicants must have secured their Ph.D. within the previous 7 years.
- Applicants can only benefit from a Post-Doctoral grant on one occasion.

## Proposals will be ranked on the following criteria:

- Scientific quality of research, novelty and timeliness, likely output.
- Feasibility.
- Cost effectiveness.
- The scientific and publication track record of the investigator.
- Demonstration that the proposed work cannot be conducted without a grant.
- Researchers that are not supported by substantial funding.
- Preference is given to applications for a single purpose (rather than top-ups of other grant applications).

## Application requirements:

Applications must be made via the IAS web site.

- Research Proposal, maximum 3 pages A4, including:
- Rationale and scientific hypothesis to be addressed
- Specific objectives of the research
- Anticipated achievements and outputs
- Methodology and approach
- Research plan

- A list of pending and previous applications for funds to support this or related research.
- CV of the applicant, maximum 2 pages A4.
- Justification of the proposed expenditure, up to 1 page of A4. If other individuals are to be involved with the project, this document must include a clear explanation of their role and costs.

## Examples of funding

- Direct costs of fieldwork.
- Laboratory analysis.
- Specialist equipment (not computers).

## Funding exclusions

The IAS does not offer funding for the following costs:

- Investigator's salary costs.
- Travel to attend a scientific conference, workshop or exhibition.
- Core funding or overheads for institutions.
- Student tuition fees and summer research bursaries.

## Deliverables

- The IAS should be acknowledged in all reports, presentations and publications produced as a result of the awarded grant.
- A report should be submitted to the IAS detailing the outcomes of the research.
- Where a publication is produced then this may be submitted in lieu of a report.

# INSTITUTIONAL IAS GRANT SCHEME (IIGS)

## IIGS Guidelines

Special IAS Grants or Institutional IAS Grants are meant for capacity building in third world countries. There exists a list of 'Least Developed Countries' (LDC) by the UN. This list categorizes countries according to income per capita and is yearly updated.

Grants are allocated to allow Geology Departments in LDC to acquire durable sedimentological equipment for teaching and research (like sieves, calcimeters, auger drilling tools, etc.) or tools that can be used by all geology students (like general geology/sedimentology textbooks, IAS Special Publications (SP), memory sticks with back issues of Sedimentology or SP, etc). Therefore, the grant application should clearly demonstrate to increase the recipient's capacity to teach sedimentology at the undergraduate level (Bachelor) in a durable way. It should also indicate in what way it would enable to support sedimentological research at the graduate level (Master).

Applicants should have a permanent position at their University and should be IAS Full Members. Applications should be submitted by email to the Office of the Treasurer (ias-office@ugent.be) and contain the following information (not exhaustive list):

- the mission statement of the University/Geology Department
- the approval of the University Authorities to accept the grant
- a list of permanent teaching and technical staff members of the Geology Department (with indication of their area of research)
- the structure of the geology undergraduate and graduate courses (Bachelor/Master programme with indication of courses and theoretical and practical lecture hours)
- the number of geology students
- the actual facilities for geology/sedimentology students
- a motivation of application
- a budget with justification
- the CV of the applicant, including a sedimentology research plan

The institutional grant scheme consists each year of 2 sessions of 1 grant of 10.000 Euro. Applications run in parallel with the PhD research grant scheme (same deadline for application and recipient notification). The IAS Grant Committee will seek recommendations from relevant National Correspondents and Council Members (eventually including visitation) before advising the IAS Bureau for final decision. Additional funds made available by the recipient's University are considered as a plus.

Items listed in the application will be bought through the Office of the IAS Treasurer and shipped to the successful applicant. By no means money will be transferred to the grant recipient.

# POSTGRADUATE GRANT SCHEME (PGS)

## PG Guidelines

IAS has established a grant scheme designed to help PhD students with their studies by offering financial support for fieldwork, data acquisition and analysis, visits to other institutes to use specialized facilities, or participation in field excursions directly related to the PhD research subject.

Up to 10 grants, each of about 1,000 Euro are awarded, twice a year. These grants are available for IAS Student Members only. Students enrolled in MSc programs are not eligible for funding and research grants are not given for travel to attend a scientific conference, nor for the acquisition of equipment.

Applicants should apply for a postgraduate grant via the IAS website. The application requires submitting a research proposal with budget and CV (template provided on the submission webpage) and a letter of support from the student's supervisor. After the deadline has passed, the IAS Bureau evaluates the submitted applications and makes a final selection. Applicants are personally informed by the Office of the Treasurer about their grant. The grants are transferred to the applicants' bank account upon submission of a short scientific and financial report.

Eligibility and selection criteria:

- Applicants must be enrolled as a PhD student;
- Applicants can only benefit from a postgraduate grant once during their PhD;
- In the evaluation process preference will be given to those applications that i) can convincingly demonstrate that the proposed work cannot be conducted without the grant, and ii) are not supported by substantial industry funding.

## Application

The application should be concise and informative, and contains the following information (limit your application to 1250 words max.):

- Research proposal (including Introduction, Proposal, Motivation and Methods, Facilities) – max. 750 words
- Bibliography – max. 125 words
- Budget – max. 125 words
- Curriculum Vitae – max. 250 words

Your research proposal must be submitted via the Postgraduate Grant Scheme application form on the IAS website before the application deadline. The form contains additional assistance details for completing the request. Please read carefully all instructions before completing and submitting your application. Prepare your application

in 'Word' and use 'Word count' before pasting your application in the appropriate fields.

A recommendation letter from the PhD supervisor supporting the applicant is mandatory, as well as a recommendation letter from the Head of Department/Laboratory of guest institution in case of laboratory visit. The letter needs to be uploaded by the candidate, when submitting his/her application, and not be sent separately to the Office of the Treasurer.

Please make sure to adequately answer all questions.

## Deadlines and notifications

Application deadline 1st session: 31 March.

Application deadline 2nd session: 30 September.

Recipient notification 1st session: before 30 June.

Recipient notification 2nd session: before 31 December.

NOTE: Students who got a grant in a past session need to wait 2 sessions (1 year) before submitting a Postgraduate Grant Scheme grant application again.

Students whose application was rejected in one session can apply again after the notification deadline of the rejected grant application

## Application Form

- Research Proposal (max. 750 words)
- Title: .....
- Introduction (max. 250 words): .....

Introduce briefly the subject of your PhD and provide relevant background information; summarise previous work by you or others (provide max. 5 relevant references, to be detailed in the 'Bibliography' field). Provide the context for your PhD study in terms of geography, geology, and/or scientific discipline.

- Proposal (max. 250 words): ...

Describe clearly your research proposal and indicate in what way your proposal will contribute to the successful achievement of your PhD. Your application should have a clearly written hypothesis or a well-explained research problem of geologic significance. It should explain why it is important. Simply collecting data without an objective is not considered wise use of resources.

- Methods (max. 125 words): .....

Outline the research strategy (methods) that you plan to use to solve the problem in the field and/or in the laboratory. Please include information on data collection, data analyses, and data interpretation. Justify why you need to undertake this research.

- Facilities (max. 125 words): .....

Briefly list research and study facilities available to you, such as field and laboratory equipment, computers, library.

- Bibliography (max. 125 words)

Provide a list of 5 key publications that are relevant to your proposed research, listed in your 'Introduction'. The list should show that you have done adequate background research on your project and are assured that your methodology is solid and the project has not been done already. Limit your bibliography to the essential references. Each publication should be preceded by a '*'-character (e.g. *Surlyk et al., Sedimentology 42, 323-354, 1995).

- Budget (max. 125 words)

Provide a brief summary of the total cost of the research. Clearly indicate the amount (in Euro) being requested. State specifically what the IAS grant funds will be used for. Please list only expenses to be covered by the IAS grant. The IAS will support field activities (to collect data and samples,

etc.) and laboratory activities/analyses. Laboratory activities/analyses that consist of training by performing the activities/analyses yourself will be considered a plus for your application as they will contribute to your formation and to the capacity building of your home institution. In this case, the agreement of the Head of your Guest Department/Laboratory will be solicited by automated e-mail.

- Curriculum Vitae (max. 250 words)

Name, postal address, e-mail address, university education (degrees & dates), work experience, awards and scholarships (max. 5, considered to be representative), independent research projects, citations of your abstracts and publications (max. 5, considered to be representative).

- Advise of Supervisor and Head of Guest Department/Laboratory

The recommendation letter from the supervisor should provide an evaluation of the capability of the applicant to carry out the proposed research, the significance and necessity of the research, and reasonableness of the budget request. The recommendation letter must be uploaded by the applicant together with the rest of the application content. Applications without letter of support will be rejected. It will be considered as a plus for your application if your PhD supervisor is also a member of IAS.

If you apply for laboratory analyses/activities, please carefully check analysis prices and compare charges of various academic and private laboratories as prices per unit might differ considerably. Please first check whether analyses can be performed within your own University. If your University is not in a position to provide you with the adequate analysis tools, visiting another lab to conduct the analyses yourself strengthens your application considerably as it contributes to your formation and to capacity building of your home University. Please check with the Head of Department/ Laboratory of your guest lab to assure its assistance during your visit. You should add a letter of support from him/her with your application.

Finally, before submitting your application, you will be asked to answer a few informative questions by ticking the appropriate boxes.

- is your supervisor a member of IAS
- was this application your own initiative
- did you discuss your application with your Supervisor
- did you already have contact in the past with the Head of the Guest Department/Laboratory (if appropriate)

# CALENDAR

## *Flügel Courses: Discover the fascination of Carbonate Rocks

*5th–16th March 2018*
*Erlangen, Germany*

*Axel Munnecke*
*axel.munnecke@fau.de*
*http://archiv.gzn.fau.de/index.php?id=1727*

---

## 2018 Western Pacific Sedimentology Meeting*

*19th–20th March 2018*
*GwangJu, Korea, South*

*https://2018wpsm.wixsite.com/home*

---

## *European Geosciences Union General Assembly 2018 EGU2018

*8th–13th April 2018, Vienna*
*Austria*

*https://www.egu2018.eu/*

---

### 7th International Maar Conference Maar2018*

*21th–25th May 2018*
*Olot, Spain*

*http://rfg2018.org/rfg/2018/home*

### POKOS 7 - Polish Sedimentological Conference organized by Polish Geological Society

*4th–7th June 2018*
*Góra Św. Anny, Poland*

*http://www.pokos.confer.uj.edu.pl*

### International Conference Resources for Future Generations 2018

*16th–21st June 2018*
*Vancouver, Canada*

*http://maar2018.com/*

### *4th Meeting of the Working Group on Sediment Generation

*27th–29th June 2018*
*Dublin, Ireland*

*https://www.tcd.ie/Geology/wgsg2018/*

### Cyclostratigraphy Intercomparison Project Workshop*

*30th July – 1st August 2018*
*Brussels, Belgium*

*http://we.vub.ac.be/en/cyclostratigraphy-intercomparison-project/workshop*

### 20th International Sedimentological Congress*

*13th –17th August 2018*
*Quebec City, Canada*

*Pierre Francus*
*Pierre.Francus@ete.inrs.ca*
*http://isc2018.org/*

### *The Indonesian Sedimentologists Forum (FOSI)

*5th–6th September 2018*
*Yogyakarta, Central Java, Indonesia,*

*www.iagi.or.id/fosi*

### *Sedimentary Records of Slope, Beach and Fluvial Processes

*6th–9th September 2018*
*Sakarya, Turkey*

*Ezher Toker Tagliasacchi*
*egulbas@pau.edu.tr*

### *VII Argentinean Meeting on Quaternary and Geomorphology

*8th–21st September 2018*
*Puerto Madryn, Argentina*

*http://www.cacg2018.cenpat-conicet.gob.ar/*

---

### Seismic Characterisation of Carbonate Platforms and Reservoirs

*10th–11th October 2018*
*London, United Kingdom*

*https://www.geolsoc.org.uk/carbonateplatforms18*

---

*** THESE EVENTS HAVE FULL OR PARTIAL IAS SPONSORSHIP**


This Newsletter has been designed by
Proedex s.l. Francisco Silvela 27
28028 Madrid, Spain editorial@proedex.com

**Contributions to be sent to:**
Vincenzo Pascucci
IAS General Secretary
Department of Architecture,
Design and Planning,
University of Sassari,
sede di Via Piandanna 4,
07100 Sassari, Italy
Tel.: +39 079228685
pascucci@uniss.it

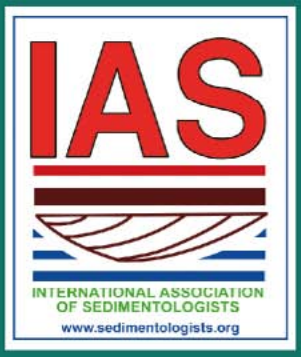
IAS
INTERNATIONAL ASSOCIATION
OF SEDIMENTOLOGISTS
www.sedimentologists.org